Fonds Régional de Développement Européen
European Regional Development Fund

ICE
INTELLIGENT COMMUNITY ENERGY

Interreg
France (Channel Manche) England

EUROPEAN UNION

ICE REPORT T1.2: ANALYSIS OF SMART GRID AND STORAGE OPTIONS IN A DEMAND SIDE ASSESSMENT CONTEXT

14/08/2018

BRETAGNE DÉVELOPPEMENT INNOVATION
SDEF
TECHNOPÔLE BREST-IROISE
Technopole Quimper-Cornouaille
PÔLE MER BRETAGNE ATLANTIQUE
UNIVERSITY OF EXETER
PLYMOUTH UNIVERSITY
UEA University of East Anglia
marine

ICE report T1.2:

Analysis of smart grid and storage options in a demand side assessment context

Hisham Mahmood, Essam Hussain, Mohammad Abusara, Philipp R. Thies, Edoardo Nerenzi

Peter M. Connor

About ICE

Supported by Interreg VA France (Channel) England, the Intelligent Community Energy (ICE) project, aims to design and implement innovative smart energy solutions for isolated territories in the Channel area. Islands and isolated communities face unique energy challenges. Many islands have no connection to wider electricity distribution systems and are dependent on imported energy supplies, typically fossil fuel driven. The energy systems that isolated communities depend on tend to be less reliable, more expensive and have more associated greenhouse gas (GHG) emissions than mainland grid systems. In response to these problems, the ICE project considers the entire energy cycle, from production to consumption, and integrates new and established technologies in order to deliver innovative energy system solutions. These solutions will be implemented and tested at our unique pilot demonstration sites (Ushant island and the University of East Anglia's campus), to demonstrate their feasibility and to develop a general model for isolated smart energy systems elsewhere. The ICE consortium brings together researcher and business support organisations in France and the UK, and engagement with SMEs will support project rollout and promote European cooperation.

Table of Contents

Abstract 10
1. Part (1): Energy Storage Management 12
Introduction 13
1.1 Energy Demand Analysis 13
1.2 Wind and Solar Resource Data 16
1.2.1 Wind Resource Analysis 17
1.2.2 Wind Direction Analysis 18
1.2.3 Wind Speed Analysis 19
1.2.4 Solar Resource Analysis 21
1.3 Energy Demand and Renewable Energy Generation Comparison Conclusions 22
1.4 Renewable Energy Technologies 23
1.4.1 Wind Power 23
1.4.2 Solar Power 25
1.4.3 Tidal Generation 26
1.5 Energy Storage Technology 26
1.6 Methodology 27
1.6.1 Energy Capacity Intervals 27
1.6.2 Energy Capacity Sizing Methodology 28
1.6.3 Power Rating Sizing 30
1.7 Energy Capacity Results 31
1.8 Case Study 32
1.9 Power Rating Sizing 39
1.10 Energy Management 40
1.10.1 Demand Side Management and Virtual Dynamic Tariff 43
1.10.2 EWH Demand Side Controller 45
1.11 100% Renewable Energy Generation 48
2. Part (2): Reliability Assessment 49
2.1 Status Quo: Reliability Assessment; Ushant Island 51
2.1.1 Power Flow Analysis of the Current Ushant Island Power Network 63
2.1.2 Reliability Analysis of the Current Ushant Island Power Network 66
2.2 Renewable Energy Integration: Reliability Assessment for existing Ushant Island Network 69
2.2.1 Power Flow Analysis 73

2.2.2 Reliability Assessment of the Future Ushant Island Power Network 76

References 79

Table of Figures

Figure 1: Annual total energy demand variations (y-axis starting from 6GWh/year for better visual representation) 14
Figure 2: Average monthly total energy demand 14
Figure 3: Average hourly demand profile per month 15
Figure 4: Power demand probability and cumulative sum of power demand probability for the average year 15
Figure 5: Power demand probability and cumulative sum of power demand probability for all six years on record (2011-2016) 16
Figure 6: Geographical location of Ushant and the considered weather station (Google Earth Pro, 2017). 17
Figure 7: Wind rose for wind resource at Brest Bretagne Airport 18
Figure 8: Wind speed probability distribution and Weibull distribution at 10m 20
Figure 9: Average hourly wind speed profile per month 21
Figure 10: Monthly average wind speed 21
Figure 11: Average hourly global irradiance 22
Figure 12: Monthly average daily sum of global horizontal irradiation 22
Figure 13: Wind shear profile (Danish Wind Industry Association, 2002) 24
Figure 14: Screenshot of program window showing input parameters in relation to the RE technologies 33
Figure 15: Screenshot of drop-down list to choose the wind turbine type 33
Figure 16: Screenshot of a 24h section for the hourly wind and solar generation and demand data 34
Figure 17: Screenshot of a 24h section for the hourly wind and solar generation and demand data 34
Figure 18: Hourly average RE generation, demand and net power profile for one day 35
Figure 19: Screenshot of key generation results 35
Figure 20: Total yearly values in MWh for RE generation, excess generation, demand and uncovered demand 36
Figure 21: Standard configuration parameters for the ESS that may be modified by the user 36
Figure 22: Screenshot of a 24h section up to 2MWh of the matrix representing the hourly SOC, considering arbitrary values for RE generation, and highlighting minimum and maximum charge 37
Figure 23: Screenshot of the section of a table from the model indicating the effect of different ESS energy capacities on the uncovered demand and excess generation 37
Figure 24: Percentage values for uncovered energy demand and excess generation for energy capacities up to 20MWh 38
Figure 25: Standard configuration parameters for the calculation of the NPV that may be modified by the user 38
Figure 26: NPV, energy capacity cost and diesel generation expenditure in year one for energy capacities up to 20MWh 39
Figure 27: Optimum energy capacity results for the five different objectives 39
Figure 28: Optimum energy capacity results for the five different objectives 40
Figure 29: Energy balance when deploying 2 MW wind generation, and 1.8 PV generation. 40
Figure 30: Annual energy balance profile when deploying 2 MW wind generation, 1.8 PV generation, and a 2 MWh battery. 41

Figure 31: Generation/demand profile on Jan 1-5, 2016. 42
Figure 32: Generation/demand profile on June 1-5, 2016. 42
Figure 33: Example for the dynamic virtual tariff that shows the energy deficit effect. 43
Figure 34: Example for the dynamic virtual tariff that shows the SOC effect. 44
Figure 35: Typical household hot water usage used in the study. 45
Figure 36: Elements of the DP control structure. 46
Figure 37: Performance of (a) the traditional simple thermostat controller, and (b) the proposed smart controller. 46
Figure 38: Dynamic virtual tariff for the 24 hours used in Figure 11-8 example. 47
Figure 39: Improvement in the annual energy balance after deploying 2 MWh battery, and employing the proposed demand response strategy. 47
Figure 40: Performance of the EWH demand response controller in comparison to the traditional controller for 5 days in January. 48
Figure 41 Ushant power network 52
Figure 42: Ushant Island power network and nodes 54
Figure 43: Example of estimating the cable length employing PlotDigitizer software 55
Figure 44: Cable cores configuration (a) Triangle, (b) Flat and (c) Trefoil 56
Figure 45 Ushant Island schematic power network diagram 59
Figure 46: Ushant Island schematic power network diagram 60
Figure 47: Total number of houses at each load node 61
Figure 48: Percentage of the load at each node 61
Figure 50: Simulink model for the Ushant power network 62
Figure 51: Load demand at each node 63
Figure 52: Node voltage drop (ΔV) under highest load demand (2.08MW) 64
Figure 53: Percentage of used cable capacity under highest load demand (2.08MW) 64
Figure 54: Connection components of the load node 67
Figure 55: Node P0002 reliability block diagram 68
Figure 56: Failure rate of individual load nodes under diesel generators 69
Figure 57: Power generation for each scenario 70
Figure 58: The recommended location of the wind turbine 71
Figure 59: The suggested locations of the wind turbine 71
Figure 60: Scenario 1 for the location of the energy generation unit 73
Figure 61: Cable used capacity under high load demand and high generation power output (scenario 1) 74
Figure 62: Voltage drop at each load node under high load demand and high generation power output (scenario 1) 74
Figure 63: Scenario 2 for the location of the energy generation unit 75
Figure 64: Cable used capacity under high load demand and high generation power output (scenario 2) 75
Figure 65: Voltage drop at each load node under high load demand and high generation power output (scenario 2) 76
Figure 66: Simplified model of PV (a) and wind turbine &tidal energy (b) for reliability study 76
Figure 67: Failure rate for the load node under fixed and equal reliability for all generator units 77

Figure 68: Failure rate for the load node under fixed and equal reliability for all generator units compared to the diesel generator units. 77
Figure 69: Failure rate for the load node under fixed reliability compared to the diesel generator units. 78
Figure 70: Change in the load node failure rate under fixed & equal reliability for all generator units and fixed reliability 78

Table of Tables

Table 1: Geographical coordinates for the weather station and Ushant (System Advisor Model, 2010) (Google Earth Pro, 2017) 17
Table 2: Key parameters for wind direction analysis 18
Table 3: Wind speed frequency distribution, probability distribution and Weibull distribution 19
Table 4: Key parameters from wind speed analysis 20
Table 5: Surface roughness length definitions (Troen and Petersen, 1989) 24
Table 6: Wind turbine characteristics (Northern Power Systems, 2015) (EWT, 2016a) (EWT, 2016b) (Enercon, 2015) (EWT, 2016c) 25
Table 7: Solar PV technologies characteristics (System Advisor Model, 2010) 26
Table 08: Key parameters for the energy storage system 27
Table 9: ESS energy capacity intervals considered for estimate of optimum size 28
Table 10: Ushant Island cable parameters 56
Table 11: Available cable capacity Island 65
Table 12 Failure rate of the main power network (YARD , A. E. Green 1978, SINTEF 1984, AME 1992, Ammirato, Silecchia et al. 2006, Jey K. JEYAPALAN 2007, Gill 2011, Chengke Zhou and Zhou 2012, Hassan M. Nemati 2015) 66
Table 13: A comparison between the suggested wind turbine locations 72
Table 14: Power demand and generation 73
Table 15 reliability of the PV unit, wind turbine and tidal energy 77

Abstract

This report is divided into two parts; energy storage management and reliability assessment of the Ushant Island.

In the first part, it addresses the challenges in energy management in order to achieve Ushant Island's goal of 70% renewable generation by 2020 and 100% by 2030. Many challenges have to be addressed carefully at all levels of the system design, sizing, and power and energy management. The main challenge is raised by the intermittent nature and daily/seasonal disparity of renewable energy generation, in addition to the misalignment of generation and demand. Consequently, it would be necessary to implement strategies to balance generation and demand, such as energy storage. Optimising the size of the battery while considering the size of the renewable energy sources and the load demand is considered as the first step towards designing an effective intelligent energy system. Consequently, this work aids at facilitating the transition of Ushant towards a more sustainable future by developing a tool in Microsoft Excel to optimise the size of the energy storage system (ESS) for the island. The program allows the user to choose between a range of renewable energy generators specifically selected to suit wind and solar resources in the area. Their hourly generation profile is then estimated from local wind speed and solar radiation data. An analysis of the hourly energy demand of the island is also carried out to better understand how the wind and solar resources could match the energy requirements of Ushant. On the other hand, at the energy management level, the Energy Management System (EMS) coordinates the operation of the energy sources and energy storage, and also manages the demand to maintain energy balance for the short term (hourly) and the long term (daily) horizon. Intelligent energy systems rely heavily on load and weather forecasts, as well as previous demand and weather data, to optimise the system operation for the next hour and 24-hour horizons. Artificial intelligence and machine learning techniques are adopted in in this work to effectively exploit all the previous and forecasted data to develop an energy management system that is trained on previous data and continues to learn and adapt while the system is operating online.

In the second part, it analyses the energy demand side options and implications for Ushant Island. In order to achieve this and provide a more generically applicable approach, a structured reliability assessment has been developed, by which the energy demand side status and renewable energy options for an island or off grid community can be assessed.

The report brings together i) the outcomes from ICE report 1.4 about the renewable energy sources types and power profiles with ii) the existing network infrastructure. The main aims of the analysis are:

- Outlining the methodology for the reliability assessment of the island/off grid power network
- Developing an assessment approach to establish/estimate any unknown data and parameters which are required for the reliability assessment
- Assessment of the current status quo for power network parameters on Ushant power network
- Analysis of current power network reliability and power quality (voltage drop) for Ushant power network

- Evaluation/comparison of traditional power generation units (Diesel Generator) with the renewable energy sources in the network reliability and power quality (voltage drop) for Ushant power network
- Evaluation of power network options to support the additional power generation units for Ushant power network.

Ushant Island power network is analysed as an example to show methodology and the effect of replacing the traditional generator units with renewable energy sources. The developed methodology is based on the available data and information, comprising of available power network data, component and hardware data sheets as well as justified assumptions, where needed. A situation with limited or restricted access to data may be a common occurrence for island and isolated communities, where the full documentation and detailed energy usage profiles may not be readily accessible. The focus of the analysis however is to perform a relative comparison between the current power network, supplied by traditional power generation units, and a sustainable energy supply through renewable generation units. This relative comparison is valid, even if the absolute parameter values have some uncertainties.

The report is structured as follows: Following an outline of the general reliability assessment methodology (section 2), the current Ushant Island power network is assessed regarding its reliability and power flow (section 3). Section 4 utilises the scenario of the renewable energy configuration, based on ICE report T1.4, in order analyse a range of load cases and their respective reliability and power flow implications for the Ushant power network. This allows a comparison between the status quo conditions and possible sustainable energy supply options (section 5).

1. Part (1): Energy Storage Management

Introduction

The French island of Ushant, off the coast of Brittany, is currently off-grid in terms of electrical energy and heating, thus heavily relies on expensive and polluting diesel generation to meet its everyday energy requirements. The overall cost of generation through fossil fuels is currently over twice as high as the national average electricity cost of €0.169/kWh (£0.149/kWh) (EDF, 2016). Due to the price volatility of fossil fuels, the generation cost is also subject to significant fluctuations over time leading to unpredictable future prices that may substantially raise the yearly expenditure on generation. This is the reason why Ushant is planning to shift away from fossil fuels towards more secure, sustainable and cheaper sources of energy. By diversifying the island's energy mix with a greater percentage of renewable energy (RE) generators, Ushant could exploit more of the abundant natural energy sources that are available in the area. Despite the fact that renewable energy sources, like wind and solar, may follow general timely patterns, they stare still intermittent and relatively unpredictable. Consequently, if more RE was planned to be installed on Ushant, it would be necessary to implement strategies to balance generation and demand, such as energy storage.

Consequently, this work aids at facilitating the transition of Ushant towards a more sustainable future by developing a tool on Microsoft Excel to correctly size an energy storage system (ESS) for the island. The program allows the user to choose between a range of renewable energy generators specifically selected to suite the wind and solar resource in the area. Their hourly generation profile is then estimated from local wind speed and solar radiation data. An analysis of the hourly energy demand of the island is also carried out to better understand how the wind and solar resources could match the energy requirements of Ushant. Depending on how well the energy demand can be directly balanced by the RE generation, the program will calculate the optimum ESS energy capacity to achieve a set of different objectives, both technical and financial. This will also take into account the recurrent need for diesel generation whenever the demand cannot be balanced by the set amount of RE and the ESS.

The tool is designed to allow the user to create the desired scenario by giving flexibility when setting the characteristics of the RE technologies, the ESS as well as further financial parameters. The program is fully automated and all the main results are clearly organised in tables and graphs.

1.1 Energy Demand Analysis

The following section investigates the power demand of Ushant with focus on exploring hourly, monthly and yearly variations. This analysis will also aid at determining the demand data to consider in the model.

The overall energy demand of the island is hourly metered and six years' worth of historical data (2011-2016) are available on an EDF online portal. Figure 1 illustrates the yearly energy demand variations between the six years on record. The average annual demand was calculated to be just under 6.6 GWh/year with a maximum deviation of approximately $\pm$ 0.5GWh/year, equal to $\pm$ 7.5% of the average value. This shows the variability of the island's energy demand, with the weather conditions probably being a major factor. The minimum and maximum energy intensive years on record are 2011 and 2013 respectively. Nevertheless, to re-create a realistic scenario that could be suitable for several future years, this project will consider the average energy demand.

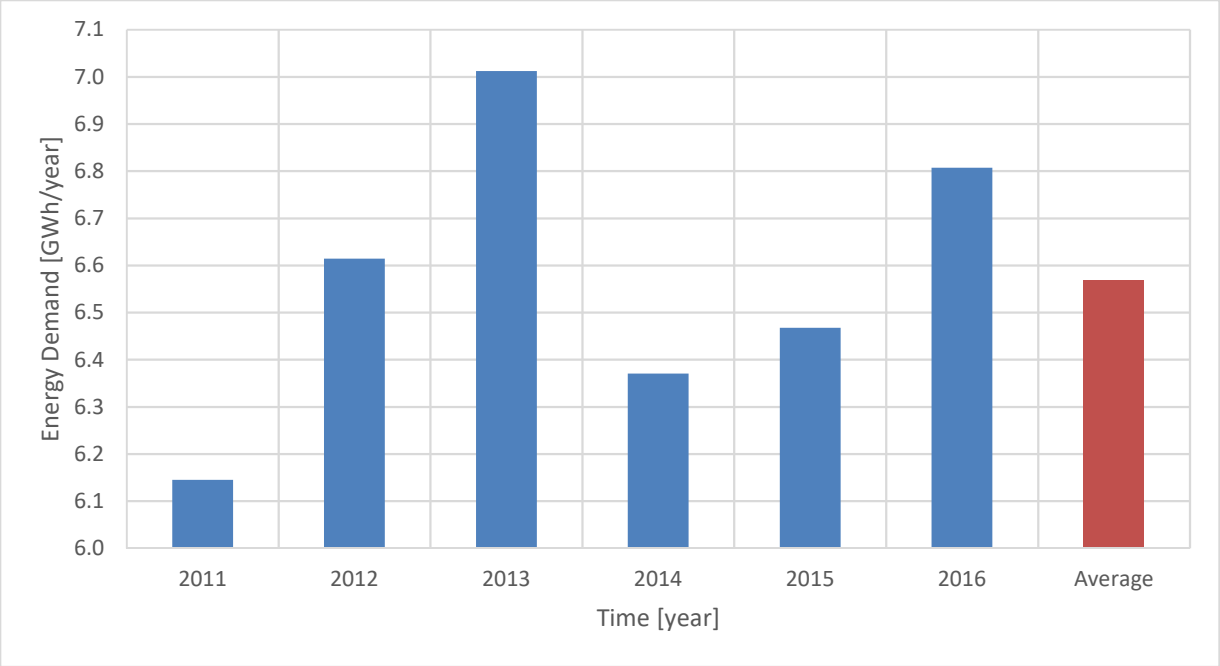

Figure 1: Annual total energy demand variations (y-axis starting from 6GWh/year for better visual representation)

Figure 2 shows the monthly variations in electricity consumption for the calculated average year. The graph highlights how the colder months (December to April) account for much greater consumption compared to the summer months. This significant difference may be attributed to the requirement for heating through electric heaters, due to Ushant not being connected to the gas mains.

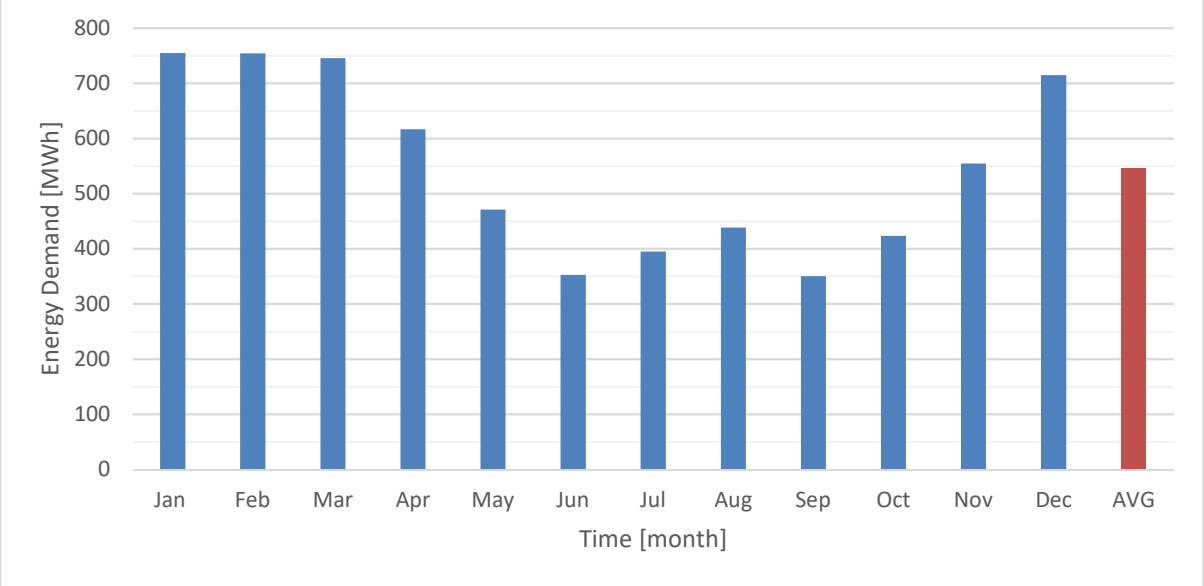

Figure 2: Average monthly total energy demand

Despite the difference in monthly total energy demand, the average hourly power demand profile is very similar between all months of the year, as shown in Figure 3. Two demand peaks are recorded

daily, a minor peak approximately between 7:00am and 12:00pm and a more substantial one between 19:00pm and 12:00am.

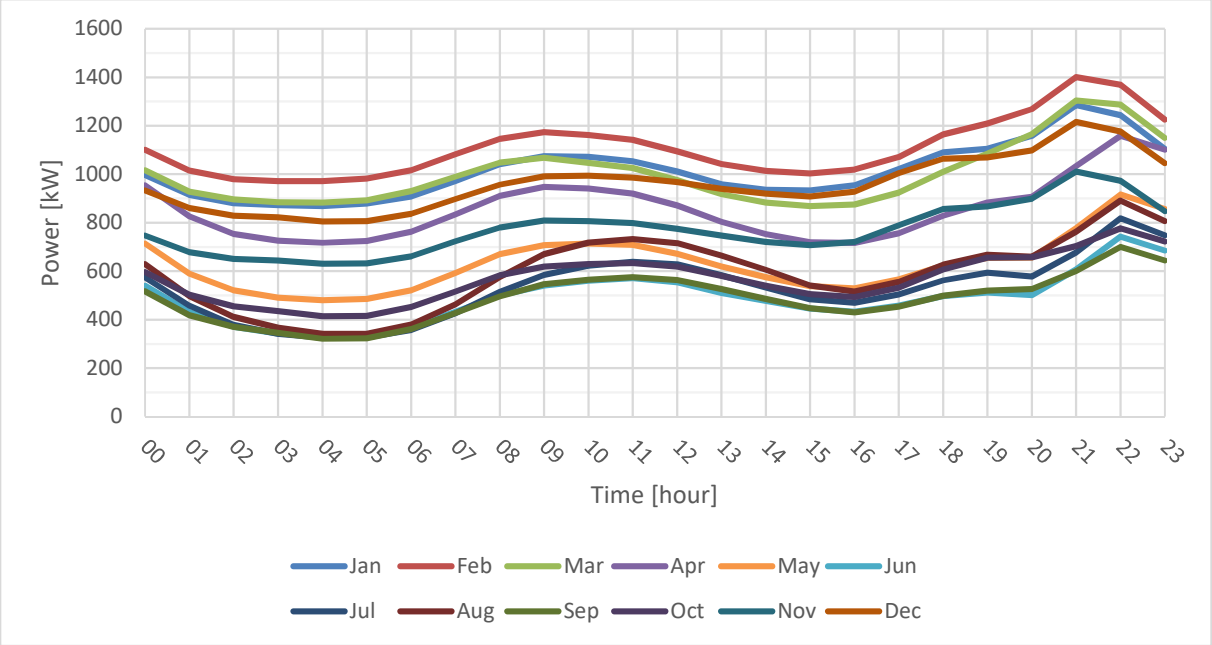

Figure 3: Average hourly demand profile per month

Figure 4 summarises the hourly power demand frequency over the considered average year. The graph shows that the demand ranges between a minimum and maximum power of 400kW and 1.7MW respectively. As indicated above the bars on the chart, demands between 1.5MW and 1.7MW rarely occur, precisely 54 times per year. Moreover, the cumulative sum curve indicates a 90th percentile in line with 1.1MW, meaning that a demand over that value only occurs 10% of the time.

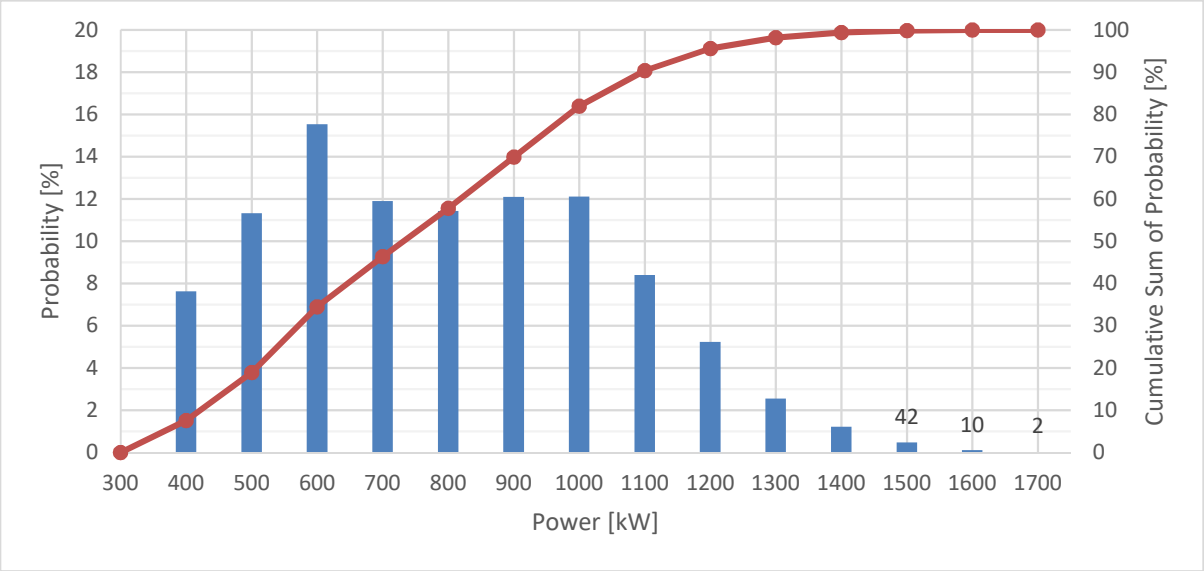

Figure 4: Power demand probability and cumulative sum of power demand probability for the average year

Nevertheless, if the same probability chart is plotted with the demand data from all six years on record, instead of only considering the average year, a broader power demand range may be observed. Figure 5 indicates the maximum power demand on record of 2.1MW which occurred twice during the most energy intensive year, 2013. Despite the broader demand range, the 90th percentile still corresponds to approximately 1.1MW, as shown in Figure 4.

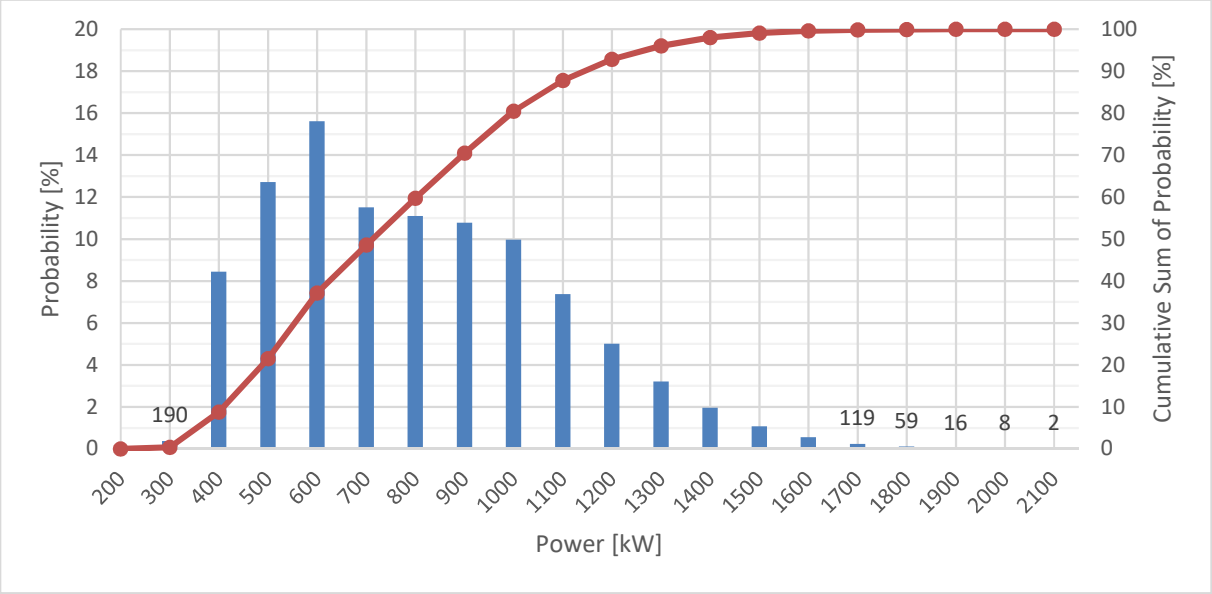

Figure 5: Power demand probability and cumulative sum of power demand probability for all six years on record (2011-2016)

This analysis has determined the yearly and daily demand distribution of Ushant which will help to better understand the balance between demand and generation from renewable energy technologies and consequently the energy storage capacity and power rating requirements.

1.2 Wind and Solar Resource Data

Specific wind and solar resource data for the island of Ushant was not found to be available online. It was even investigated whether the local airport on the island might have had a weather station, however it was determined that no weather data recording equipment was present. The data for nearby weather stations was downloadable from the renewable energy sizing software "System Advisor Model (SAM)" by the National Renewable Energy Laboratory (NREL) (System Advisor Model, 2010). The wind data was recorded by the weather station at Brest Bretagne Airport (Station ID: 071100), on mainland in Brittany approximately 50 km from Ushant as shown in Figure 6. While the typical hourly solar data for the same location was originally sourced from the International Weather for Energy Calculations (IWEC) data files by ASHRAE (IWEC Weather Files, 2012). The datasets span over the same time range of one year (EnergyPlus, n.d.), however it is not specified which one in particular.

Figure 6: Geographical location of Ushant and the considered weather station (Google Earth Pro, 2017).

Table 1: Geographical coordinates for the weather station and Ushant (System Advisor Model, 2010) (Google Earth Pro, 2017)

	Latitude	Longitude	Altitude
Ushant	48°27'17'' N	5°05'52''W	30m
Brest Weather Station	48°27'00''N	4°25'12''W	103 m

1.2.1 Wind Resource Analysis

The wind dataset includes hourly wind direction and speed recordings at 10m above ground level. These datasets are analysed in Section 1.2.2 and 1.2.3 respectively.

A more accurate analysis could have been carried out if more detailed data was available, such as half-hourly or even 10-minute recordings. Nevertheless, that data is currently not available, consequently the hourly data had to suffice for the scope of this project.

Furthermore, the different geographical location and characteristics between Ushant and the weather station suggest that the analysis may underestimate the actual wind resource on the island. This is due to Ushant being surrounded by the sea, thus receiving direct wind with no obstacles that may slow down the air stream. Conversely, the weather station is located on mainland approximately 25 km from the coast, thus surrounded by several obstacles such as hedgerows and buildings.

1.2.2 Wind Direction Analysis

The recorded direction data is measured in azimuth degrees and approximated to the nearest ten. Below, Figure 7 show the wind rose of the site:

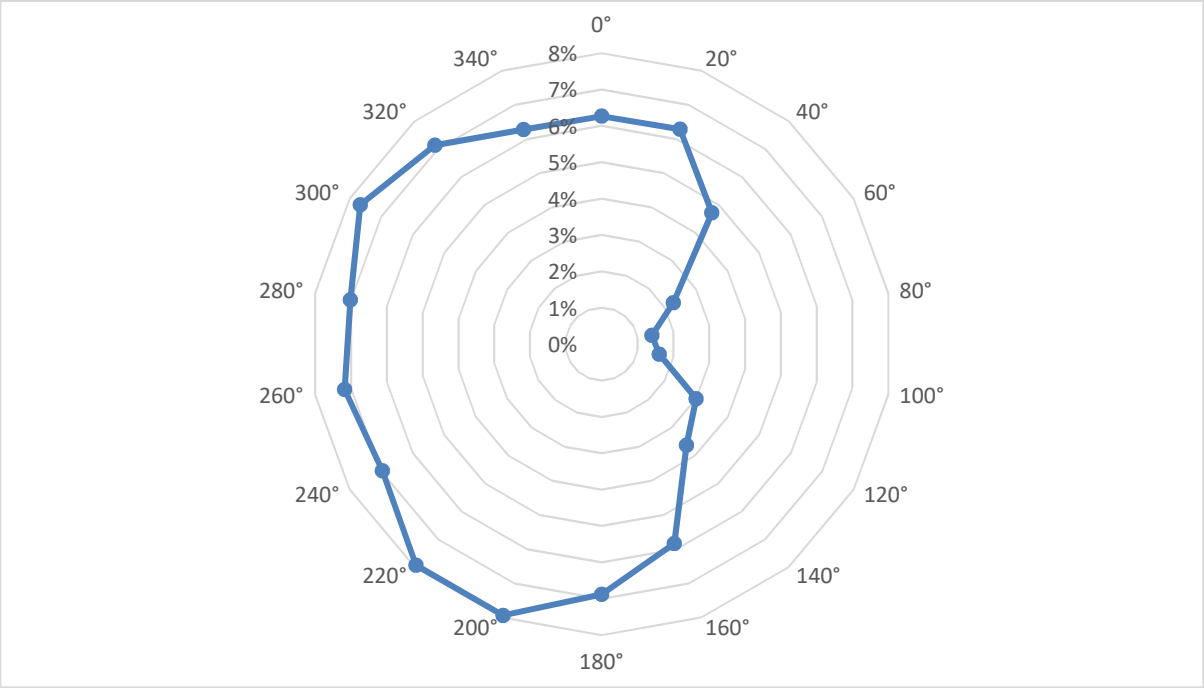

Figure 7: Wind rose for wind resource at Brest Bretagne Airport

As the wind rose shows, the prevailing wind blows from a westerly direction fading out towards north and south. This highlights how the wind typically blows from the Atlantic Ocean thus hitting Ushant at maximum speed. Some key parameters regarding the wind direction are summarised in Table 2.

Table 2: Key parameters for wind direction analysis

Mean	**212°**
Median	230°
Mode	200°-220°
Standard Deviation	104°

It is important to note that 443 of the 8760 wind direction data points were assigned a value of 999°. The reason for this is unknown, however it may be assumed that the cause was a malfunctioning of the recording equipment. Consequently, these values were excluded from the above analysis.

1.2.3 Wind Speed Analysis

Following is an analysis of the wind speed recordings from the weather station, with Table 3 and Figure 8 illustrating the findings. The actual wind speed probability distribution was matched with a Weibull distribution that was calculated on Excel by means of an embedded formula. The Weibull distribution at 10 m above ground level was found to have a shape factor, k, of 1.89, thus indicating a fairly broad wind speed distribution (Homer Energy, n.d.).

Table 3: Wind speed frequency distribution, probability distribution and Weibull distribution

Wind Speed [m/s]	Frequency	Probability [%]	Weibull [%]
0	97	1.1%	0.0%
1	488	5.6%	7.8%
2	225	2.6%	12.9%
3	1427	16.3%	15.4%
4	1425	16.3%	15.5%
5	1288	14.7%	13.8%
6	1150	13.1%	11.2%
7	831	9.5%	8.3%
8	699	8.0%	5.7%
9	558	6.4%	3.7%
10	293	3.3%	2.2%
11	147	1.7%	1.2%
12	67	0.8%	0.6%
13	41	0.5%	0.3%
14	10	0.1%	0.1%
15	11	0.1%	0.1%
16	2	0.0%	0.0%
17	1	0.0%	0.0%
18	0	0.0%	0.0%

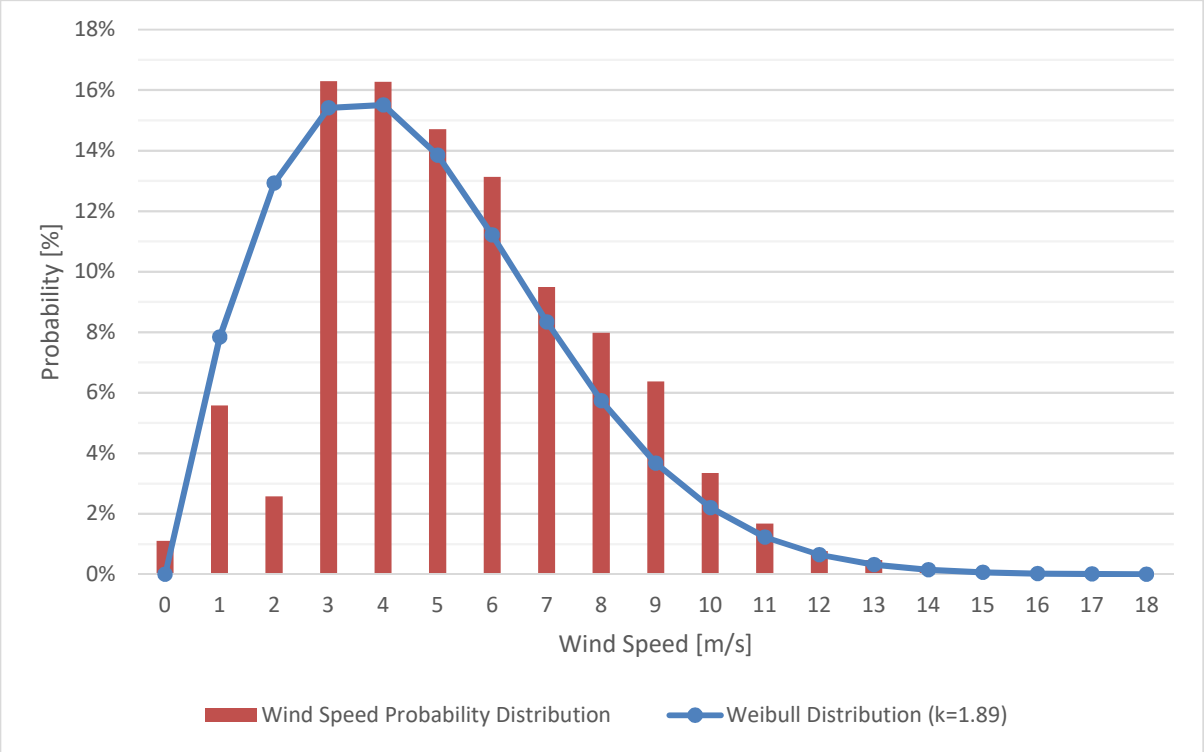

Figure 8: Wind speed probability distribution and Weibull distribution at 10m

Following are some key parameters regarding the wind resource:

Table 4: Key parameters from wind speed analysis

Mean [m/s]	**4.7**
Median [m/s]	4.1
Mode [m/s]	3.1
Standard Deviation [m/s]	2.6

The average hourly wind speed variations per month are illustrated in Figure 9. The average wind speed profile is similar for all months and greater average speeds may be recorded in the central hours of the day, thus approximately between 10am and 6pm.

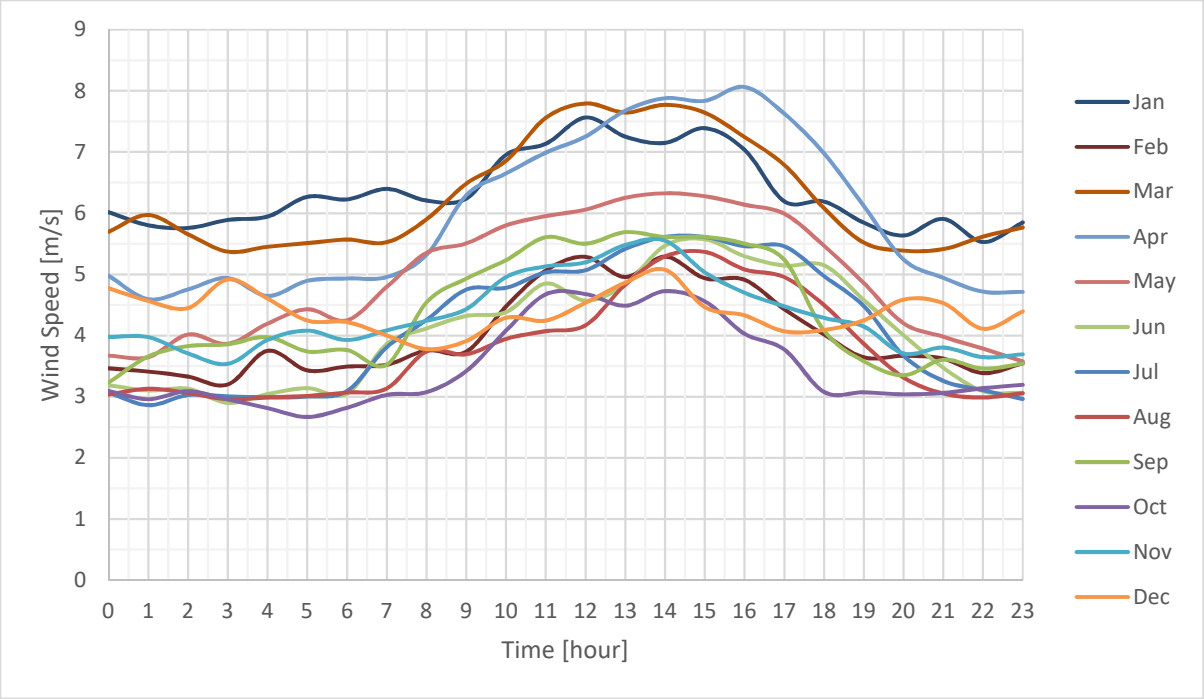

Figure 9: Average hourly wind speed profile per month

Figure 10 displays the monthly variations in average wind speed, highlighting the greater wind resource during winter and spring months, except for February. The wind resource in February may be assumed to be anomalous for the considered year and perhaps it would be in line with the adjacent months if wind recordings from other years were available.

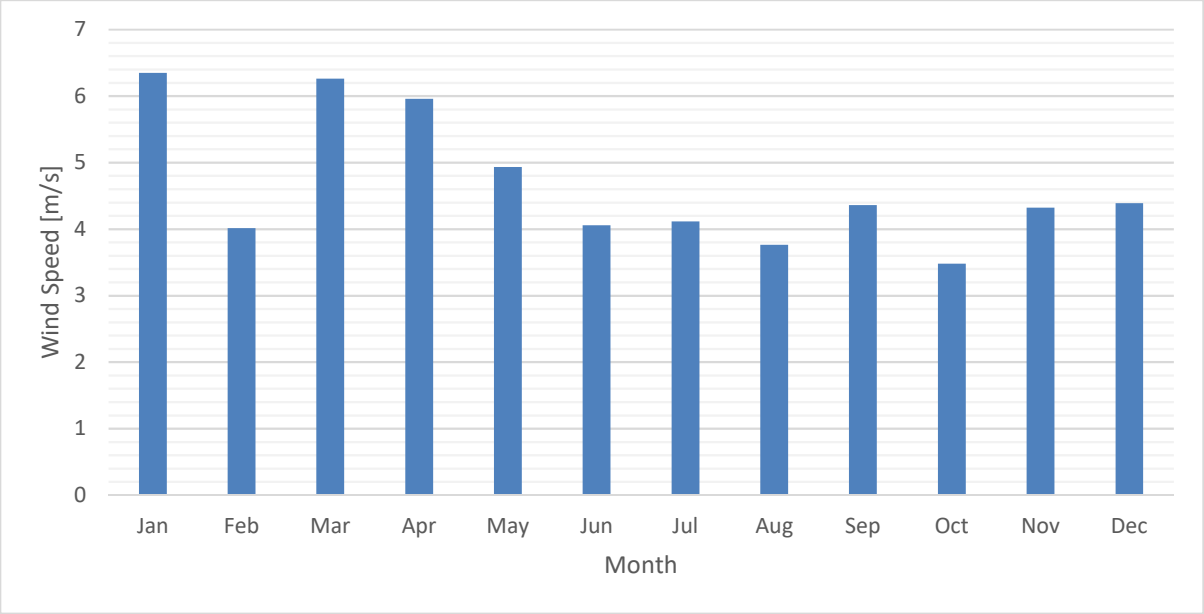

Figure 10: Monthly average wind speed

1.2.4 Solar Resource Analysis

The hourly solar resource was analysed by considering the global solar radiation. This could be calculated with the summation of the available direct beam radiation and the diffuse radiation data (Marion et al., 1992).

Figure 11 shows the average hourly profile for every month highlighting the significantly more intense radiation as well as longer radiation periods during summer.

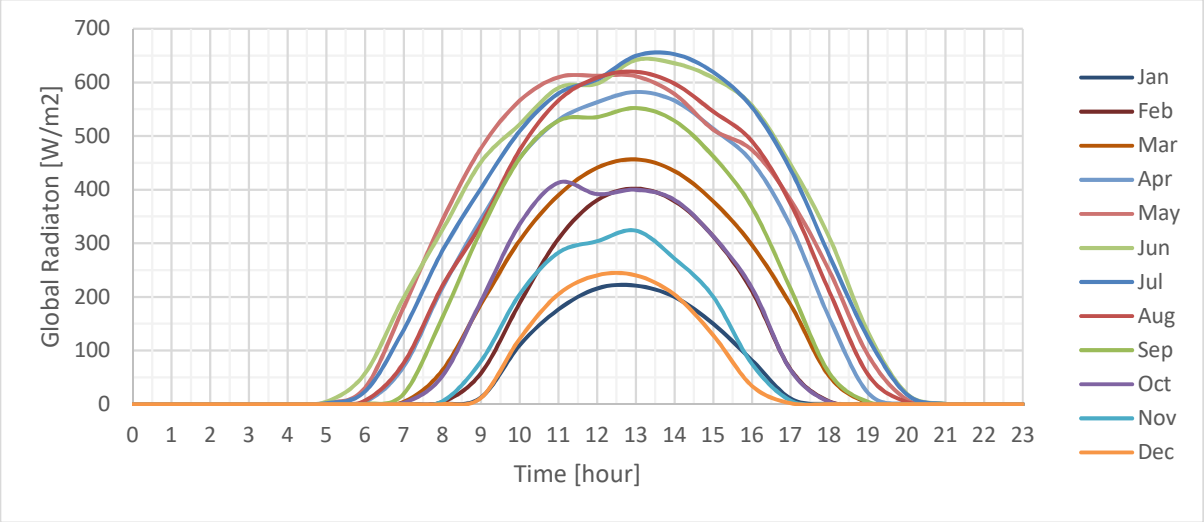

Figure 11: Average hourly global irradiance

Figure 12 shows the average daily sum of global irradiation. The summer months receive a substantial amount of energy with June being the one receiving the greatest and December receiving the least overall radiation respectively.

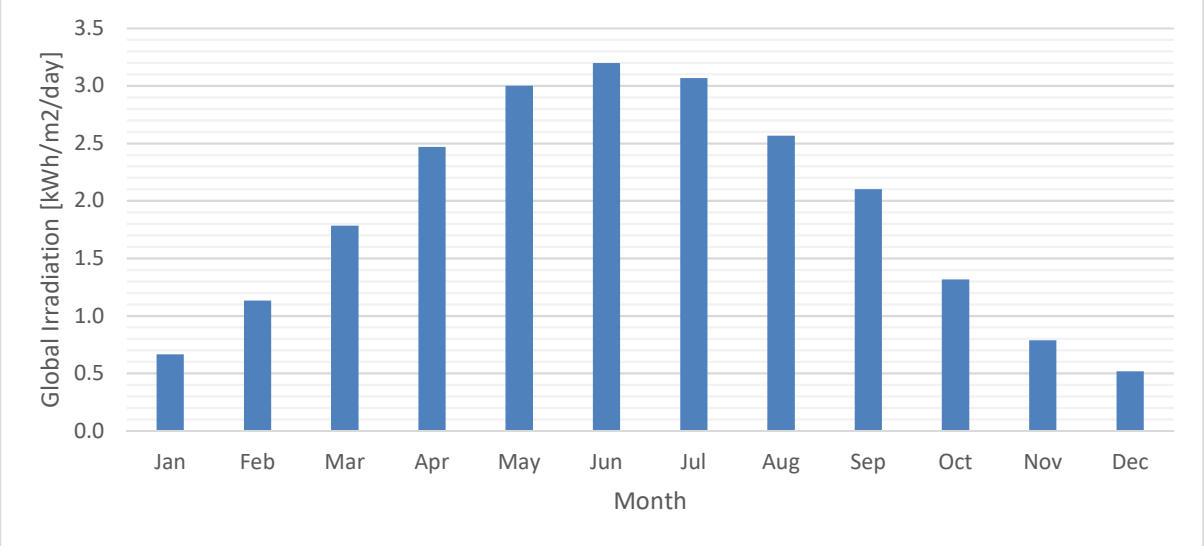

Figure 12: Monthly average daily sum of global horizontal irradiation

1.3 Energy Demand and Renewable Energy Generation Comparison Conclusions

Sections 1.1 and 1.2consist in a detailed analysis of the timely patterns for both the energy demand of Ushant and the regional solar and wind resources. A comparison of the findings can allow a better understanding of how, on average, the generation from renewable energy resources could match the energy demand.

Accounting for the monthly patterns of wind speed, consisting in a greater resource in the winter and spring months, wind power would be suitable for satisfying the demand of the island, that also peaks in the same period. Nevertheless, despite the hourly wind speed peaks in correspondence of the minor daily demand peak, it decreases just before the greater demand peak thus, on average, not following the same trend.

In contrast to the wind resource, the solar resource peaks in the summer months thus not following the monthly energy demand pattern. Similarly to the wind speed, the hourly pattern peaks in the central hours of the day thus covering the minor demand peak. Nevertheless, the second demand peak occurs after sunset, thus preventing the solar resource to directly satisfy the demand.

This first non-detailed analysis shows how renewable energy generation could only partially contribute to satisfying the island's energy demand. In fact, the intermittency of renewable energy resources does not allow them to directly satisfy the demand at all times. Even at high penetration, wind and solar would fully satisfy the demand only at certain times, meaning that when RE generation is low, other solutions to cover the demand need to be implemented. These include energy storage and diesel generators and will be discussed later in the report.

1.4 Renewable Energy Technologies

Solar and wind are the only two renewable energy sources considered for this project. The following sections explain how these resources were implemented into the model according to theoretical principles. The sections also discuss the reasons for the chosen types of generator included in the model and how their characteristics may be adjusted.

1.4.1 Wind Power

A range of different wind turbines were considered in the model to give the user the possibility to choose the most suitable type depending on various aspects. As the wind measurements were recorded at 10 m above ground level, the wind speed dataset needed to be adjusted accordingly to the selected hub height. In fact, wind speed increases with height due to the terrain roughness slowing down the wind passing closer to the ground (Parajuli, 2016). This phenomenon called wind shear is illustrated in Figure 13.

The principles of boundary layer flow, with the log law given in Equation 1, were applied to estimate the wind speed at different heights.

Equation 1 (Ray, Rogers and McGowan, 2006)

$$U(z) = U(z_r)^{\ln(z/z_0)} \Big/ \ln(z_r/z_0)$$

The parameters z and z_r are the selected hub height and reference height (10 m) respectively, with $U(z)$ and $U(z_r)$ their respective wind speeds. z_0 is the surface roughness length, a parameter to indicate the terrain roughness whose definitions from the European Wind Atlas are summarised in Table 5. A roughness length of 0.2 m was estimated for the met mast in Brest due to the high density of tall hedgerows surrounding the site.

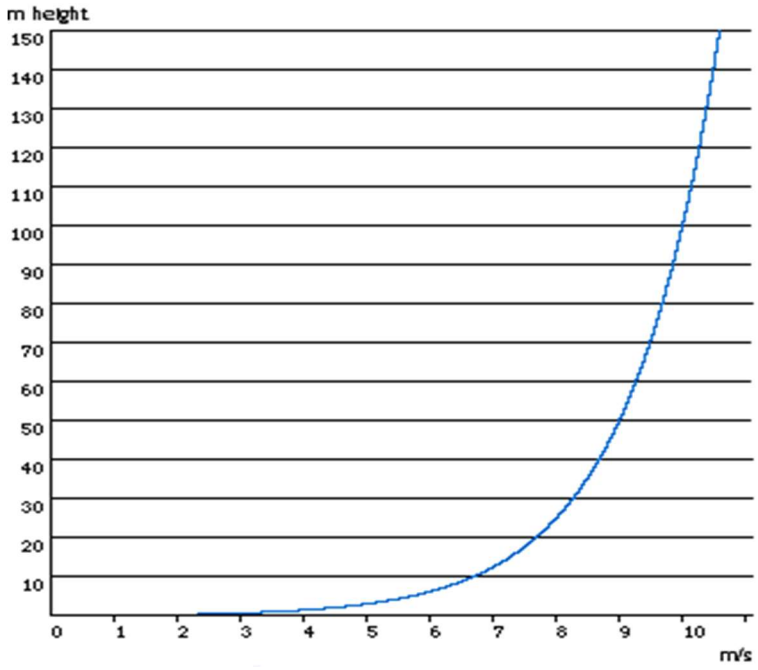

Figure 13: Wind shear profile (Danish Wind Industry Association, 2002)

Table 5: Surface roughness length definitions (Troen and Petersen, 1989)

Roughness Length [m]	Landscape Type
0.0002	Water surface
0.0024	Completely open terrain with a smooth surface
0.03	Open agricultural area with very scattered buildings
0.055	Agricultural land with some houses and tall sheltering hedgerows with a distance of 1250m
0.1	Agricultural land with some houses and tall hedgerows with a distance of 500m
0.2	Agricultural land with many houses, shrubs and plants, or tall hedgerows with a distance of 250 metres
0.4	Villages, small towns, agricultural land with many or tall hedgerows or forests
0.8	Larger cities with tall buildings
1.6	Very large cities with tall buildings and skyscrapers

1.4.1.1 Wind Turbine Selection

The considered turbines were accurately selected accounting for a range of aspects such as availability, manufacturing country and wind resource suitability. In fact, all turbines are currently under production in European countries, furthermore the turbine models were specifically selected with larger rotors for optimum performance in sites with a wind resource classified under IEC class IIIA (V_{avg}=7.5m/s) (Zhang, 2015). This choice accounts for the assumption that the wind resource in Ushant is underestimated in relation to the measurements from Brest.

The wind turbines considered in the model are listed in Table 6 with some key parameters. A range of different power ratings up to 900kW was included so that the most suitable turbine could be considered depending on power output requirements and structure dimension, which strictly affects the impact on the landscape. Furthermore, every turbine has the option to consider different hub heights, allowing, for example, the minimisation of the visual impact with lower towers or the exploitation of higher wind speeds at greater altitudes. The model automatically adjusts the wind speed dataset according to the chosen hub height as explained in Section 1.4.1. Finally, an efficiency of 95% is assumed for all wind generators (Ozdemir, Selamogullari and Elma, 2014).

Table 6: Wind turbine characteristics (Northern Power Systems, 2015) (EWT, 2016a) (EWT, 2016b) (Enercon, 2015) (EWT, 2016c)

	Northern Power 100C-24	EWT 250 DW54	EWT 500 DW54	Enercon E53	EWT 900 DW54
Rated Power [kW]	100	250	500	800	900
Rotor Diameter [m]	24	54	54	53	54
Hub Height [m]	22-29-37	35-40-50-75	35-40-50-75	50-60-73	35-40-50-75
Cut-in Wind Speed [m/s]	3	2.5	2.5	1.5	2.5
Rated Wind Speed [m/s]	12	9	10	13	14
Cut-out Wind Speed [m/s]	25	25	25	28	25

1.4.2 Solar Power

For the scope of this project, the solar PV power output was calculated by means of the "System Advisor Model (SAM)" software. It was assumed that the panels would be more likely to be roof-mounted rather than ground-mounted in order to minimise their environmental impact. Therefore, the tilt was set at 45° in line with the average traditional house roof pitch in the north of France (Davies, 2013) which also approximately corresponds to the optimum solar panels tilt at that latitude.

During the analysis, it was assumed that the arrays would only be installed on roofs within a 135° and 225° azimuth angle, thus approximately facing south for best performance. Consequently, the model allows the user to calibrate the average solar panels azimuth between south-east (135°), direct south (180°) and south-west (225°) depending on the proportion of solar arrays facing each direction.

1.4.2.1 Solar PV Panels Selection

Mono-crystalline, poly-crystalline and thin film are currently the most popular solar PV technologies on the market. These were considered in the model accounting for several intrinsic properties thus resulting in an accurate estimate of their power output.

Table 7: Solar PV technologies characteristics (System Advisor Model, 2010)

	Standard	Premium	Thin Film
Technology	Poly-crystalline	Mono-crystalline	Thin Film
Efficiency	15%	19%	10%
Temperature Coefficient [%/°C]	0.47%	0.35%	0.20%

Despite mono-crystalline panels having greater efficiency, their optimum performance occurs in direct light conditions. Conversely, thin film have a broader spectrum absorption range, thus performing better than crystalline panels in diffused and weak light conditions, for instance during cloudy days (Fthenakis, 2012). Furthermore, the lower temperature coefficient of thin film allows the panels to have lower efficiency degradation in the summer months when the panels can reach temperatures of up to 45°C. This allows the thin film technology to be better suited to Brittany than crystalline panels. In fact, for this specific scenario, their overall generation was calculated to be similar to crystalline panels, although thin film panels are significantly cheaper (Kalogirou, 2014).

1.4.3 Tidal Generation

Tidal stream generation would be a great way to diversify the energy mix of the island thus increasing the probability of meeting the energy demand without the aid of an energy storage system for balancing. However, unfortunately, the generation from the D10 Sabella turbine cannot be considered in this model due to the impossibility of gaining access to the historical generation data from Sabella (Hardwick, 2017). Furthermore, it would be extremely complicated to estimate the generation by simply considering data related to tides or perhaps by considering tidal generation data from other devices deployed in different regions. Nevertheless, the model is designed to allow the user to easily implement the generation from the turbine in case Sabella will release hourly or sub-hurly generation data in the future.

1.5 Energy Storage Technology

Lithium-ion is the energy storage technology suggested for this application due to its great suitability for load and renewable energy generation balancing applications. This is one of the most popular types of batteries and may be considered a reliable solution for meeting the requirements of Ushant. Fast response, deep depth of discharge, high efficiency, long cycle life and their immunity to the memory effect (RegenSW, 2016) (Chen, Gooi and Wang, 2012) are some of the main advantages of lithium-ion batteries and the reason why they would suit this application.

Table 08 shows some key parameters related to the energy storage system (ESS) that have been assumed in order to create a standard scenario. If only a primary analysis was carried out, these parameters may be kept unchanged. Nevertheless, to allow the user maximum flexibility and level of detail, the model was designed so that these parameters may be modified and tailored to the specific case and energy storage technology considered.

Table 08: Key parameters for the energy storage system

Energy Storage System Efficiency (one way)	**95%**
Maximum Depth of Discharge (DOD) Allowed	80%
Energy Storage System Cost [£/kWh]	400

The specified efficiency accounts for the efficiency of both batteries and inverters. Meanwhile, the maximum depth of discharge (DOD) was set at 80% of the battery capacity in order to improve the longevity of the batteries thus maximising their cycle life (Schiffer et al., 2007). The indicated costs are taken from the industry therefore may be considered accurate enough for a primary analysis.

1.6 Methodology

For a realistic estimate of the energy storage optimum capacity, a whole year worth of hourly demand and generation data was considered in order to account for not only daily and weekly variations but also seasonal ones. The hourly datasets were considered as a continuous sequence of recordings rather than as separate 24h or 48h cycles. Subsequently, the adopted approach assumes that the ESS will be charged or discharged whenever a surplus or shortage of RE generation occurs, respectively. In the case that the RE generation and the stored energy in the ESS are not sufficient to cover the load, the existing diesel generators are assumed to be capable of meeting all the remaining demand (Xiao et al., 2014)

1.6.1 Energy Capacity Intervals

Before discussing in detail the adopted methodology, it is required to specify that the following analysis and formulas were applied to a wide range of ESS capacities. In this way, the results may be compared between different ESS capacities in order to evaluate the most suitable configuration.

Table 9 illustrates the energy capacity intervals considered, which vary depending on the capacity range. This is because different levels of accuracy are required for different capacity ranges. In fact, for instance, no ESS with energy capacity over 20MWh would realistically be feasible, which is why only 5MWh intervals are considered. However the capacity would still be considered in the analysis in order to give an approximate value for optimum size if it happened to be over 20MWh. Conversely, if the optimum capacity was below 10MWh, then more accuracy would be required as an ESS of that capacity could actually be feasible. This decision was made to minimise the number of intervals thus reducing the number of data points on the Excel spreadsheet.

Table 9: ESS energy capacity intervals considered for estimate of optimum size

Range	Intervals
0 – 500kWh	100 kWh
500 kWh – 10 MWh	500 kWh
10 MWh – 20 MWh	1 MWh
20 MWh – 50 MWh	10 MWh

1.6.2 Energy Capacity Sizing Methodology

Following is a technical explanation of the adopted methodology with a discussion of the formulas implemented into the program.

The adopted methodology is based on Equation 2, Equation 3 and Equation 4. These functions aid at determining the hourly uncovered demand, excess generation and the state of charge (SOC) of the ESS. The **uncovered demand** consists in the demand that neither the RE generation (sum of wind and solar generation) nor the ESS discharge are capable of balancing. This consequently means that the ESS is at minimum charge. Therefore, the uncovered demand consists in the energy demand that needs to be met by diesel generation. Whereas, the **excess generation** consists in that surplus RE generation that can not be stored in the ESS due to it being already at maximum charge. As a result, this generation will need to be dissipated through a dump load.

Following is an explanation of the three formulas and the parameters included:

If *Load(t) > RE Generation(t)*:

Equation 2

$$\begin{cases} SOC(t+1) + \boldsymbol{Uncovered\ Demand}(t+1) + \gamma = SOC(t) + [RE\ Generation(t) - Load(t)] \\ SOC_{min} \leq SOC \leq SOC_{max} \\ 0 \leq t \leq 8760 \\ SOC(t) = SOC_{max} \qquad t = 0 \end{cases}$$

Therefore, if *Uncovered Demand ≠ 0* then $SOC(t+1) = SOC_{min}$.

If *RE Generation(t) > Load(t)*:

Equation 3

$$\begin{cases} SOC(t+1) + \boldsymbol{Excess\ RE\ Generation}(t+1) + \gamma\ = SOC(t) + [RE\ Generation(t) - Load(t)] \\ SOC_{min} \leq SOC \leq SOC_{max} \\ 0 \leq t \leq 8760 \\ SOC(t) = SOC_{max} \qquad t = 0 \end{cases}$$

Therefore, if *Excess Generation ≠ 0* then $SOC(t+1) = SOC_{max}$.

If *RE Generation(t) = Load(t)*:

Equation 4

$$\begin{cases} SOC(t+1) = SOC(t) + [RE\ Generation(t) - Load(t)] \\ SOC_{min} \leq SOC \leq SOC_{max} \\ 0 \leq t \leq 8760 \\ SOC(t) = SOC_{max} \qquad t = 0 \end{cases}$$

Therefore, no excess generation or uncovered demand would be recorded. Moreover, the SOC of the ESS would be unchanged over the two consecutive hours.

Where:

- γ represents the energy losses due to the efficiency of the ESS when charging or discharging. The ESS efficiency may be either the standard configuration value of 95% (one-way), as explained in Section 1.5 and shown in Table 08, or a specific value chosen by the user;

- *SOC* is the state of charge of the battery in kWh, whose maximum value is SOC_{max} (100% charge), equal to its energy capacity, and minimum value is SOC_{min}. The latter strictly depends on the chosen DOD, as shown in Equation 5:

Equation 5

$$SOC_{min} = Battery\ Capacity\ \times\ (1 - DOD)$$

Where the *DOD* may be either the standard configuration value, 80%, as explained in Section 1.5 and shown in Table 08, or a specific value chosen by the user;

- *t* is time divided into hours, from the start of the year, hour *0*, to the end of the year, hour *8760*;

- The ESS is also assumed to be fully charged at the start of the dataset. This is just an assumption that was arbitrarily made and, in the same way, the ESS could be assumed to be fully discharged (SOC_{min}) at *t=0*.

The above equations may then be modified into the summations in Equation 6 and Equation 7 to calculate the yearly total values for uncovered demand and excess RE generation respectively.

If *Load(t) > RE Generation(t)*:

Equation 6

$$\boldsymbol{Yearly\ Total\ Uncovered\ Demand}\ [\boldsymbol{MWh}] = \sum_{t=0}^{8760} \begin{cases} SOC(t) + [RE\ Generation(t) - Load(t)] - SOC(t+1) - \gamma \\ SOC_{min} \leq SOC \leq SOC_{max} \\ SOC(t) = SOC_{max} \qquad t = 0 \end{cases}$$

If *RE Generation(t) > Load(t)*:

Equation 7

$$\boldsymbol{Yearly\ Total\ Excess\ RE\ Generation}\ [\boldsymbol{MWh}] = \sum_{t=0}^{8760} \begin{cases} SOC(t) + [RE\ Generation(t) - Load(t)] - SOC(t+1) - \gamma \\ SOC_{min} \leq SOC \leq SOC_{max} \\ SOC(t) = SOC_{max} \qquad t = 0 \end{cases}$$

The results from Equation 6 and Equation 7 are then compared to the yearly values for total demand and total RE generation respectively, thus determining their percentage values with respect to the total.

As it may be understood, the greater the energy capacity of the ESS, the greater the amount of excess RE generation that can be stored thus allowing more uncovered demand to be satisfied. Nevertheless, there will not always necessarily be enough excess generation to meet all the uncovered demand or enough uncovered demand to use up all the excess generation.

Consequently, due to the significant number of scenarios that may be created by varying the RE mix, and the range of goals that the user may be trying to achieve, it was decided to design the model so that it would output different optimum energy capacities in relation to a diverse variety of objectives. These objectives and the final results are discussed in Section 1.7.

1.6.3 Power Rating Sizing

For this project, the power rating of the ESS is simply sized in order to cover most of the net power demand. It was estimated that the power rating should cover approximately 90% of the net power demand. The power rating was calculated by grouping the net power demand into bins and then calculating their probability of occurrence. Subsequently, this allowed the calculation of the cumulative sum of the hourly net power demand probability of occurrence, thus the power rating would be in correspondence to the 90th percentile.

The energy for each energy capacity that the power rating can not cover is actually much lower than 10% of the total stored energy due to the batteries being for a proportion of the time at maximum or

minimum charge, thus not charging or discharging. Consequently, the power that the inverters may not cover leads to a minor amount of uncovered energy compared to the total thus may be assumed to be negligible for the rest of the calculations in the program.

1.7 Energy Capacity Results

Once the yearly uncovered energy demand and excess generation are calculated for the whole range of ESS capacities, the results may be utilised to find the optimum energy capacity. The model was designed to output five different energy storage capacities in relation to five different targets that the user may want to achieve. However, depending on the set input values relative to the RE generation, some of these may not be achievable. Following is an explanation of the considered objectives and what kind of scenarios they are more suitable for:

- 70% of demand met by renewable energy generation:
  Ushant is currently planning to achieve 70% of RE generation by 2020. The specified ESS capacity would allow the storage and supply of sufficient RE generation to meet 70% of the total demand.
  The achievement of this objective requires the total RE generation to be equal or greater to 70% of the total demand. Moreover, a diverse generation mix with high RE penetration may allow the objective to be achieved with a more economically feasible ESS;

- 100% of demand met by renewable energy generation:
  Ushant is planning to be fully powered by RE by 2030. The indicated ESS capacity would allow the storage and supply of all the energy required to meet the island's remaining demand.
  This objective requires a minimum total RE generation equal to the total demand. Furthermore, similarly to the previous objective, a diverse energy mix with high RE penetration may allow a more economically feasible ESS;

- 100% excess generation usage:
  This objective aims at storing and supplying all the yearly excess RE generation. Consequently, the total RE generation is required to be equal or lower than the total demand. This objective makes the most of the cheap electricity from RE in comparison to the diesel generators.
  In contrast to the two previous objectives, this is more suitable for low RE penetration scenarios, thus achievable with a smaller and more economically feasible ESS;

- 30% excess generation usage:
  Similarly to the previous objective, this targets the excess RE generation. However, in this case, only 30% of the excess generation is required to be stored and re-delivered. Therefore, for this objective to be achievable, the uncovered demand needs to be greater than 30% of the excess RE generation.
  Conversely to the previous objective, this may also be suitable for scenarios with a higher penetration of RE generation.

- Maximum Net Present Value (NPV):

This is the only financially orientated objective within the model and perhaps the most valuable one as it considers the monetary benefit of the ESS over time. In fact, despite the significant capital cost of energy storage, a further reduction in uncovered demand by storing and re-dispatching RE may lead to substantial savings on diesel generation.

Consequently, this objective aids at finding the ESS capacity, within the considered range of energy capacities, with the maximum NPV (lowest net present cost). The NPV is calculated by considering the capital cost of energy storage, estimated at 400£/kWh as shown in Table 08 (this figure may be modified by the user), and the yearly expenditure on diesel generation to meet the remaining uncovered demand.

The calculation assumes an inflation rate of 2.5% and a discount rate of 7%, however these parameters may be adjusted by the user depending on specific requirements. Furthermore, the ESS is assumed to have a lifespan of 20 years.

1.8 Case Study

This section considers a case study to explain in detail the structure of the program and the adopted strategies to clearly present the results and to perhaps allow the user to carry out a further analysis. In this case, renewable energy generation scenario 3 from Task 1.4 is considered. Under this scenario wind turbines with total power rating of 2 MW, and PV arrays with a total power rating of 1.8 MW are considered.

It is crucial to mention that the program is designed to only require the initial user's input information in regards to the RE technologies and the energy storage system. In fact, once this information has been input, the model automatically goes through all the required calculations to output the desired results and present them on suitable graphs.

Initially, the user is required to input the desired specifications related to the RE technologies as shown in Figure 14. As Figure 15 demonstrates, the information may be input through drop down lists in order to give to the user multiple clear options.

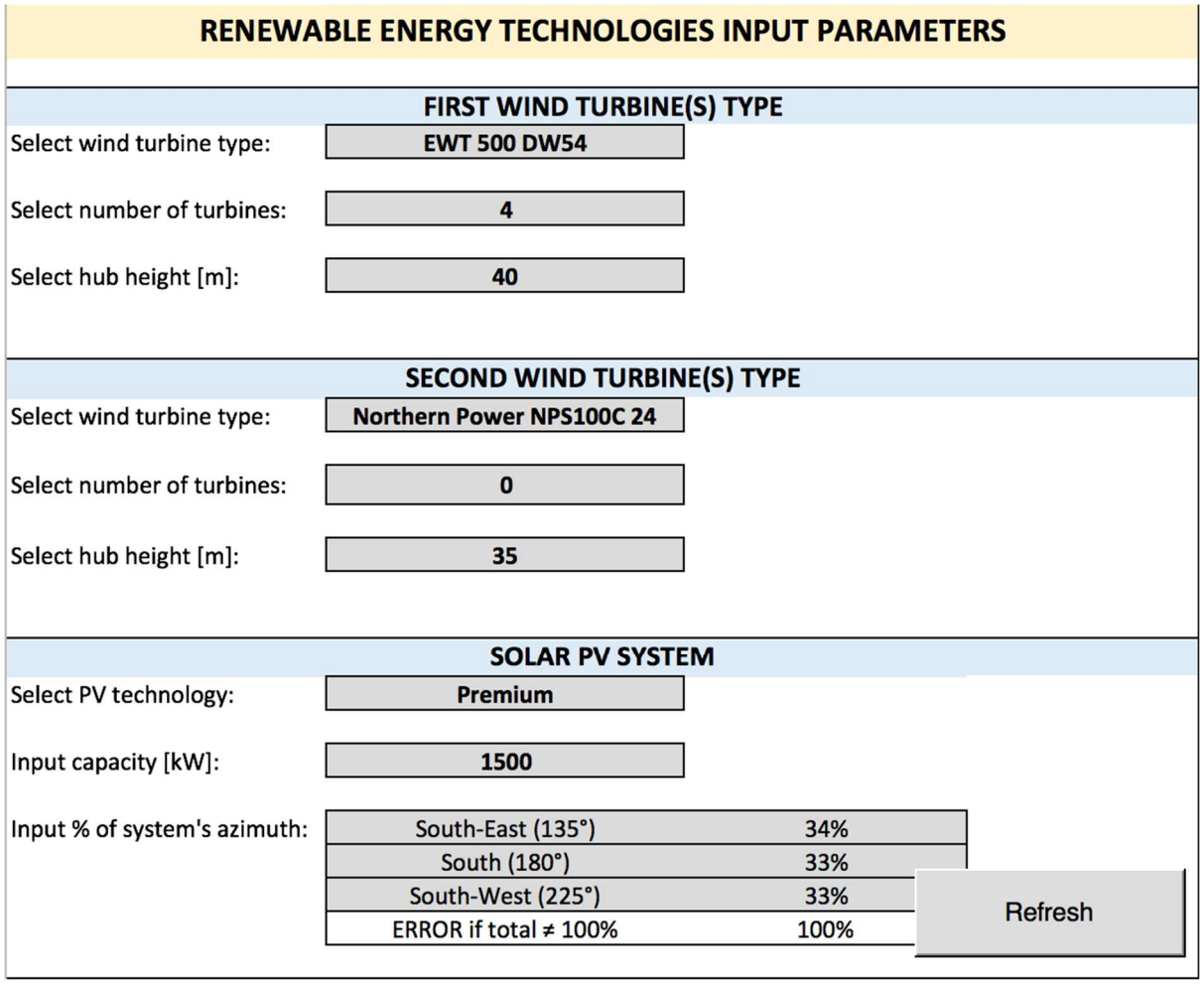

Figure 14: Screenshot of program window showing input parameters in relation to the RE technologies

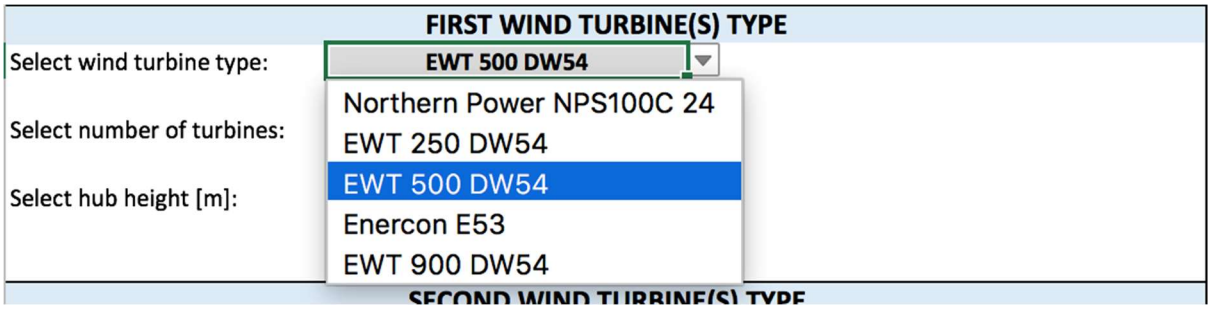

Figure 15: Screenshot of drop-down list to choose the wind turbine type

This case study will consider the generation from four EWT 500kW wind turbines with a hub height of 40m and a total solar PV capacity of 1.5MW. This assumes mono-crystalline to be the most popular technology and the installations to be evenly distributed between azimuths of South-West, South and South-East.

Once the RE technologies input parameters have been set, the program automatically calculates the hourly generation data for the chosen devices over one year following the principles explained in Section 1.2. The hourly generation is then subtracted from the hourly demand highlighting in red and green when there is a shortage ad an excess of RE generation respectively. A 24h section of the Excel table summarising the hourly and generation data is shown in Figure 16 and Figure 17 (the figures had to be split to be included into the report, however the tool shows the data on the same level).

TIME			RENEWABLE ENERGY GENERATION		
			WIND		
Month	Day	Hour	First Turbine(s) Power Out [kW]	Second Turbine(s) Power Out [kW]	Turbine(s) Tot Power Output [kW]
1	1	0	151	0	151
1	1	1	52	0	52
1	1	2	151	0	151
1	1	3	52	0	52
1	1	4	151	0	151
1	1	5	257	0	257
1	1	6	151	0	151
1	1	7	626	0	626
1	1	8	881	0	881
1	1	9	881	0	881
1	1	10	1850	0	1850
1	1	11	1480	0	1480
1	1	12	1900	0	1900
1	1	13	881	0	881
1	1	14	1900	0	1900
1	1	15	1480	0	1480
1	1	16	1850	0	1850
1	1	17	881	0	881
1	1	18	1850	0	1850
1	1	19	1214	0	1214
1	1	20	1480	0	1480
1	1	21	1900	0	1900
1	1	22	1900	0	1900
1	1	23	1900	0	1900

Figure 16: Screenshot of a 24h section for the hourly wind and solar generation and demand data

		DEMAND	
SOLAR	TOTAL		
Solar PV Power Out [kW]	Total RE Generation [kW]	AVG Power Demand [kW]	Dem - RE Gen [kW]
0	151	1409	1258
0	52	1275	1222
0	151	1189	1038
0	52	1132	1079
0	151	1098	947
0	257	1087	830
0	151	1097	946
0	626	1131	504
0	881	1194	313
0	881	1278	397
16	1866	1340	-526
42	1522	1369	-152
58	1958	1344	-614
63	944	1287	343
53	1953	1243	-710
33	1514	1208	-306
34	1884	1209	-675
0	881	1280	399
0	1850	1371	-479
0	1214	1400	186
0	1480	1473	-8
0	1900	1599	-301
0	1900	1541	-359
0	1900	1368	-532

Figure 17: Screenshot of a 24h section for the hourly wind and solar generation and demand data

The hourly data for one year from Figure 16 and Figure 17 is then averaged over one day in order to produce Figure 18, which shows the profiles for RE generation, demand and net power (Demand minus RE Generation) for the average day. The curve describing the net power profile assumes positive or negative values when there is a shortage or a surplus of RE generation respectively.

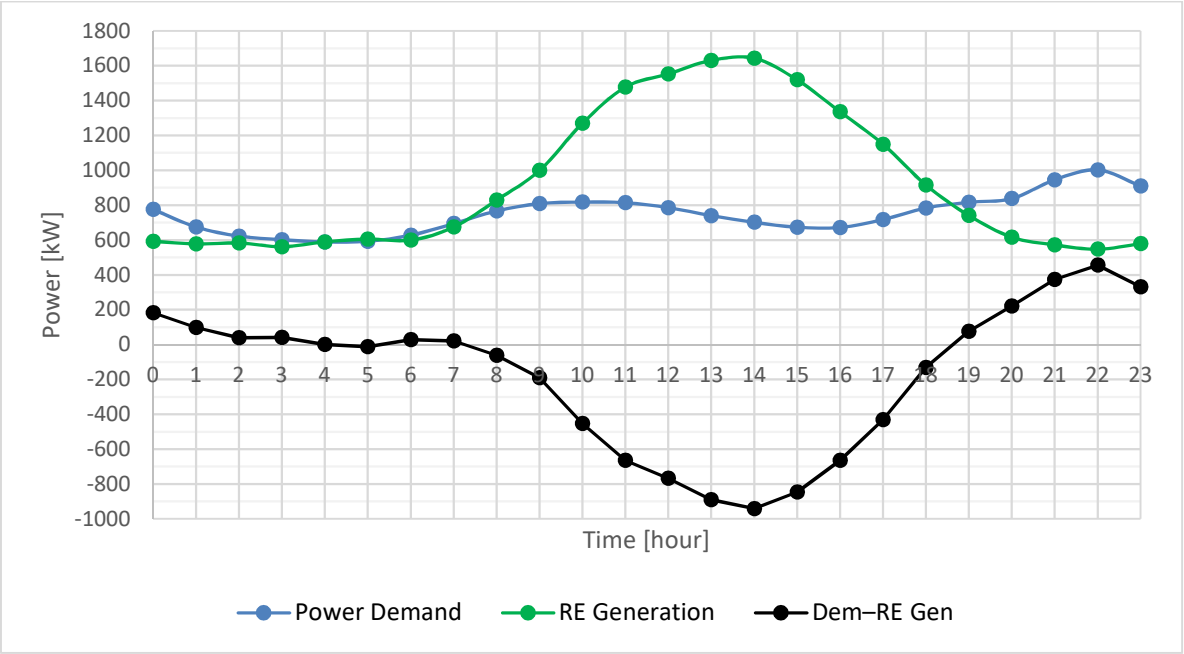

Figure 18: Hourly average RE generation, demand and net power profile for one day

The hourly generation and demand data is then utilised to calculate the total yearly generation and demand data from Figure 19. This figure also shows the approximate amount of uncovered demand and excess generation if no ESS was installed.

GENERATION KEY RESULTS			
	Tot Capacity [kW]	Tot Gen [MWh/year]	Capacity Factor
First Wind Turbine(s)	2000	6708	38%
Second Wind Turbine(s)	0	0	0%
Solar PV System	1500	1379	10%

GENERATION & DEMAND DATA RESULTS			
Tot Gen [MWh]	8087		
Excess Gen [MWh]	3850	% Excess Gen	48%
Tot Dem [MWh]	6559		
Uncovered Dem [MWh]	2321	% Uncovered Dem	35%

Figure 19: Screenshot of key generation results

The results from Figure 19 are then plotted on a bar chart, as in Figure 20, for a better visual understanding of how generation compares to the demand.

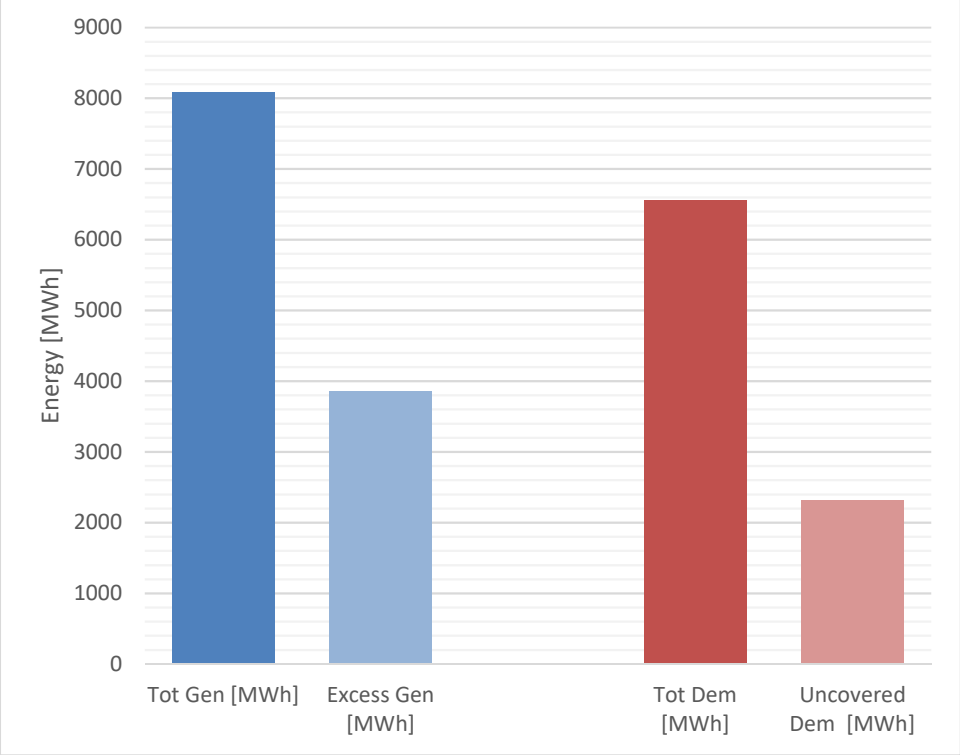

Figure 20: Total yearly values in MWh for RE generation, excess generation, demand and uncovered demand

At this point, the ESS comes into place and, as explained in Section 1.5, its main characteristics need to be specified unless the standard configuration parameters are suitable for the considered scenario. Figure 21 is the section of the program where the user may modify the ESS parameters.

ENERGY STORAGE SYSTEM INPUT PARAMETERS	
ESS Efficiency (one way)	95%
Minimum Battery Charge	20%
ESS Cost [£/kWh]	400

Figure 21: Standard configuration parameters for the ESS that may be modified by the user

Subsequently, the hourly net power data from Figure 17 is input into Equation 2, Equation 3 and Equation 4 to calculate the hourly SOC of the ESS throughout the year for every energy capacity considered (energy capacity intervals shown in Table 9). The SOC hourly results are then visually represented in an Excel table as shown in Figure 22.

		Energy capcities in kWh							
hour	Gen-Dem [kWh]	100	200	300	400	500	1000	1500	2000
0	-1258	20	40	60	80	100	200	300	676
1	-1222	20	40	60	80	100	200	300	400
2	-1038	20	40	60	80	100	200	300	400
3	-1079	20	40	60	80	100	200	300	400
4	-947	20	40	60	80	100	200	300	400
5	-830	20	40	60	80	100	200	300	400
6	-946	20	40	60	80	100	200	300	400
7	-504	20	40	60	80	100	200	300	400
8	-313	20	40	60	80	100	200	300	400
9	-397	20	40	60	80	100	200	300	400
10	526	100	200	300	400	500	700	800	900
11	152	100	200	300	400	500	844	944	1044
12	614	100	200	300	400	500	1000	1500	1628
13	-343	20	40	60	80	139	639	1139	1267
14	710	100	200	300	400	500	1000	1500	1941
15	306	100	200	300	400	500	1000	1500	2000
16	675	100	200	300	400	500	1000	1500	2000
17	-399	20	40	60	80	80	580	1080	1580
18	479	100	200	300	400	500	1000	1500	2000
19	-186	20	40	104	204	304	804	1304	1804
20	8	27	47	111	211	311	811	1311	1811
21	301	100	200	300	400	500	1000	1500	2000
22	359	100	200	300	400	500	1000	1500	2000
23	532	100	200	300	400	500	1000	1500	2000

Figure 22: Screenshot of a 24h section up to 2MWh of the matrix representing the hourly SOC, considering arbitrary values for RE generation, and highlighting minimum and maximum charge

As previously explained, the net power is highlighted in red or green when there is a shortage or a surplus in RE generation, therefore when the ESS is delivering or absorbing power respectively. The SOC is also coloured in green and red indicating when the battery is at maximum and minimum charge, therefore when there happen to be excess RE generation and uncovered demand respectively. Consequently, for every energy capacity, green indicates when RE generation is wasted and red when the diesel generators come into work.

This visual representation allows the user to easily understand how frequently excess generation and uncovered demand occur with respect to different energy capacities. Furthermore, their timely variations throughout the year may be visualised by scrolling down the table.

Using the data from the Excel table represented in Figure 22, the program calculates, for every energy capacity, the yearly results for total uncovered demand (MWh) and total excess generation (MWh) alongside their percentage value in relation to the total demand and total RE generation respectively. These results are then organised in a table, Figure 23, and plotted on a graph, Figure 24, to visually illustrate their variation with changing ESS size.

Storage Capacity	0	100	200	300	400	500	1000	1500	2000
Uncovered Energy Dem [MWh]	2278	2273	2264	2250	2231	2208	2099	2015	1932
Excess Gen [MWh]	4159	4155	4144	4133	4118	4104	4008	3916	3831
Energy Covered by ESS [MWh]	0	4	13	27	47	69	179	263	346
Uncovered Energy Dem [%]	35%	35%	35%	34%	34%	34%	32%	31%	29%
Excess Gen [%]	49%	49%	49%	49%	49%	49%	47%	46%	45%

Figure 23: Screenshot of the section of a table from the model indicating the effect of different ESS energy capacities on the uncovered demand and excess generation

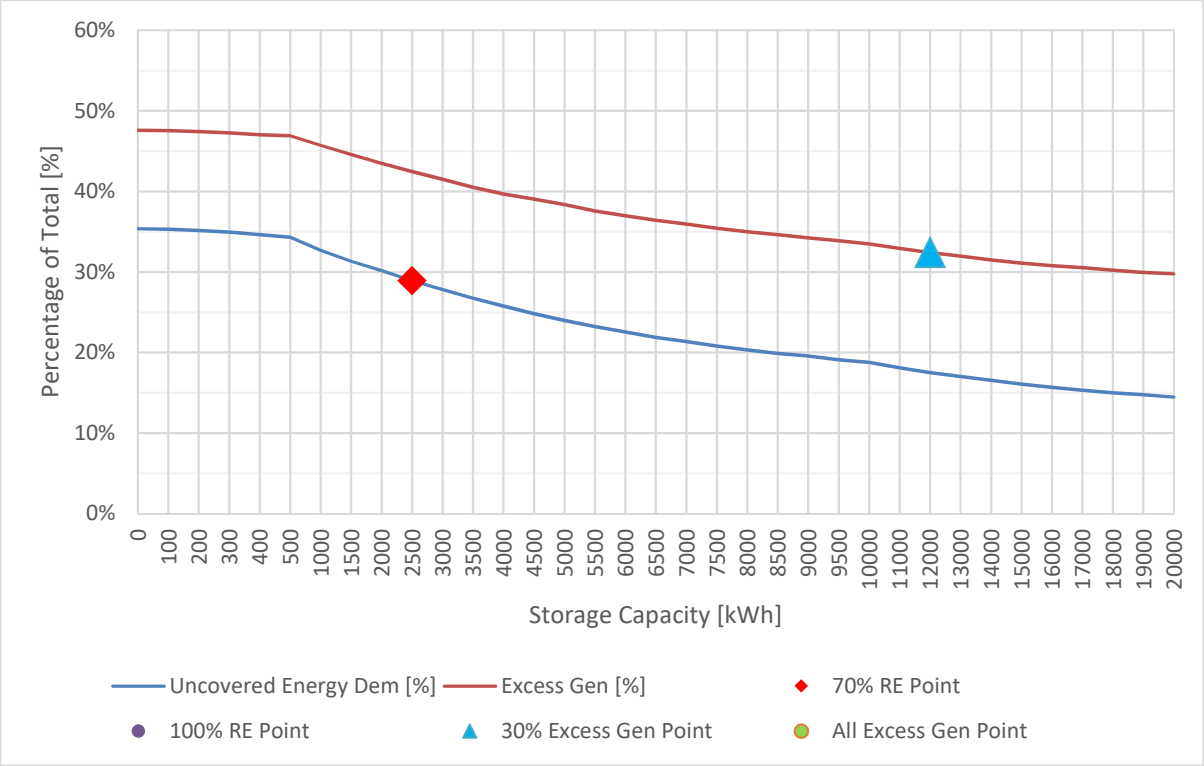

Figure 24: Percentage values for uncovered energy demand and excess generation for energy capacities up to 20MWh

Finally, the NPV for every energy capacity is calculated as explained in Section 1.7, considering the cost of energy storage and the yearly expenditure on diesel generation over 20 years. The model allows the user to adjust the standard configuration parameters in Figure 25 to meet specific requirements.

FINANCIAL PARAMETERS FOR NPV	
Diesel Generation Cost [£/kWh]	0.35
Discount Rate	7%
Inflation Rate	2.5%

Figure 25: Standard configuration parameters for the calculation of the NPV that may be modified by the user

Once the financial parameters are set, the model calculates the discounted cash flow over 20 years for all energy capacities and plots the costs and NPVs on a graph, Figure 26. The diesel generation expenditure needed to be plotted on a secondary axis with a different scale due to its values being too small when compared to the NPVs or energy storage costs. Figure 26 also highlights the maximum NPV recorded, that in this case corresponds to an energy capacity of 7 MWh.

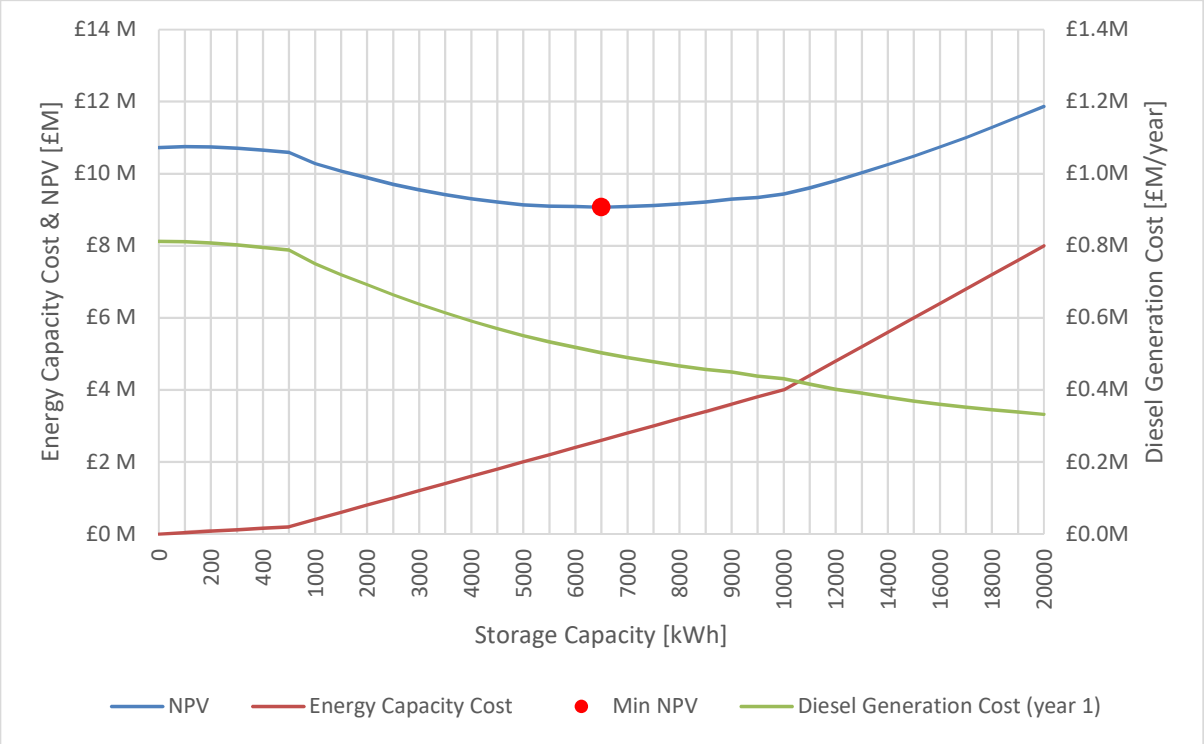

Figure 26: NPV, energy capacity cost and diesel generation expenditure in year one for energy capacities up to 20MWh

In Section 1.7, it was explained that the model calculates the optimum energy capacity for five different objectives. Figure 27 shows the optimum capacities for the considered scenario.

OPTIMUM ENERGY CAPACITY RESULTS	
70% RE Supply [kWh]	2500
100% RE Supply [kWh]	Over 50MWh
100% Excess Gen Usage [kWh]	Not Achievable
30% Excess Gen Usage [kWh]	12000
Minimum NPV [kWh]	6500

Figure 27: Optimum energy capacity results for the five different objectives

Furthermore, both Figure 25 and Figure 26 highlight the optimum energy capacity point on the respective curves when they are within the 50MWh limit.

In this case, the "100% excess generation usage" target is not achievable due to the total RE generation being greater than the total demand, as it can be clearly seen from Figure 20.

1.9 Power Rating Sizing

For the sizing of the power rating the cumulative sum of the net power demand probability was calculated and the probability data organised into a table. This is then plotted on a graph as shown in Figure 28. The cumulative sum of probability curve then allows to determine its 90th percentile which in this case corresponds to a power rating of about 1.1 MW.

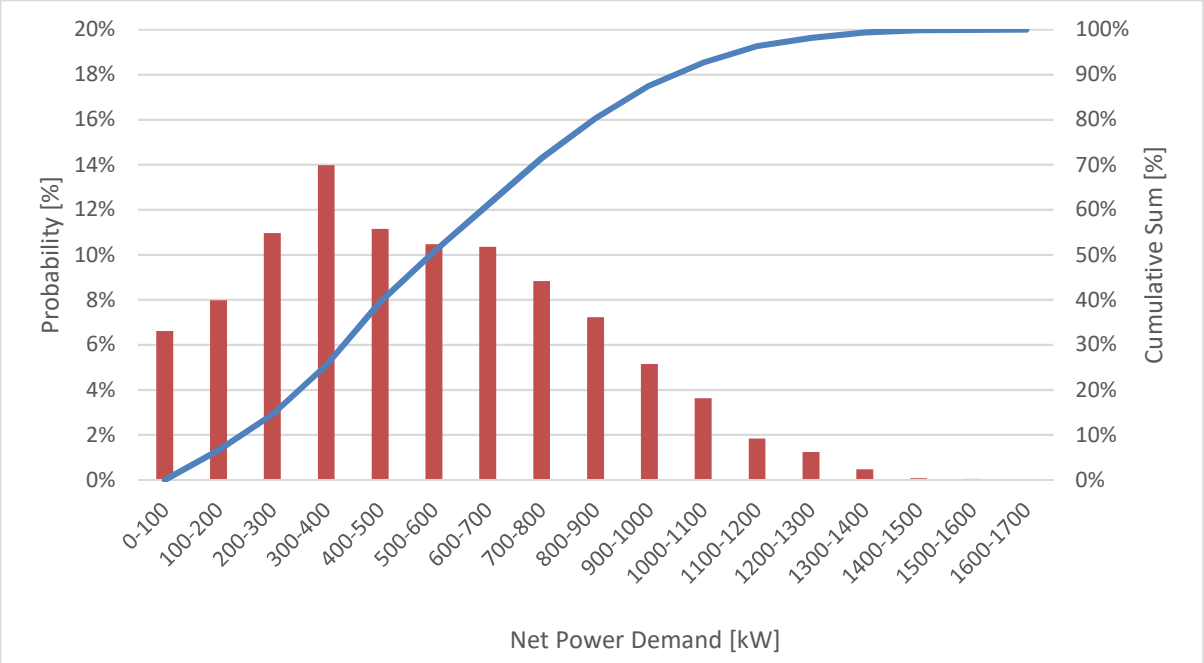

Figure 28: Optimum energy capacity results for the five different objectives

1.10 Energy Management

In this section, main challenges with energy management will be investigated while considering one of the renewable energy generation scenarios proposed in Task report 1.4. In this scenario, 2 MW wind generation, and 1.8 MW PV generation are considered. Using this scenario along with the weather forecast for 2016 and the averaged load demand profile, the annual energy balance will be as shown in Figure.29. In this figure, the deficit represents the uncovered energy that must be supplied by diesel generators, and the surplus represents the energy that exceeded the demand and had to be curtailed. Considering an average annual generation of 6.6 GWh, the renewable energy generation would supplie about 65% of the total annual demand.

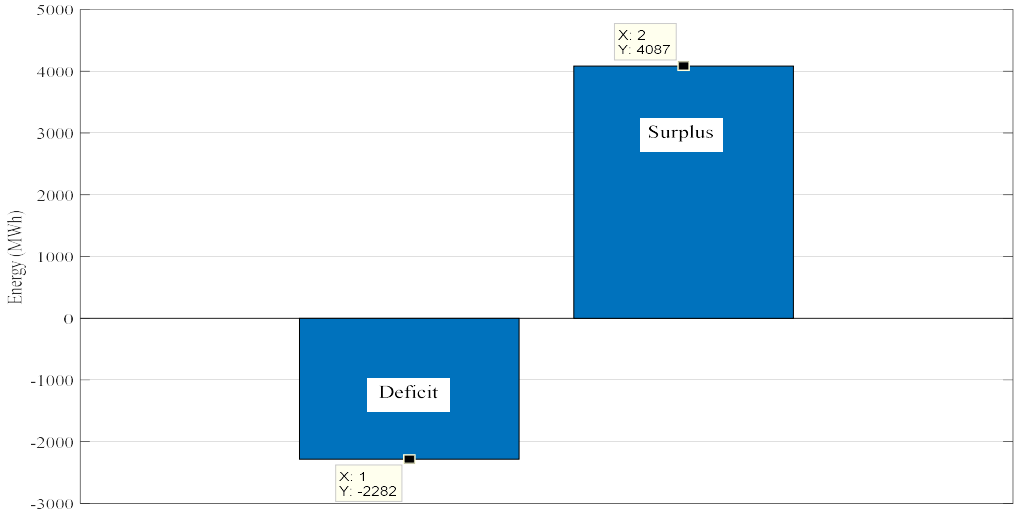

Figure 29: Energy balance when deploying 2 MW wind generation, and 1.8 PV generation.

To reach the first goal of 70% renewable energy generation, a battery storage system is considered to make use of some of the surplus renewable energy to meet the demand. According to the battery sizing tool, a 2 MWh battery is required to meet the 70% renewable generation goal. Deploying this battery will result in the energy balance profile shown in Figure 30. As can be seen from this figure, the battery storage results in 246 MWh saving, and 71.7% renewable energy generation.

Even though the first goal has been achieved; however, it still results in a considerable amount of surplus energy that is wasted. To investigate the reason for this inefficient utilization of renewable energy, the generation/demand profile for the first five days in January 2016 is shown in Figure 31. This figure shows a great disparity between generation and demand from day to day. On the other hand, the 2 MWh battery contribution to the energy balance is limited to 2-3 hours due to the high hourly load in winter months.

In addition, there is a seasonal disparity in generation/demand as can be noticed in Figure 32, which shows the generation/demand profile for 5 days in June as an example for summer days.

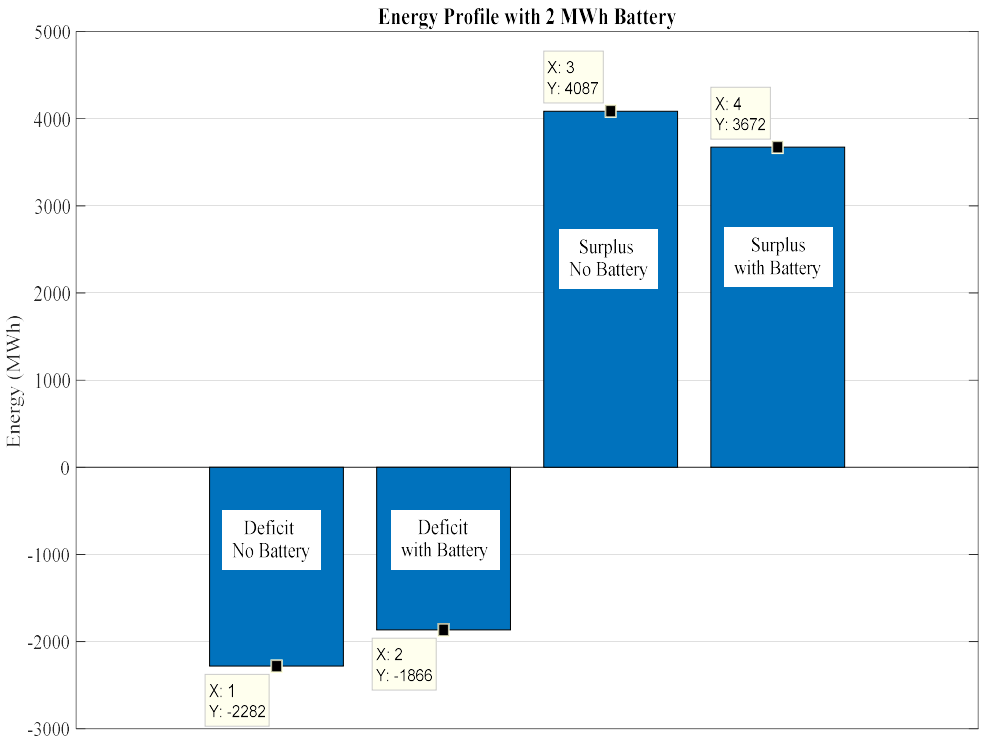

Figure 30: Annual energy balance profile when deploying 2 MW wind generation, 1.8 PV generation, and a 2 MWh battery.

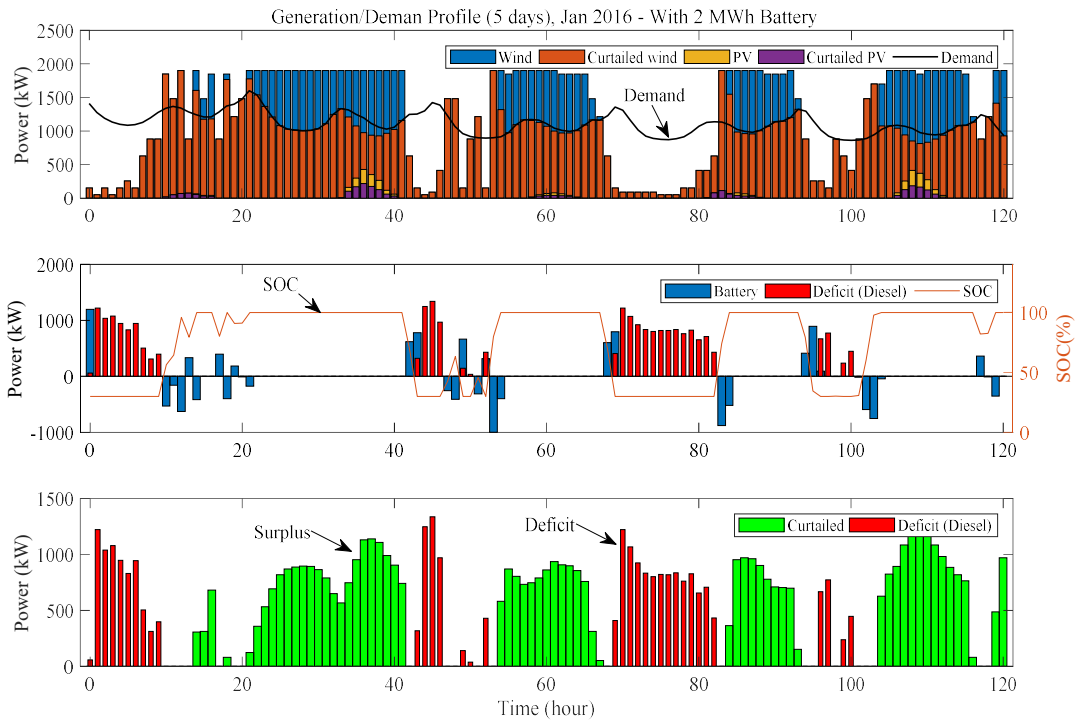

Figure 31: Generation/demand profile on Jan 1-5, 2016.

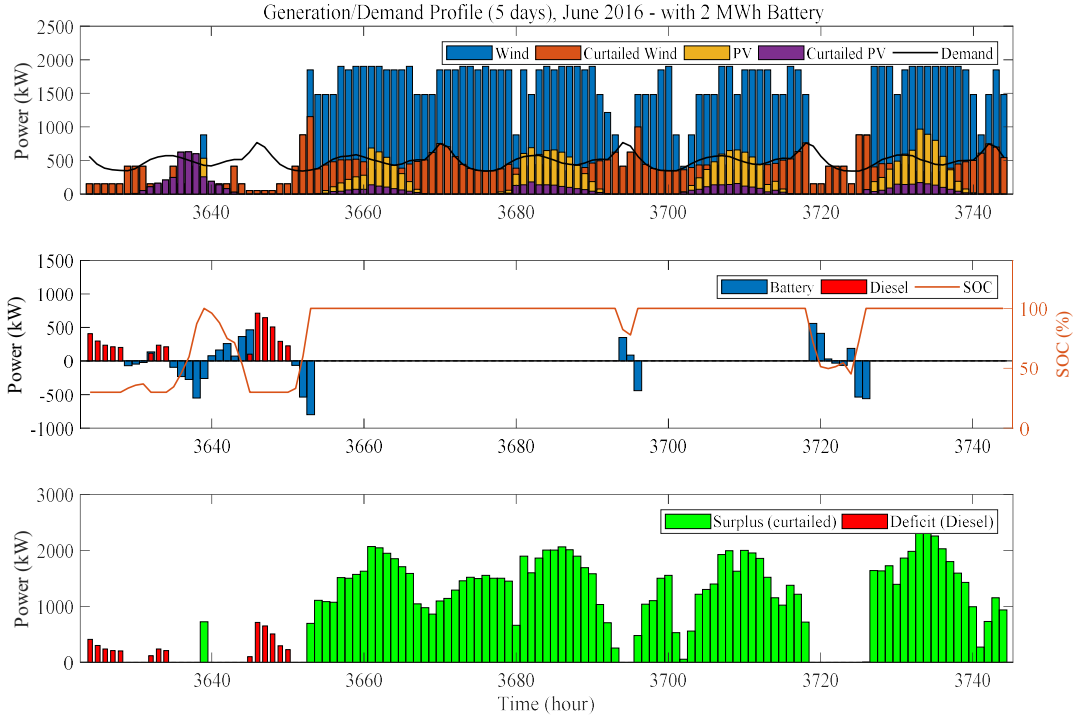

Figure 32: Generation/demand profile on June 1-5, 2016.

1.10.1 Demand Side Management and Virtual Dynamic Tariff

It is concluded in task report 1.4 that the main cause for high load in winter and for the seasonal disparity in demand is the heating load. In other words, the contribution of the heating load to the deficit power can be significant. One approach, to mitigate the heating load contribution to the energy deficit, is to use Demand Side Management, which is also called Demand Response. The main aim of the demand response is to shift the load demand to time periods when electric energy is cheaper. In Ushant Island's case, this is translated into shifting the load demand as much as possible to the time of the day when there is surplus in the renewable energy generation. However, the energy tariff on Ushant is fixed; hence, there is no way for the demand response controller at the load to evaluate the energy availability at any time.

To overcome this hurdle, a new method is proposed in this report to generate a dynamic virtual tariff 24 hours ahead. This tariff reflects the availability/shortage in renewable energy generation 24 hours ahead. This is achieved by exploiting the weather forecast, demand forecast, and the energy balance model of the power system to predict this virtual tariff. The central Energy Management System on the island is responsible for calculating this hour tariff and broadcasting it to all smart loads, i.e. loads equipped with demand response capabilities. This virtual tariff is assigned to a value of 5 for each hour, in the 24-hour horizon, with predicted deficit in energy, and a value of 0 for each hour with predicted surplus. Thereafter, the tariff values are averaged for every 3-hour interval in the 24-hour horizon. This is done because the optimization algorithm in the smart load controller is designed to operate on a 3-hour sampling basis, as will be discussed later in this section. Also, the predicted battery SOC is utilized to raise the tariff when there is no deficit, but low battery SOC. Accordingly, the virtual tariff will be between 0 – 3, for SOC value between 100% and SOC_{min}. Examples for the proposed virtual tariff are shown in Figures 33 and 34.

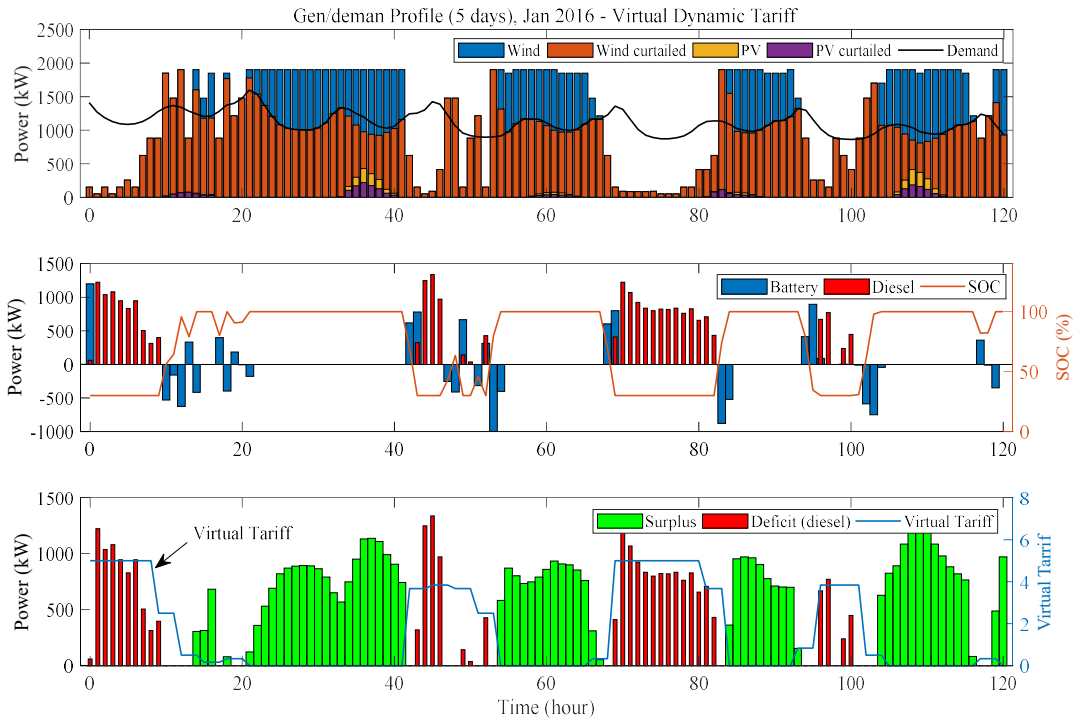

Figure 33: Example for the dynamic virtual tariff that shows the energy deficit effect.

At the smart load, an intelligent control algorithm is designed to utilize the received 24-hour tariff profile to schedule the load operation. To examine the proposed control strategy, electric water heater (EWH) loads are considered as an example. A 50 gallon, 5kW EWH is used in this study. The model for this heater can be found in (Du, et. al. 2011). Since, there is no data available for the average household hot water usage on the island, a typical household water usage is adopted from (Gelažanskas, et. al. 2015), and shown in Figure 35.

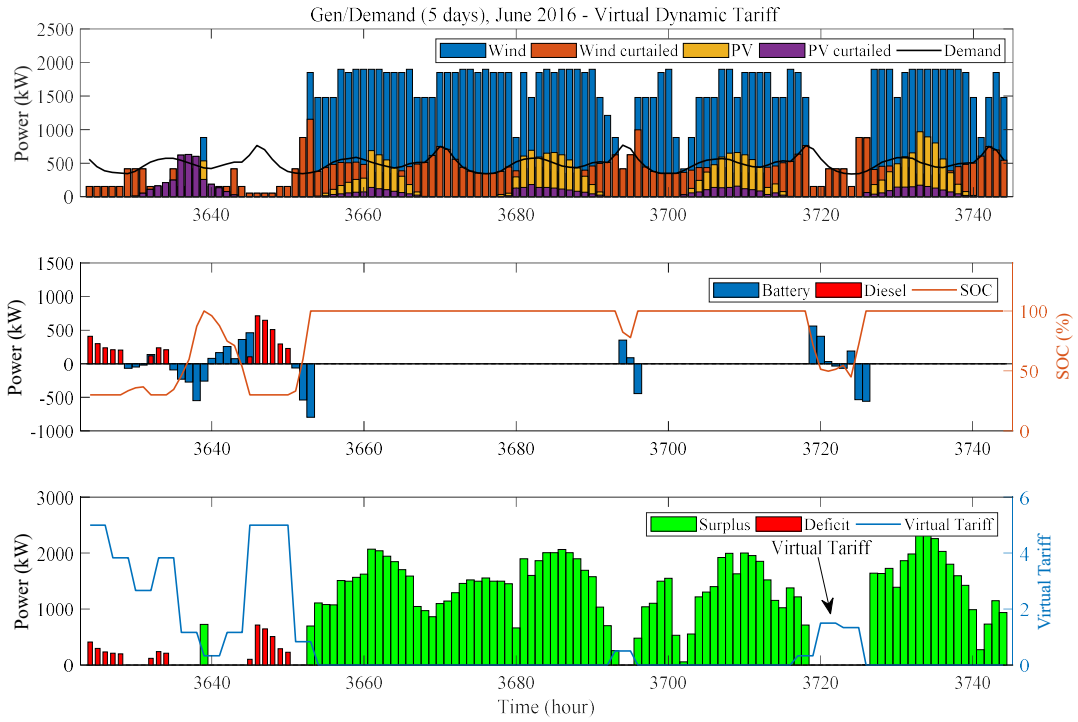

Figure 34: Example for the dynamic virtual tariff that shows the SOC effect.

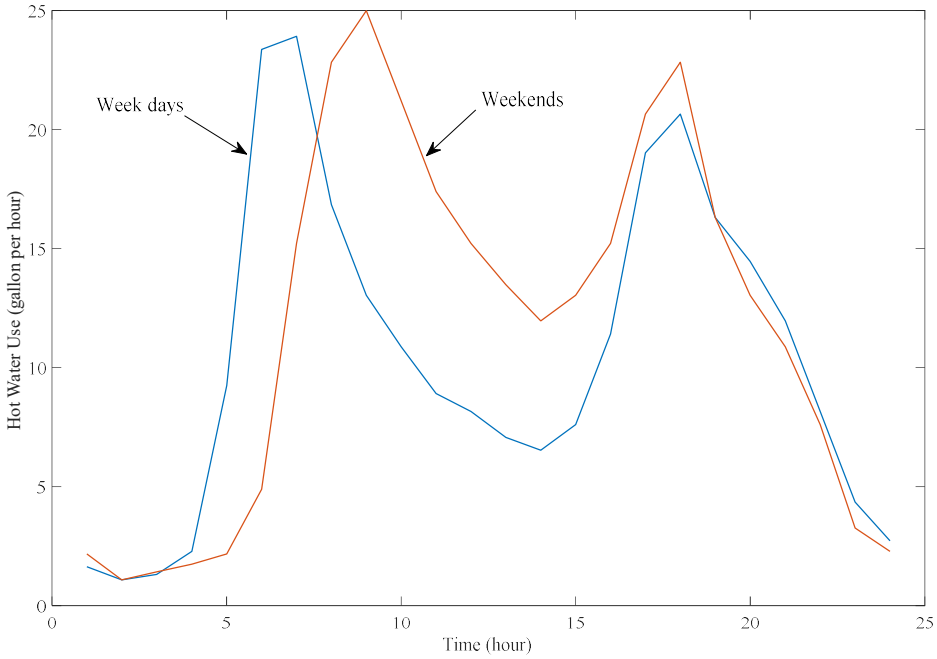

Figure 35: Typical household hot water usage used in the study.

1.10.2 EWH Demand Side Controller

At the EWH, the controller uses a dynamic programming (DP) algorithm called Q-iteration (Busoniu et. al. 2010). The elements of the dynamic programming based control system are shown in Figure 36. The process in this case is the EWH dynamic model, which is modelled as a Markov Decision Process. The reward is the electric energy cost using the virtual tariff. The state is a combination of physical variables that describe the process unique physical state, e.g., three variables are used to describe the process; these variable are: time of day (TOD), tariff, and the water temperature (T). In the considered design, TOD is divided into 8 intervals of 3 hours each, the tariff is discretized into 5 levels, and the temperature is discretized into 5 levels between 55 C^o and 75 C^o. Therefore, the combination of these variable level results in a 200 discrete states that describe process behaviour. The action is the control algorithm output which is considered to be the temperature reference. In this design under consideration, the action can be either 60 C^o or 70 C^o.

In Figure 37, the performance of the traditional EWH controller, which uses a simple hysteresis thermostat, is compared with the performance of the smart controller that uses the forecasted virtual tariff and Q-iteration algorithm. The virtual tariff forecast for that day is shown in Figure 38.

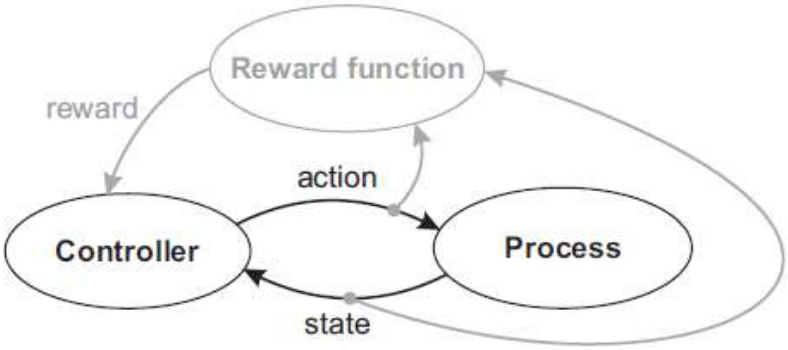

Figure 36: Elements of the DP control structure.

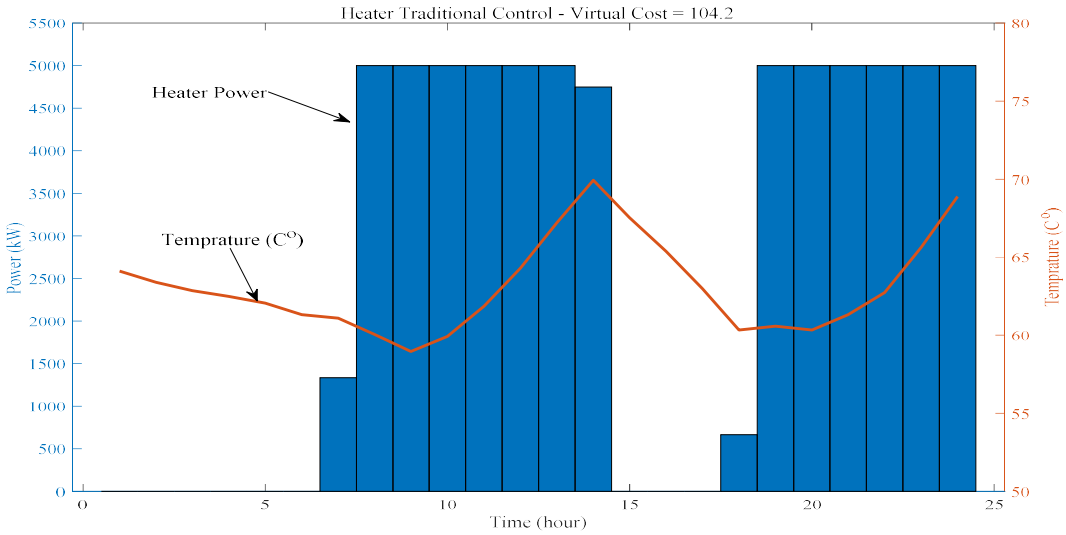

(a)

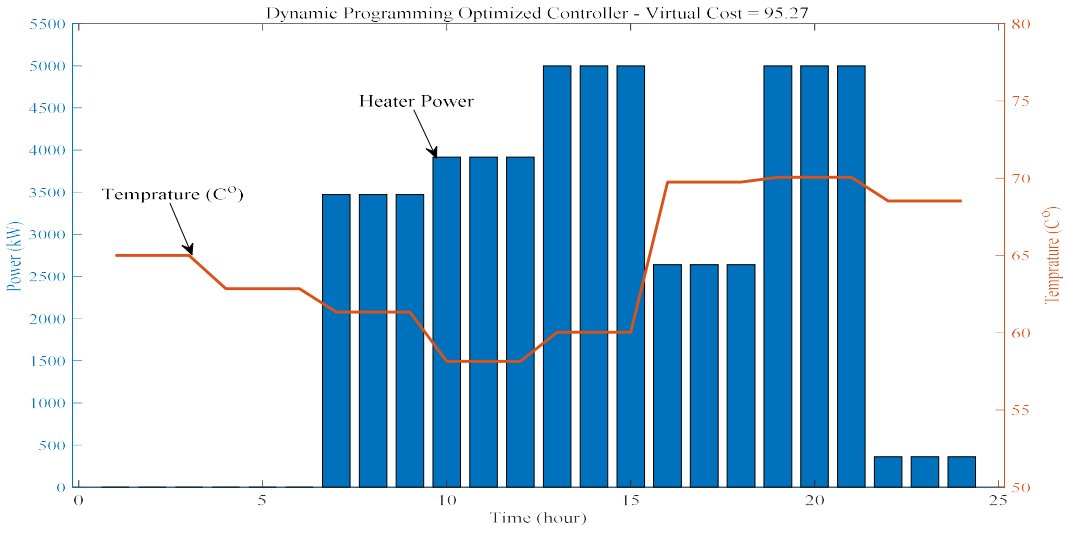

(b)

Figure 37: Performance of (a) the traditional simple thermostat controller, and (b) the proposed smart controller.

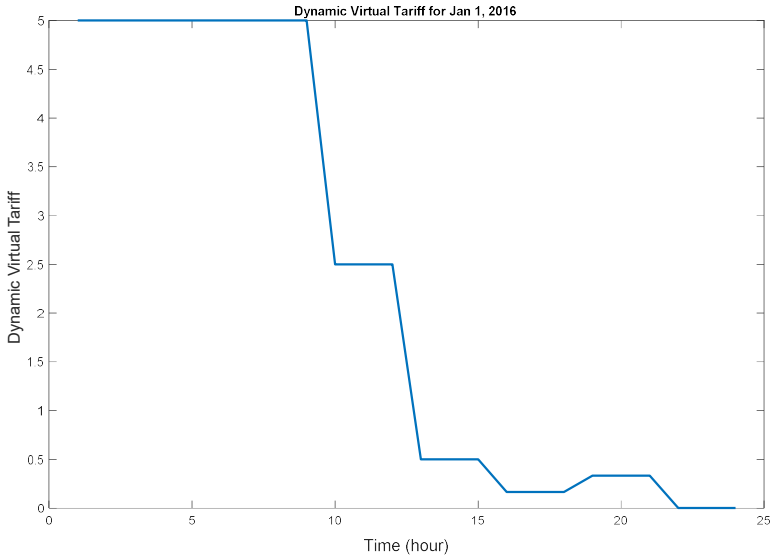

Figure 38: Dynamic virtual tariff for the 24 hours used in Figure 11-8 example.

Using the proposed demand side management for a group of 150 electric water heaters on the island, the energy balance profile improved as shown in Figure 39. It can be seen that demand response has reduced the annual deficit by 246 MWh, which is more than half the saving achieved by the 2 MWh battery.

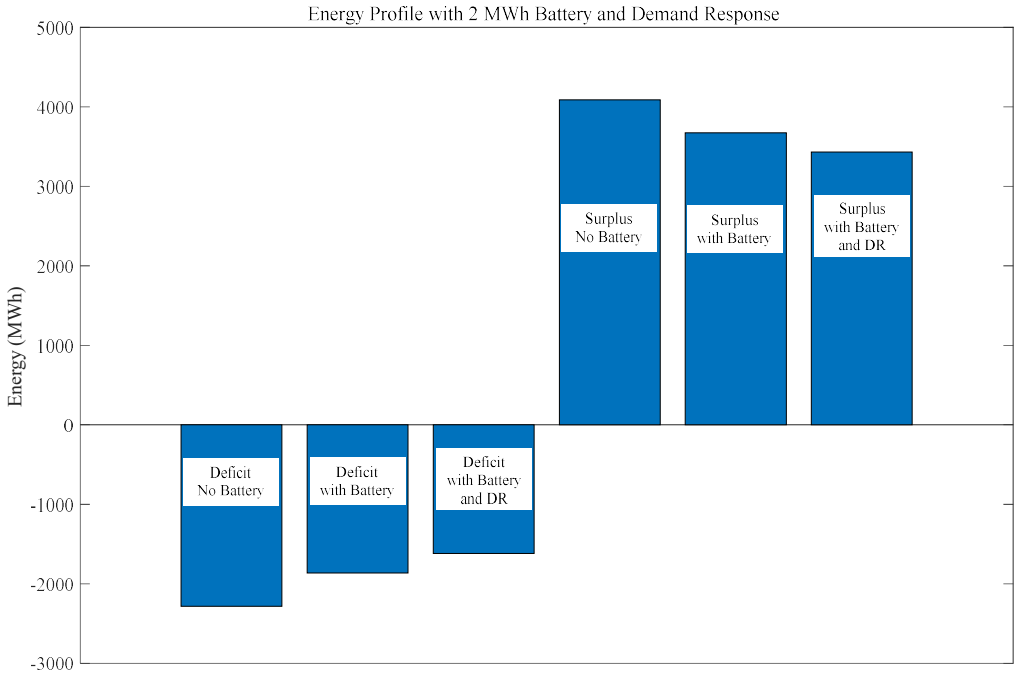

Figure 39: Improvement in the annual energy balance after deploying 2 MWh battery, and employing the proposed demand response strategy.

The performance of the smart EWH in comparison to that of the traditional controller is shown in Figure 40 for the first 5 days in January.

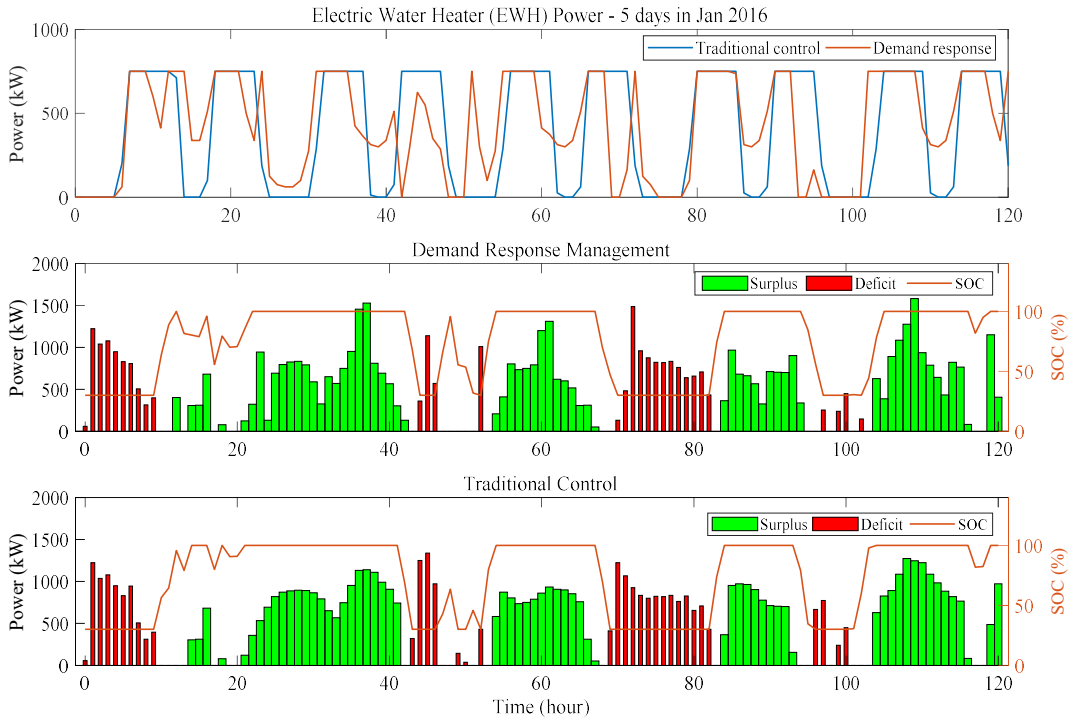

Figure 40: Performance of the EWH demand response controller in comparison to the traditional controller for 5 days in January.

1.11 100% Renewable Energy Generation

For the same considered renewable energy resources rated at 1.8 MW PV and 2 MW wind power, to achieve 100% renewable energy generation on the island, a battery of more than 300 MWh needs to be installed, which is unrealistic. Even though, this battery will make use of the surplus energy already available from renewable energy sources, the cost for such a battery will be unrealistic. This challenge can be approached differently, for example: 1) increase the deployed renewable energy generation, and/or 2) use long term energy storage types such as pumped hydro storage or pumped air storage would be more realistic and cost effective. These solutions will be the investigated in the future work.

2. Part (2): Reliability Assessment

The main aim of the reliability study is to develop a methodology to assess the impact of different reliabilities on the parameters, measuring reliabilities of energy security and availability, assessing target reliability/availability and prioritising possible supply and generation mix options.

In order to assess the island power network in term of reliability and assessing the supply and generation mix, two distinct analysis are required:

1. An analytical reliability study of the network, translating electrical distribution network into a Reliability Block Diagram (RBD) system employing a software such as ReliaSoft. One of the primary objectives of the reliability analysis is to obtain a life distribution that describes the times-to-failure of a component, subassembly, assembly or system. This analysis is based on the time of successful operation or time-to-failure data of the item (component) either under use conditions or from existing failure information databanks.
2. A quantitative power flow analysis, which analyses the voltage for each load node, the effect of introducing new renewable energy sources on the network and the capability of the network to supply the load and transfer the power. Software such as Matlab Simulink can be employed for power flow analysis.

To perform these assessments, ta range of primary data is required, including, but not limited to:

- A schematic diagram of the island power system network and the network operating voltage
- The hardware specifications of the main components of the island network such as power cables, transformers, circuit breakers and generators units:
    - The cables type, length and size
    - The transformer parameters, terminals voltage, parameters and type
    - The electrical generator parameter (power, type and impedance)
    - The circuit breaker information, location and type
- Failure rate information of the main network components or a failure record of each network components, covering 5 years or more
- The annual load demand (active and reactive power) at each load connection node for a duration of at least one year

As mentioned, the data may not always be directly available. However, a range of techniques and approaches has been used to infer, derive and/or estimate the data:

- A schematic diagram can often be obtained from the supplier, depicting a basic diagram of the network, which shows the main network lines and connections.
- A site visit allows to identify the main networks components, including network components such as transformers, generators, circuit breakers.
- The cable length can be inferred by employing a Google Earth map in conjunction with the network diagram and connection diagrams. This allows to estimate t the cable length, and depending on the core materials and the size of the cable the equivalent inductance, resistance and the capacitor values. For any missing data, the standard parameters or these

data can be get form a well know or reported networks which have a similarity in term of voltage and power can be used.

- The active and reactive power of the load at each node, can be obtained from the energy supplier or estimated. The estimated active and reactive power are based on the number of houses supplied from the same node. In conjunction with the average household load profiles, a reasonable load estimate can be made for each node. If the total load of the network is known, the load at each node can also be estimated based on the percentage of the total houses/building connected with this power node to the total number of houses/building of the island, assuming that the households follow an average use profile.
- The failure rate data for the reliability analysis can be sourced from published work/reports, stating extensive failure rate data for the most common power system components. Depending on the power and voltage specification, a matching between the available data and the required data for the reliability assessment can be employed. A particularly useful source for the reliability data is IEEE 493 which have reliability Data of Industrial Plants, for transformers, breakers, cables and other electrical components.

2.1 Status Quo: Reliability Assessment; Ushant Island

Ushant (Fr: Ouessant) is selected as a representative case study for an isolated island community energy system. It is an island community located off the northwest coast of Brittany in the Iroise Sea, at the southern end of the western entrance to the Channel. The island is the largest and most westerly of the Îles du Ponant, with an area of 15.01km^2. It is largely flat, with the highest elevation at just 61m above mean sea level. The island is a rocky surface covered with many grass fields and there is very little woodland. Around the edge of the island are rocky cliffs interspersed with several sandy beaches, and the surrounding waters contain many small islands and outcrops (ICE report T1.4).

The power network of the Ushant Island is managed by the local network operator SDEF. According to the information provided, the Ushant grid consists of two main networks; high voltage network (HTA) and low voltage network/distributed network (BT). The total length of the HTA is about 28.4 km and all the cables are underground. Only the HTA network was available for this analysis. An overview map is shown in Figure 41.

The dashed lines represent the HTA cable. The blue circles represent the node connection between the HTA and BT network via a step down transformer. The cable size and its core material are displayed on the map. The HTA network cable size are 150mm^2, 95mm^2 and 50mm^2 respectively. Each load node has a unique name identification such as P0009. According to the available map, there are 35 nodes/connections for load distribution.

The generation portfolio comprises four off 1.2MW Diesel Generators and a 0.5MW Diesel Generator. Additionally, a 0.045MWp Solar PV array is instllalled on the roof of the Sport Hall rooftop since 2014. Hence the total peak generating capacity is 5.345MWp, with less than 1% from renewable energy sources.

Figure 41 Ushant power network

The present analysis makes the following assumptions for the Ushant network:

- Only the HTA network is considered
- All loads are referred to the HTA
- For reliability, each load node connected to the HTA via a step up transformer and a circuit breaker
- Constant failure rate for the power network components are considered.
- Only the four diesel generators are consider

The individual steps for the reliability and power flow analysis are:

1. In order to estimate the required data for the reliability and power flow analysis the connection between cable segments for the distributed points in the cable must be identified. Figure 2 shows the identification name for the connection nodes and distributed nodes (N). The blue circles are the additional load nodes names and the black circles are the additional cable connections nodes. The red circles are the nodes names assigned by SDEF. According to Figure 42, the grid consists of 51 nodes 54 cable segments.

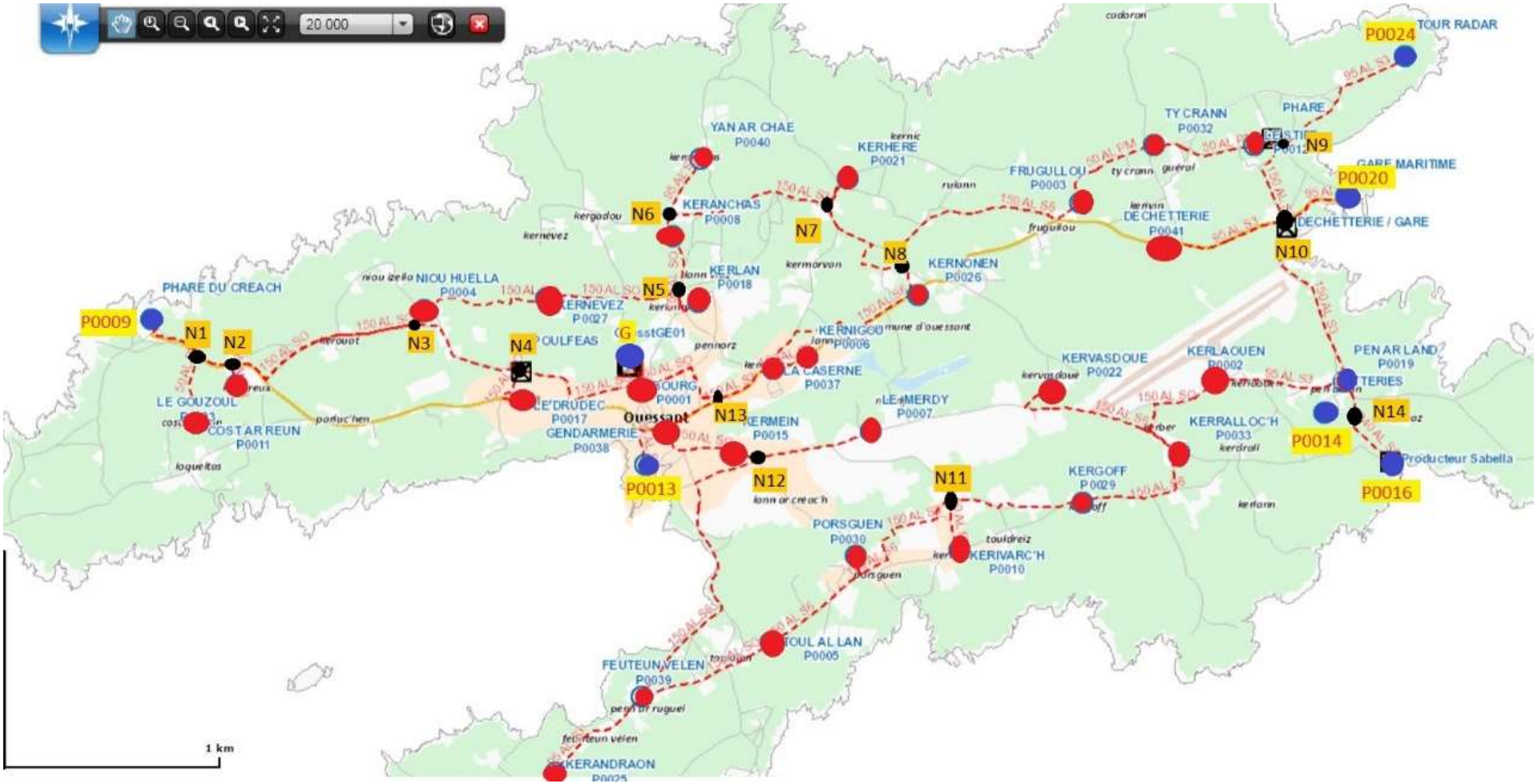

Figure 42: Ushant Island power network and nodes

By employing PlotDigitizer software , the cable length between load nodes can be estimated as shown in Figure 43 Depending on the length, core materials and the size of the cable the equivalent inductance, resistance and the capacitor can then be inferred. The total estimated length of the cable is 23.771 km, which is less than the reported one (28.082km). This error is likely to be caused by slight deviations in the actual building configuration of the cables in situ. To account for this difference, all the cable estimated length are scaled to match the actual one by multiplying by 1.1646.

Figure 43: Example of estimating the cable length employing PlotDigitizer software

Subsequently, the cable parameters can be estimated according to the following equations (*http://nepsi.com/.)* .

$$c = \frac{2.24 \times SIC}{\log\left(\frac{D}{d}\right)} \times \frac{L}{10^6} \quad (1)$$

$$L_c = 0.3048 \frac{\left(0.1404 \times \log_{10} \sqrt[3]{\frac{A \times B \times C}{d}} + 0.0153\right)}{10^6} \times K \times L \quad (2)$$

$$R = \rho \frac{L}{a} \quad (3)$$

Where:

C	Total capacitance of the cable (µf)
SIC	Dielectric constant of the cable insulation
D	Diameter over the insulation
d	Diameter of the conductor
L	Length of the Cable in Feet
LC	Cable Inductance (mH)
A, B, C	Spacing per the figure, see Figure 44.
K	Installation correction factor
ρ	Cable core resistivity
a	Cable core area

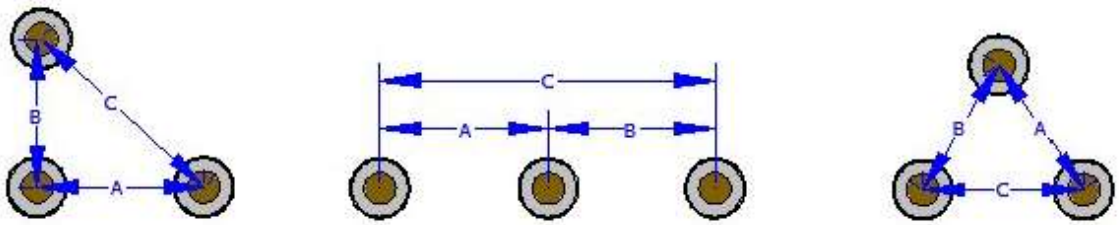

(a) (b) (c)

Figure 44: Cable cores configuration (a) Triangle, (b) Flat and (c) Trefoil

For a 5.5kV cable, the typical insulation thickness is 2.25mm. A Cross-linked polyethylene (XLPE) type cable is assumed of the cable which have lowest directed constant 2.3. The highest correction factor is chosen (1.5). These specifications are considered to emulate the worst conditions. The chosen cable core configuration is Trefoil (c) in Figure 44. The core martial of the cable is Aluminium. Based on this information, the cable resistance, inductor and capacitor are estimated as shown in Table 10.

Table 10: Ushant Island cable parameters

Node - From	Node - To	Cable Length (estimated) [m]	Cable Size [mm²]	Cable Length (Scaled) [m]	R [Ω]	C [µF]	L [mH]
P0009	N1	347.32	150	410	0.07	0.18	0.23654
N1	N2	162.807	150	192	0.03	0.09	0.11088
N1	P0011	322.611	50	381	0.20	0.11	0.30406
N2	P0023	109.501	95	129	0.04	0.05	0.08568
N2	N3	966.495	150	1142	0.20	0.51	0.65821
N3	P0004	77.378	150	91	0.02	0.04	0.05270
P0004	P0027	610.928	150	722	0.13	0.32	0.41606
P0027	N5	616.743	150	729	0.13	0.33	0.42002
N5	P0018	182.815	150	216	0.04	0.10	0.12450
N5	P0008	257.573	150	304	0.05	0.14	0.17542
P0008	N6	105.199	150	124	0.02	0.06	0.07164
N6	P0040	285.736	95	338	0.09	0.12	0.22358
N6	N7	760.264	150	898	0.16	0.40	0.51776
N7	P0021	175.727	150	208	0.04	0.09	0.11968
N7	N8	561.45	150	663	0.12	0.30	0.38237
N8	P0026	139.998	150	165	0.03	0.07	0.09534
N8	P0003	1,021.59	150	1207	0.21	0.54	0.69574
P0003	P0032	509.628	50	602	0.32	0.17	0.48033

Node - From	Node - To	Cable Length (estimated) [m]	Cable Size [mm^2]	Cable Length (Scaled) [m]	R [Ω]	C [µF]	L [mH]
P0032	P0012	477.833	50	564	0.30	0.16	0.45036
P0012	N9	136.639	50	161	0.09	0.05	0.12878
N9	P0024	763.324	95	902	0.25	0.33	0.59729
N9	N10	385.605	150	456	0.08	0.20	0.26261
N10	P0020	310.407	95	367	0.10	0.13	0.24289
N10	P0019	833.852	150	985	0.17	0.44	0.56788
P0019	N14	165.333	240	195	0.02	0.11	0.09717
N14	P0016	291.854	240	345	0.04	0.19	0.17153
N14	P0014	135.646	240	160	0.02	0.09	0.07972
P0019	P0002	619.77	95	732	0.20	0.27	0.48496
P0002	N17	432.644	150	511	0.09	0.23	0.29464
N17	P0022	736.766	150	870	0.15	0.39	0.50176
N17	P0033	150.358	150	178	0.03	0.08	0.10240
P0033	P0029	626.307	150	740	0.13	0.33	0.42654
P0029	N11	640.008	150	756	0.13	0.34	0.43587
N11	P0010	239.642	50	283	0.15	0.08	0.22586
N11	N18	641.999	150	758	0.13	0.34	0.43722
N18	P0030	99.366	150	117	0.02	0.05	0.06767
N18	P0005	530.68	150	627	0.11	0.28	0.36141
P0005	P0039	709.896	150	839	0.15	0.37	0.48346
P0039	P0025	529.555	95	626	0.17	0.23	0.41437
P0039	N12	1,517.61	150	1793	0.32	0.80	1.03354
N12	P0007	526.213	150	622	0.11	0.28	0.35837
N12	P0015	112.546	150	133	0.02	0.06	0.07665
P0015	P0038	384.642	150	454	0.08	0.20	0.26195
P0038	P0013	294.596	95	348	0.10	0.13	0.23052
P0038	N13	281.831	150	333	0.06	0.15	0.19194
N13	P0001	469.54	150	555	0.10	0.25	0.31977
N13	P0006	298.872	150	353	0.06	0.16	0.20354
P0037	P0006	166.581	150	197	0.03	0.09	0.11345

Node - From	Node - To	Cable Length (estimated) [m]	Cable Size [mm^2]	Cable Length (Scaled) [m]	R [Ω]	C [μF]	L [mH]
P0006	P0026	861.9	150	1018	0.18	0.45	0.58698
P0001	G	117.79	150	139	0.02	0.06	0.08022
P0001	N4	658.518	150	778	0.14	0.35	0.44847
N4	P0017	221.299	150	261	0.05	0.12	0.15071
N4	N3	595.633	150	704	0.12	0.31	0.40565
N10	P0041	593.105	95	701	0.20	0.26	0.46409

2. The second step is to draw the schematic diagram of the Ushant network. According to the Ushant network map shown in Figure 42, the schematic diagram of the network can be implemented as shown in Figure 45. The green circles are the load nodes and the red circles are the generator units. A different colour and thickness of the lines represent the different diameters of the cables. Red lines denote 150mm^2 diameter, green - 50mm^2 and so on. The blue blocks represent the cable between nodes.
3. The third step is to estimate the load for each node. This can be estimated by establishing a catchment area for each node and count the number of houses/building in this area based on a reference house model as shown in Figure 46. The catchment area is drawn based on the nearest building to the node. The base model of the house is chosen to be a small house (70m^2). According to the proposed technique to estimate the load at each node, the number of houses for each node is shown in Figure 47 and the percentage of the building for each node is shown in Figure 48. The total number of buildings is 1,105, which is more than the number of people living on the island permanently (850) and indicates that about 2/3rd of the buildings are likely to be holiday homes/ serve tourism. The percentage of the load at each node is shown in Figure 49. As been expected the main load demand is in the city centre area.
4. Once the system parameters of the cable and power network are established, a Simulink model, using Matlab Simulink, is developed to study the power flow of the network. The complete Simulink model with all nodes and connections for the island is shown in Figure 50.

Now all essential data of the Ushant Island to analysis the power network in term of reliability study and power flow is estimated. In the next sections a power flow and reliability analysis are presented.

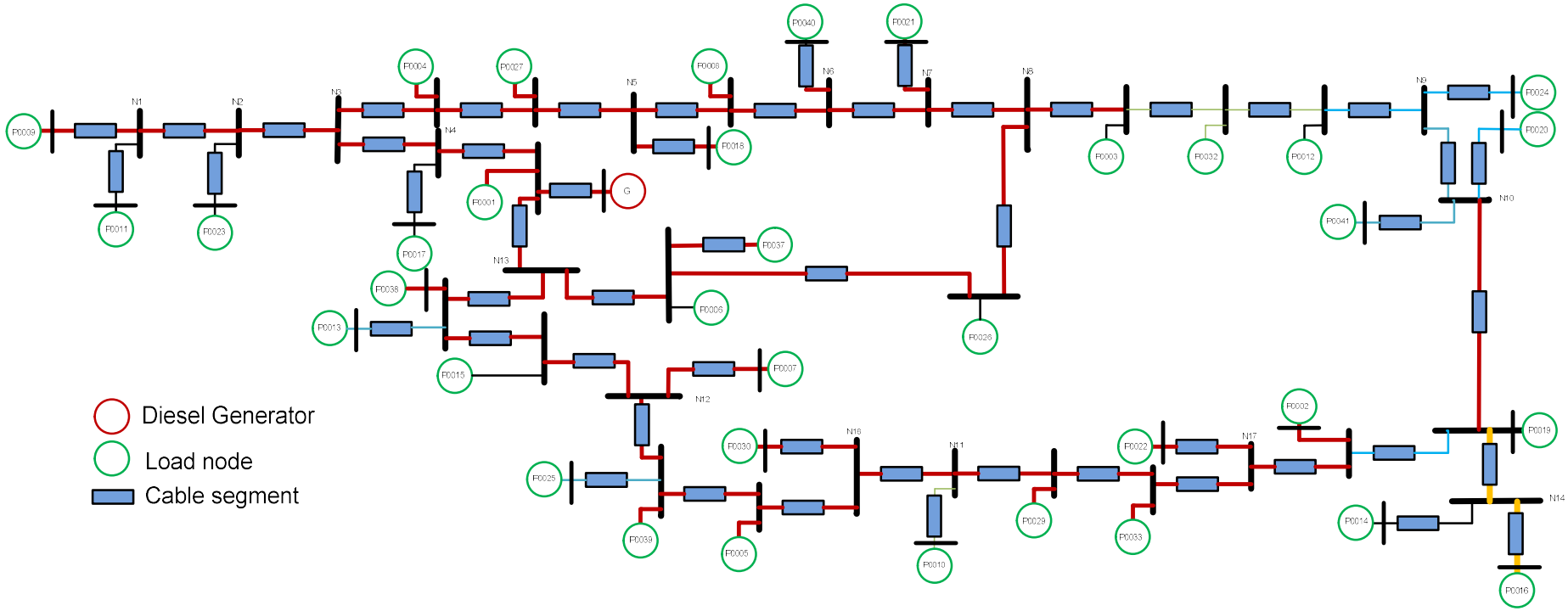

Figure 45 Ushant Island schematic power network diagram

Figure 46: Ushant Island schematic power network diagram

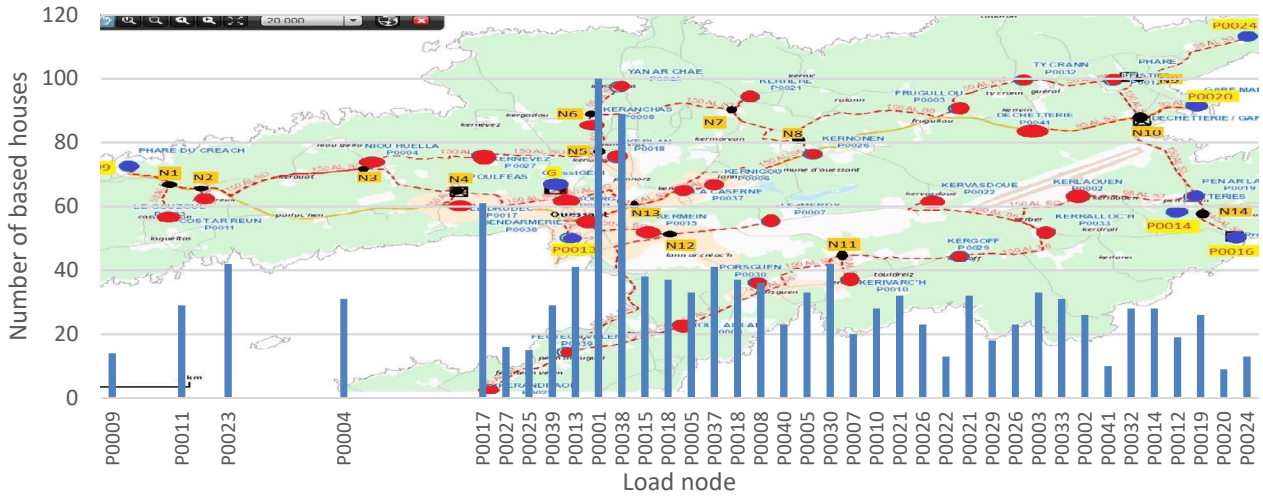

Figure 47: Total number of houses at each load node

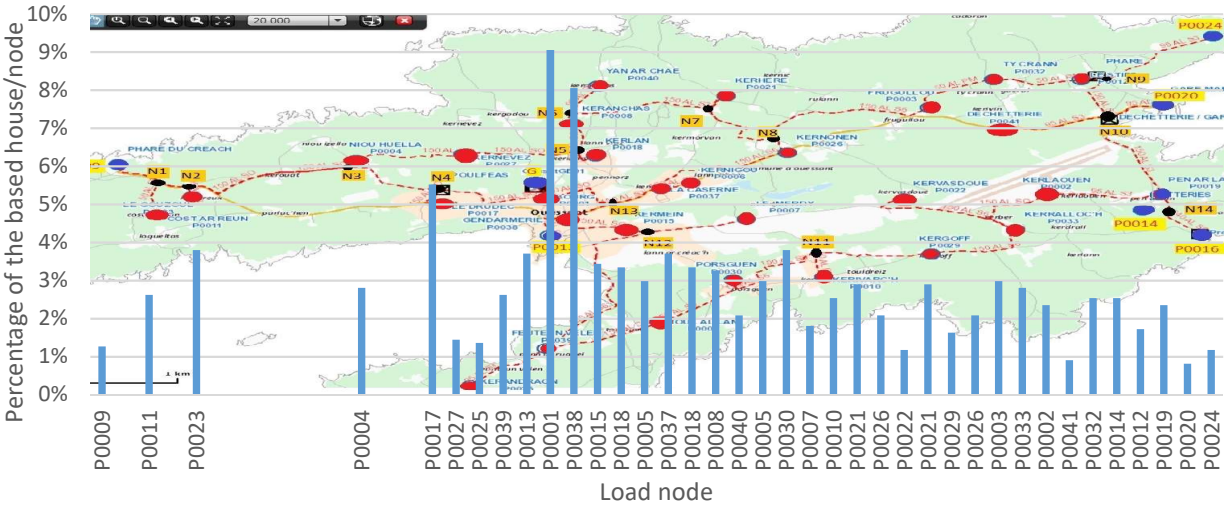

Figure 48: Percentage of the load at each node

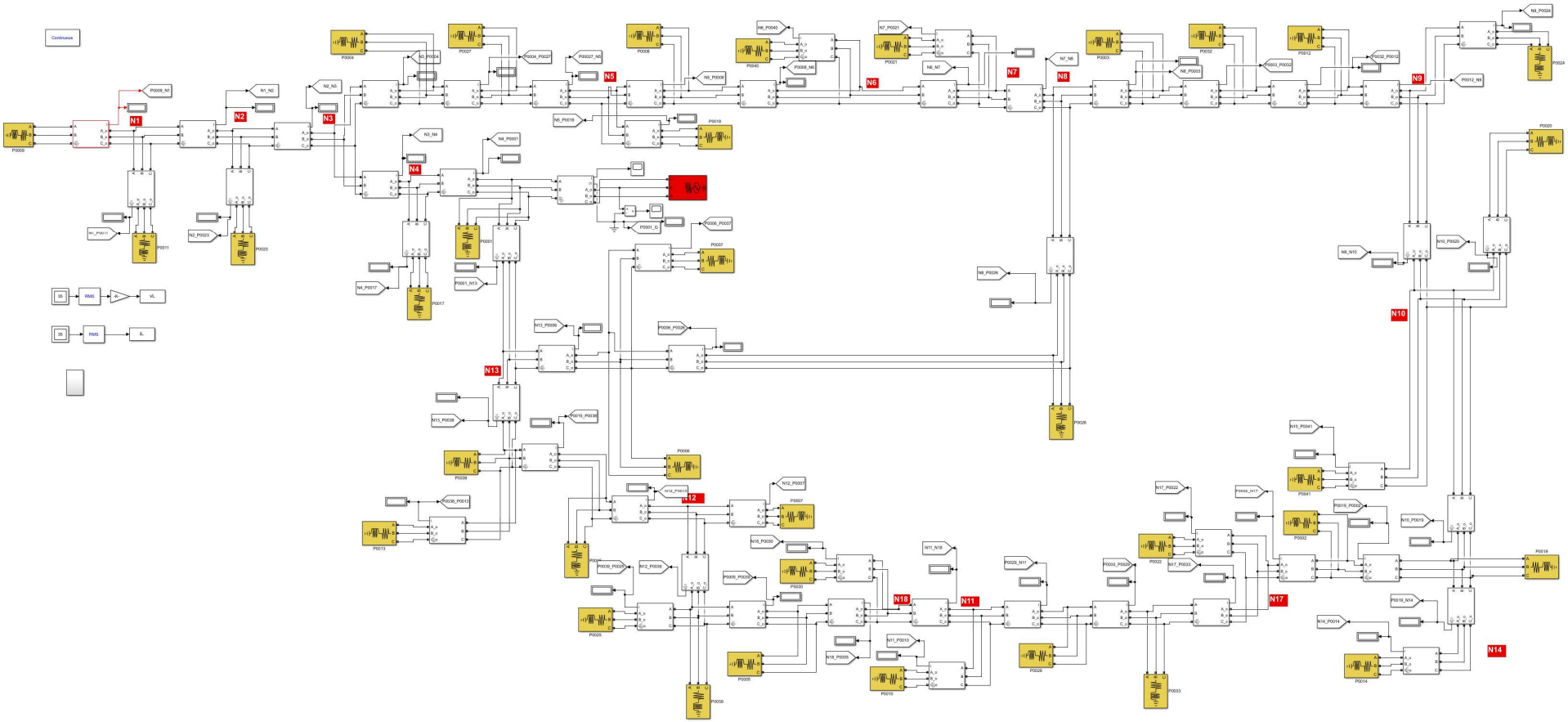

Figure 49: Simulink model for the Ushant power network

2.1.1 Power Flow Analysis of the Current Ushant Island Power Network

It is worth to study and analysis the current Ushant power network without introducing the renewable energy to the network. This helps to understand the power quality of the grid regarding the voltage at each load node and the capacity usage of the power cable. Furthermore, the failures of the load node according to the reliability analysis of the network can be analysed as reference case. This analysis can then inform the selection of the most suitable locations for renewable energy deployments from a power network perspective. It indicates the potential rated power of renewable energy generation and location, which the existing network can support without requiring network upgrade investments.

The existing generation capacity is located in the city centre. The peak energy demand recorded throughout the six years of available data is 2.08MW, in March 2013 (ICE report T1.4 Report), indicating an overcapacity in the generation capacity by a factor of 2.5.

The peak demand of 2.08MW is employed for the power flow analysis of the Ushant network. The power factor of the load node is assumed to be 0.7 which is normally the lower power factor of the grid (Papathanassiou and Santjer 2006). Based on this peak load, the load demand at each node is calculated as the percentage of the number of building at each node. Figure 51 shows the resulting load demand estimates at each node.

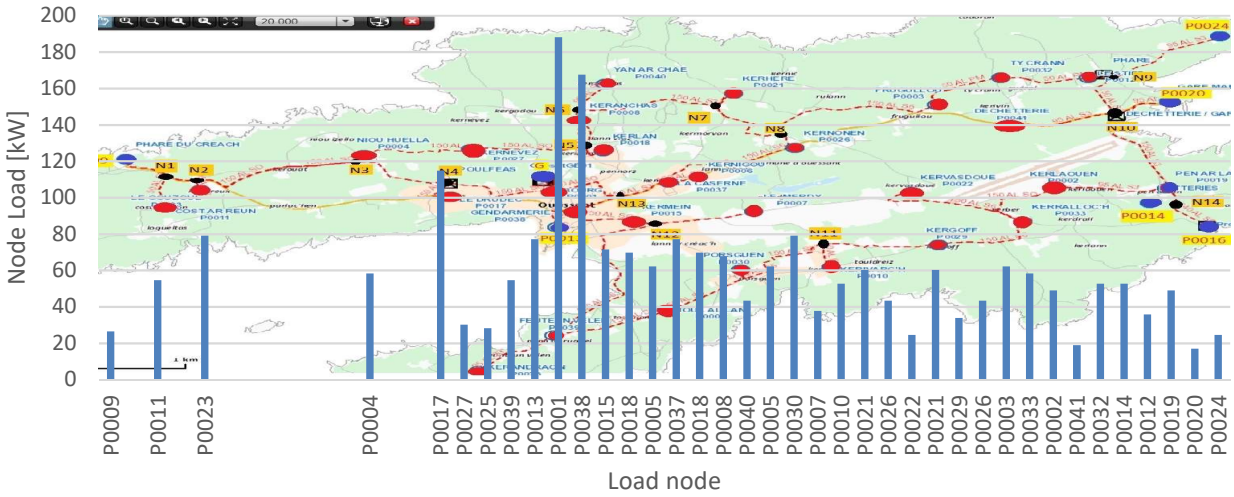

Figure 50: Load demand at each node

Figure 51 indicates that the maximum load demand occurs at the city centre (190kW). The percentage voltage drops at each node are shown in Figure 52. The percentage of the voltage drops is calculated based in the nominal high voltage network (5.5kV). The further away the load nodes are located from the generation units, the higher is voltage droops at the load node. The range of the load node voltage drops is between 0.5% to 2% depending on their distance from the diesel generators units. This voltage drops range is lower than the maximum voltage variation ranges according France grid regulations, 6%-8% (Republic 2003).

It is also worth to analyse the cable current capacity under the highest load demand. Figure 53 shows the percentage of cable current capacity usage under the highest load demand (2.08MW). The highest cable capacity usage is at the city centre (58%). It seems that the Ushant power network is capable of

adding more loads and generation units. The cable capacity analysis indicated that as much as 2.7MVA (1.87MW at 0.7pf) could be added as power generation capacity.

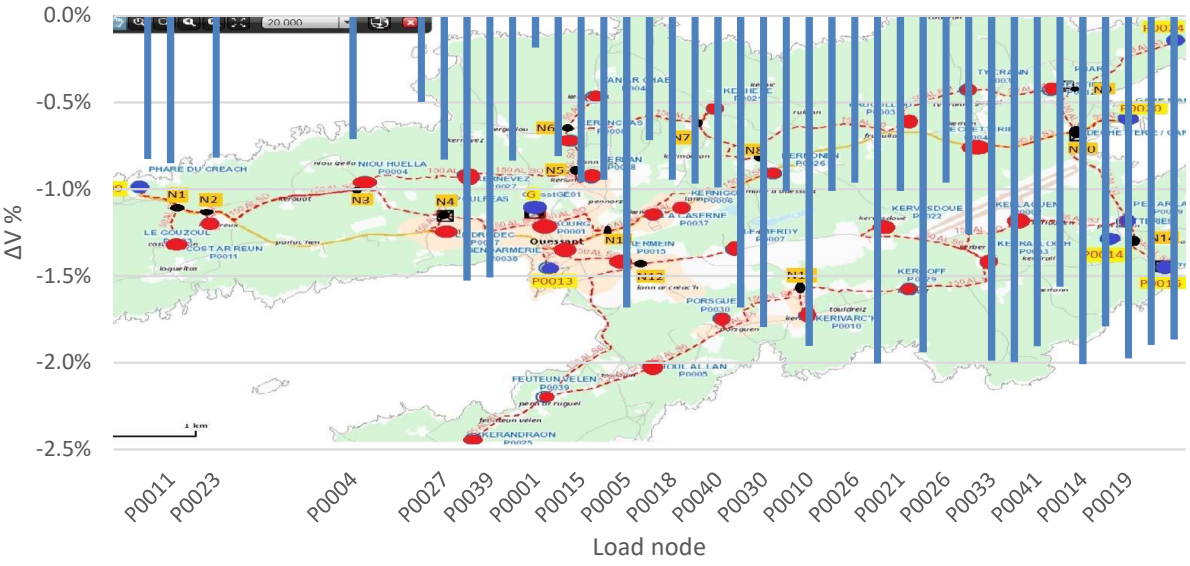

Figure 51: Node voltage drop (ΔV) under highest load demand (2.08MW)

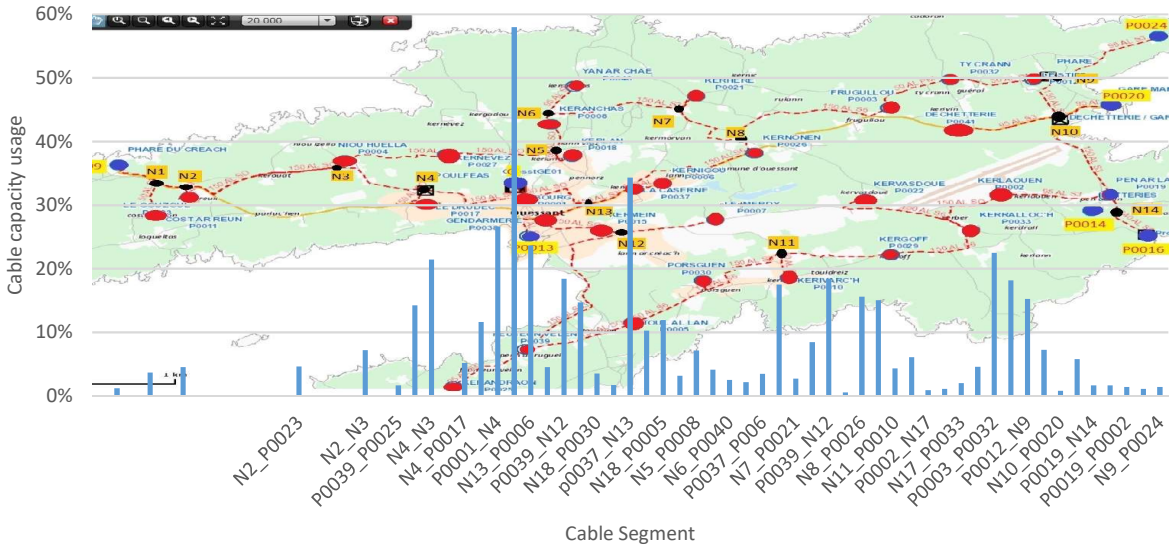

Figure 52: Percentage of used cable capacity under highest load demand (2.08MW)

Table 11: Available cable capacity Island

FROM	TO	Available cable capacity [MVA]
P0009	N1	3.1
N1	N2	3.0
N1	P0011	1.6
N2	P0023	2.3
N2	N3	2.9
N3	P0004	2.7
P0004	P0027	2.8
P0027	N5	2.8
N5	P0018	3.0
N5	P0008	2.9
P0008	N6	3.0
N6	P0040	2.4
N6	N7	3.1
N7	P0021	3.1
N7	N8	3.1
N8	P0026	2.7
N8	P0003	2.7
P0003	P0032	1.3
P0032	P0012	1.4
P0012	N9	1.5
N9	P0024	2.4
N9	N10	2.9
N10	P0020	2.4
N10	P0019	3.0
P0019	N14	4.4
N14	P0014	4.4
P0019	P0002	2.9
P0002	N17	3.1
N17	P0022	3.1
N17	P0033	3.1
P0033	P0029	3.0
P0029	N11	3.0
N11	P0010	1.6
N11	N18	2.9
N18	P0030	3.0
N18	P0005	2.8
P0005	P0039	2.7
P0039	P0025	2.4
P0039	N12	2.6
N12	P0007	3.1
N12	P0015	2.5
P0015	P0038	2.4
P0037	P0013	2.3

FROM	TO	Available cable capacity [MVA]
P0037	N13	2.1
N13	P0001	1.3
N13	P0006	2.4
P0037	P0006	3.0
P0006	P0026	2.6
P0001	N4	2.3
N4	P0017	3.0
N4	N3	2.5
N10	P0041	2.4
P0001	G	1.6

2.1.2 Reliability Analysis of the Current Ushant Island Power Network

A reliability analysis of the current Ushant network gives an indication regarding the failure rate/year of each node. i.e. how often in the year there is no power at a specific load node. Moreover, it provides a general estimate of the power network reliability.

For Ushant Island, there is no available/recorded data of the cables, transformers, generator and circuit breaker failure rates. Published papers and literature can be used to as an estimated of the failure rate of the most common network elements. An overview of typical failure rates data for power network components is shown in Table 12. The average data is derived and summarised from (YARD , A. E. Green 1978, SINTEF 1984, AME 1992, Ammirato, Silecchia et al. 2006, Jey K. JEYAPALAN 2007, Gill 2011, Chengke Zhou and Zhou 2012, Hassan M. Nemati 2015).

Table 12 Failure rate of the main power network (YARD , A. E. Green 1978, SINTEF 1984, AME 1992, Ammirato, Silecchia et al. 2006, Jey K. JEYAPALAN 2007, Gill 2011, Chengke Zhou and Zhou 2012, Hassan M. Nemati 2015)

Element	Failure rate /year	Element	Failure rate /year
Cable (1kV-33kV)	0.0386/km	AC generator >200kW	0.0877
Transformer (3.3kV-33kV)	0.0526	Power inverter	0.0433
Circuit Breaker (415V-11kV)	0.0131		

All the failure rates of the mechanical system of the renewable energy sources such as turbine, diesel generator mechanical parts and gearbox are neglected for this analysis, as the focus lies on the electrical infrastructure and network, rather than on the mechanical system. In this reliability study, the reliability block diagram is built for each load node, modelling the AC generators, power cables, a transformer at the node and a circuit breaker connecting the load to the grid. Figure 54 shows the building blocks of each load node: the power network consists of AC generator and cable connection configuration according to the network schematic diagram.

An example of a load node reliability block diagram is shown in Figure 55. At least two out of four diesel generators should be operational together to supply the load demand. Based on the assumed

failure rates and the given Ushant power network, the calculated failure rate for each load node is shown in Figure56.

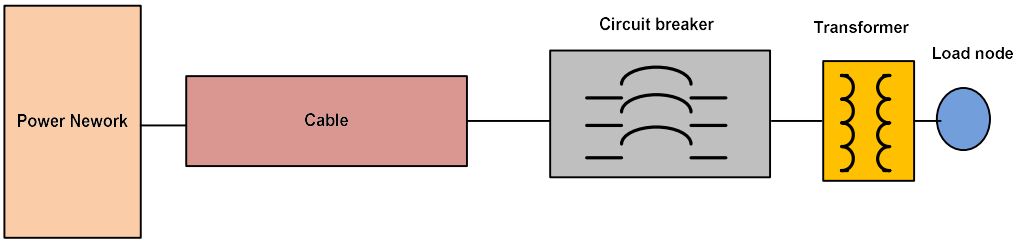

Figure 53: Connection components of the load node

From Fig, 56, the lowest failure rate of the load node is the one closest to the generators. The highest failure rate is 0.125 failure/year at the load node P0011. This means that during 10 years of grid operation one expects an average of 1.25 failures at this load node.

With the established reference case, in the next section the existing diesel generators are replaced by renewable energy sources. Different scenarios are considered and compared with the current network. This is to quantify the possible benefits and implications of the renewable energy in term of power system quality and network / supply reliability.

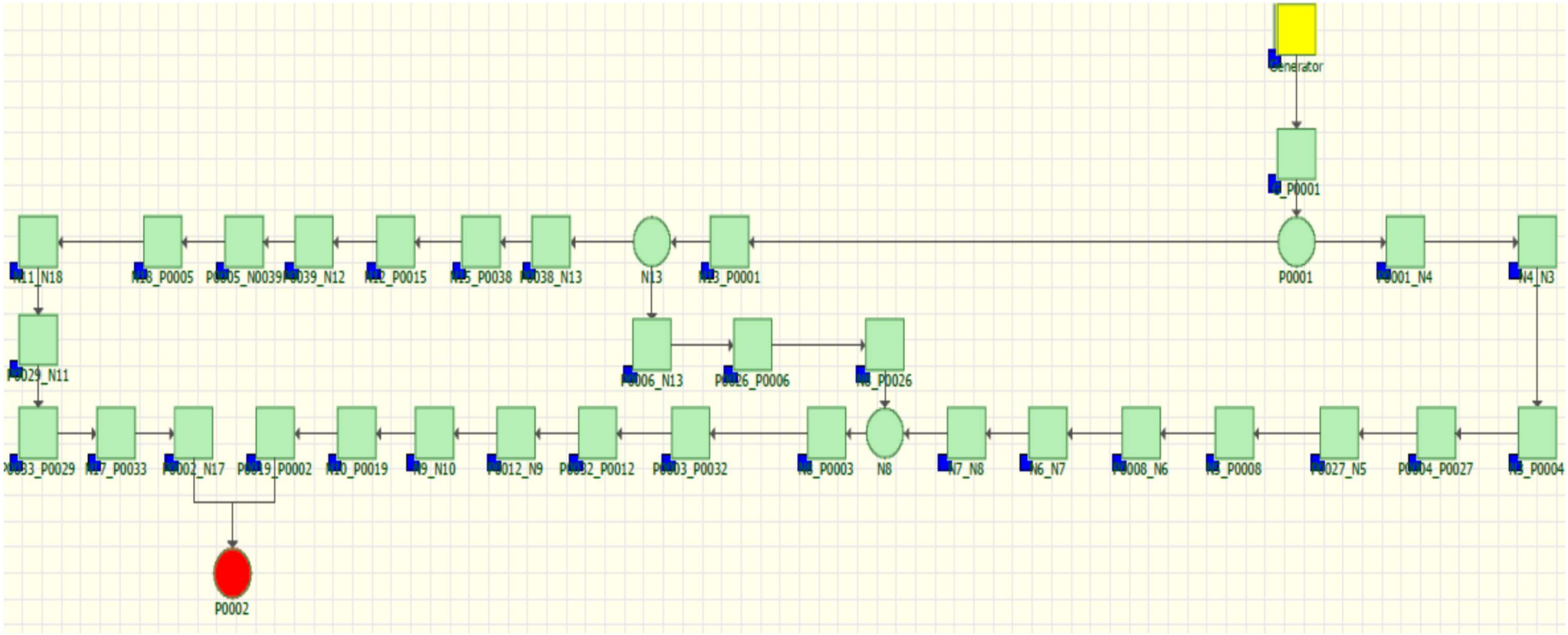

Figure 54: Node P0002 reliability block diagram

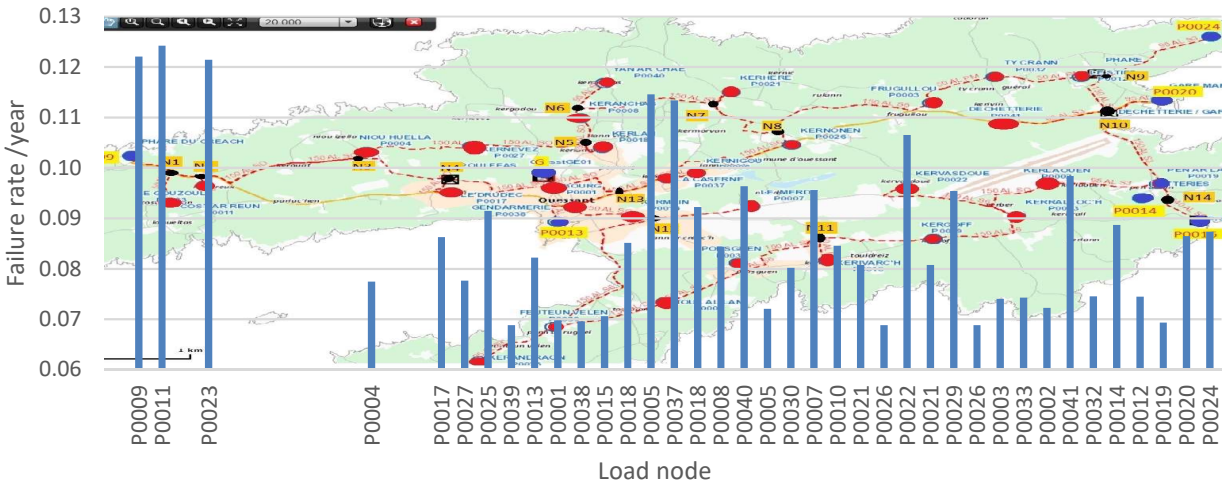

Figure 55: Failure rate of individual load nodes under diesel generators

2.2 Renewable Energy Integration: Reliability Assessment for existing Ushant Island Network

As can be seen from the previous analysis of the current Ushant grid in term of voltage drops, load node failure rate and cable power capacity usage:

- There is a plenty of cable power usage capability which can support the growth of the load demand or introduce renewable energy sources to the grid (and average of 1.87MW)
- The load nodes which are quite far from the diesel generator units have high voltage drops (2%), high failure rate (0.125/year) and less power cable capacity usage (1%).

In this section, the same analysis of the Ushant power network under diesel generators is repeated here but under renewable energy sources. It is assumed that there is a storage unit such as batteries that can handle the mismatching between the generation and the demand (see first part of the report).

According to ICE report T1.4, there are seven suggested scenarios for the type and rating of the renewable energy sources as follows:

- Scenario 1: Planned solar installations (5 sites, total capacity 293.5kW$_p$) and one 300kW wind turbine
- Scenario 2: Extensive solar (20% of rooftops, the solar installations are estimated to provide 3888.93MWh to the grid per annum) and one 800kW wind turbine
- Scenario 3: Extensive solar (20% of rooftops, the solar installations are estimated to provide 3888.93MWh to the grid per annum) and one 2MW wind turbine
- Scenario 4: Sabella D10 tidal turbine (average power 100.4kW, ICE report T1.4) and planned solar (5 sites, total capacity 293.5kW$_p$)

- Scenario 5: Sabella D10 tidal turbine average power (100.4kW, ICE report T1.4) and extensive solar installations (20% of rooftops, the solar installations are estimated to provide 3888.93MWh to the grid per annum)
- Scenario 6: Two Sabella D10 tidal turbines (100.4kW, ICE report T1.4) and planned solar installations (5 sites, total capacity 293.5kW$_p$)
- Scenario 7: Sabella D10 tidal turbine (100.4kW, ICE report T1.4), extensive solar installations (20% of rooftops, the solar installations are estimated to provide 3888.93MWh to the grid per annum) and an 800kW wind turbine

The generation for each scenario during the summer and winter as shown in Figure 57 compared to the demand. Only scenarios 3 & 7 are capable of supply the required energy to the load during the winter and summer seasons. Scenario 7 have the highest power generation during the winter and it have three power sources, which increases the system reliability. Therefore, scenario 7 is selected as a case study of the system reliability and power flow analysis.

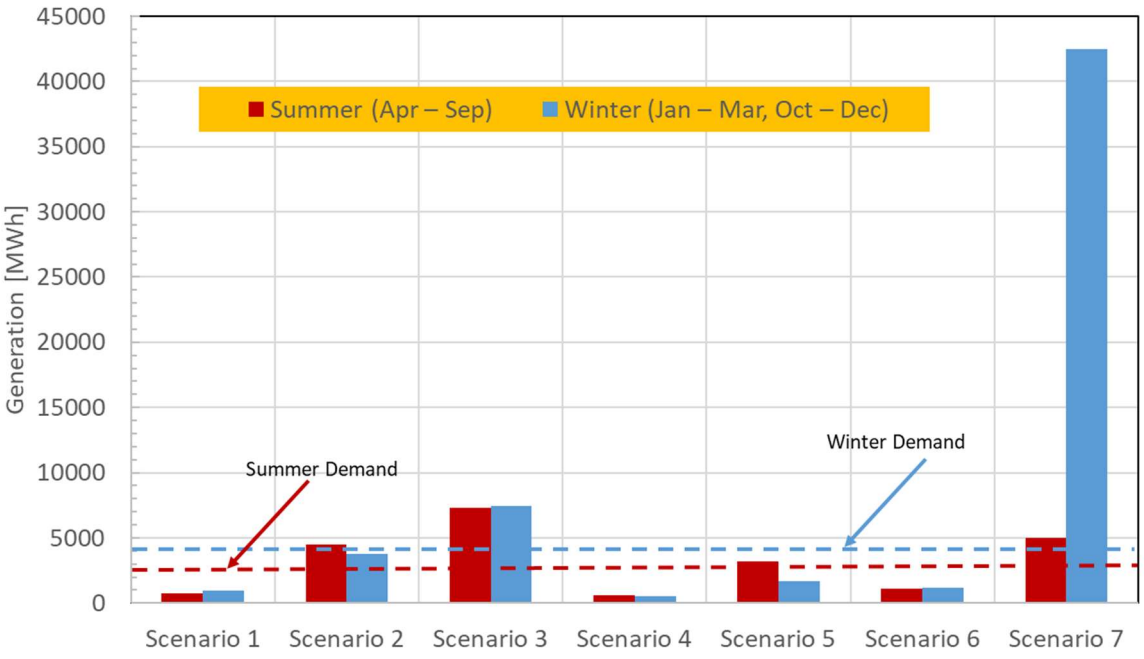

Figure 56: Power generation for each scenario

Scenario 7 suggested three power generation units, Sabella D10 tidal turbine, extensive solar installations (20% of rooftops) and an 800kW wind turbine. The location of the tidal turbine is nearly selected to be in the south weast of the island where there is a connection point and a cable(240mm^2). For the wind turbine location, ICE report T1.4 sugested areas where not allowed to install the wind turbine due to the saftey and regulation issues as shown in Figure 58 where the yellow and blue areas should be avoided for the wind turbine location. There are seven suitable locations for wind turbine as shown in Figure 59. These location are chosen based on the nearest to the network node, avoid the city centre, be a way from the possible location of tide energy unit.

Table 13 shows a comparison between the suggested wind turbine locations based on the nearest node load, cable size and cable capacity used, additional power which cable can support, reliability

and voltage drop. It can be said that the location WT_P0025 and WT_0021 are the most suitable locations for the wind turbine. This is because the connection node have:

- The higher voltage drop which can be reduced by connection a generation unit
- The higher failure rate, which can be reduced by adding a generation unit.
- The higher additional power which cable can be supported

Therefore, by adding the wind turbine at one of these locations can improve the reliability and reduce the node voltage drop. Therefore, two scenarios are considered for power flow.

Figure 57: The recommended location of the wind turbine

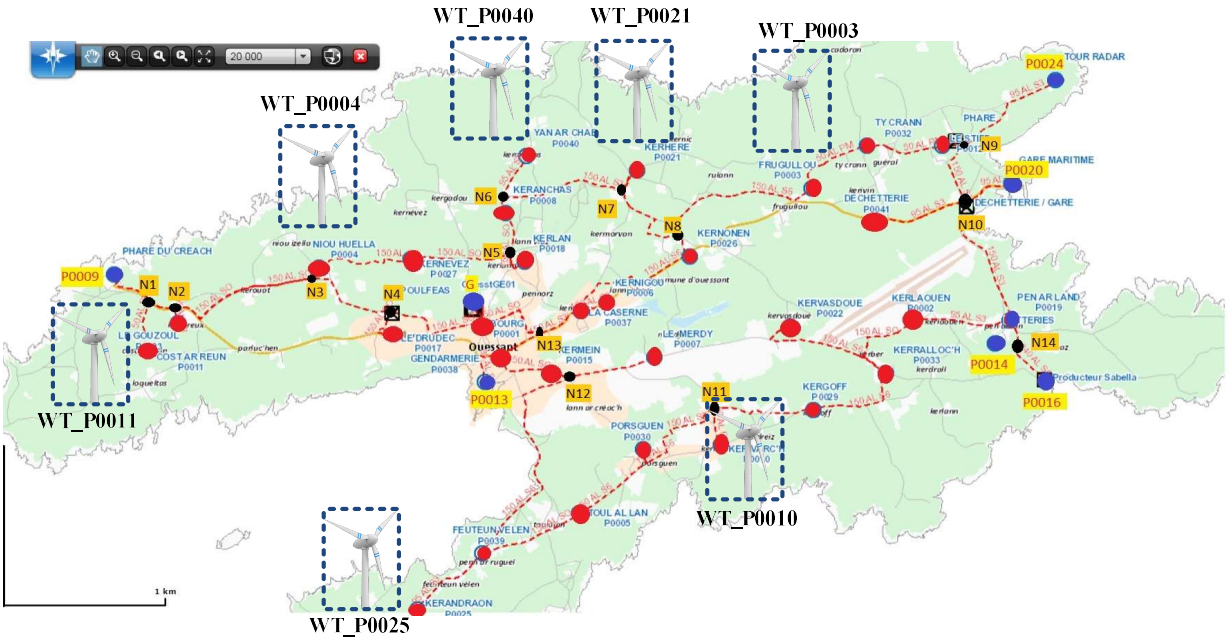

Figure 58: The suggested locations of the wind turbine

Table 13: A comparison between the suggested wind turbine locations

WT Location	Connection Node	Cable Size [mm2]	Cable Current Rating [A]	Cable usage (with DG only)	Additional Cable power [MVA]	Node Failure rate [Failure/year]	Voltage drop
WT_P0011	P0011	50	180	5%	1.63	0.0804	0.86%
WT_P0004	P0004	150	330	13%	2.73	0.0375	0.74%
WT_P0040	P0040	95	255	3%	2.36	0.0775	1.05%
WT_P0021	P0021	150	330	3%	3.05	0.0837	1.09%
WT_P0003	P0003	150/50	255	19%	1.97	0.1167	1.39%
WT_P0010	P0010	50	180	4%	1.65	0.11	1.81%
WT_P0025	P0025	95	255	2%	2.38	0.0974	1.5%

2.2.1 Power Flow Analysis

Two cases are considered, maximum load demand and maximum generation output. According to the recorded data for the Ushant Island in 2016 (ICE report T1.4) and the maximum load and maximum generation output are shown in table 14.

Table 14: Power demand and generation

	Solar (20%)	wind_800kW	tidal	Total Generation	Load Demand
Case 1 (maximum load)	0kW	810 kW	2.7 kW	812.7 kW	1706.7 kW
Case 2 (maximum power generation)	1930kW	780 kW	480.3 kW	3190.3 kW	859.2 kW

There is battery storage system, which is capable of storage the surplus the generation energy and inject the shortage in energy demand. It is located on the diesel generator building. Two scenarios of wind turbine location are considered; WT_P0025 and WT_P0021. In each scenarios two load cases are considered ; maximum load and maximum power generation.

2.2.1.1 Scenario 1: Wind Turbine at Location WT_P0025

The location for the WT and tide energy conversion (Sabella D10) are shown in Figure 60. The 20% of the rooftops for PV is considered at each load node by adding an energy source at each node. The power of this additional energy source is related to the percentage of the number of building at the node and the total PV generated power. For example, if the total power generated form PV is 1000kW and the percentage of the number of building at a node is 10%. Therefore, the injected power at this node is 100kW.

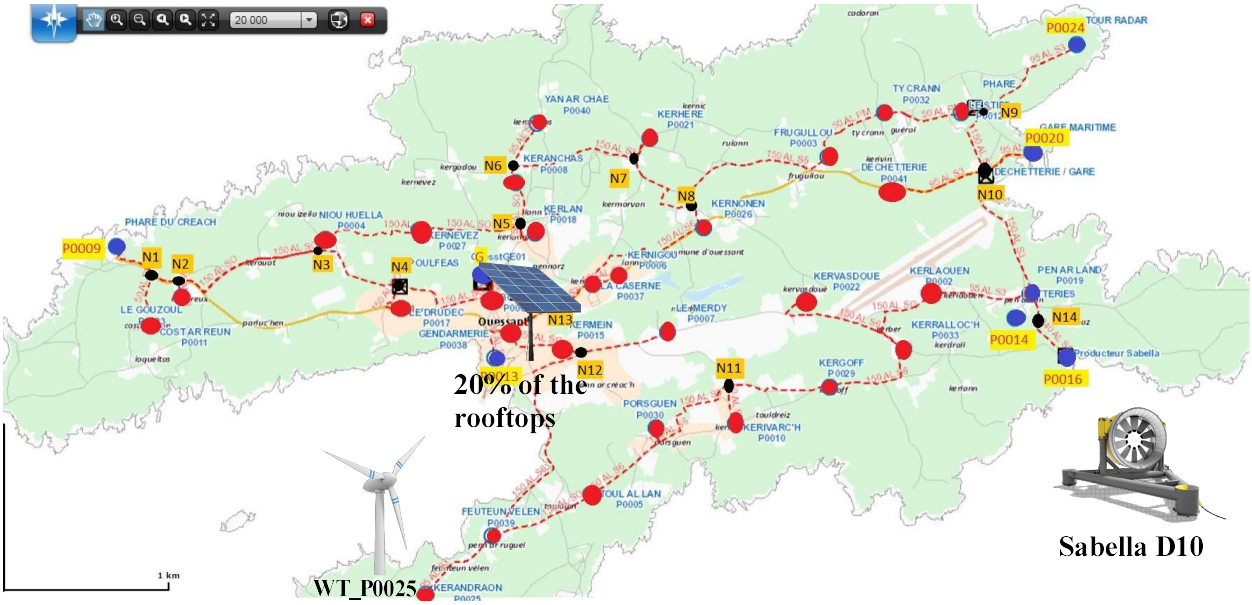

Figure 59: Scenario 1 for the location of the energy generation unit

According these data, the cable capacity usage under two load cases are shown in Figure61. It can be seen that under maximum power generation (3.2MW) the cable capacity usage is high especial at the

city centre where the storage system located (58%). This is due to there is surplus in energy generation (2.3MW) which is transferred to the battery storage unit. Moreover, the PV power is concentrated at the city centre.

Under the maximum load demand, the cable capacity usage is no more than 40% at the city centre. The rest of the cable capacity usage are small (1% to 20%).

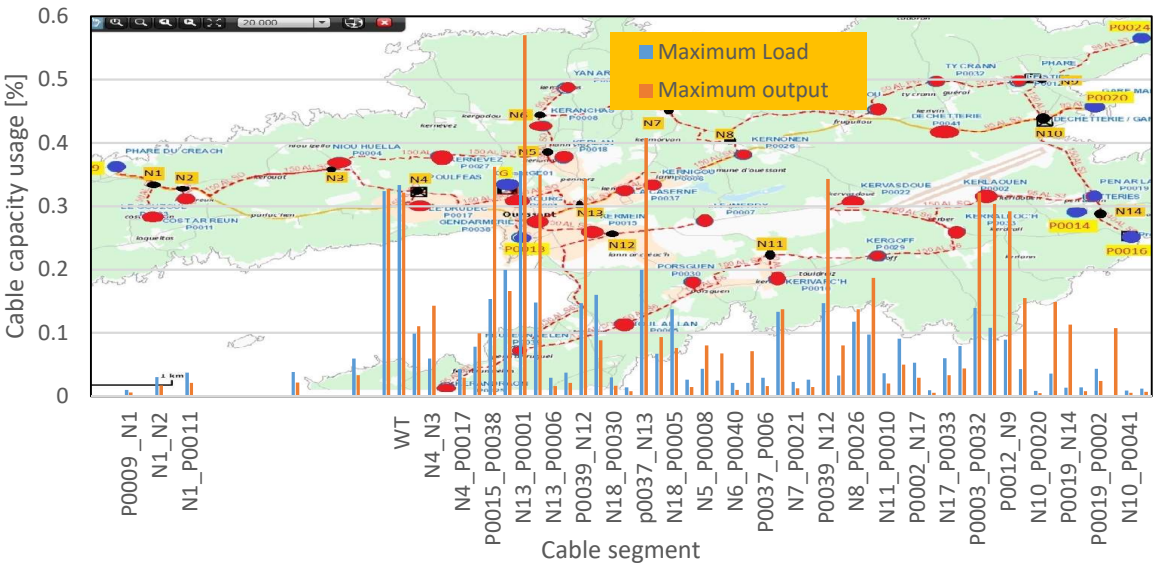

Figure 60: Cable used capacity under high load demand and high generation power output (scenario 1)

The percentage of the voltage drop (ΔV) under two load cases are shown in Figure62. The voltage drops range is -0.5% to 3%. This voltage drops range is lower than the maximum voltage variation ranges according France grid regulations, 6%-8% (Republic 2003).

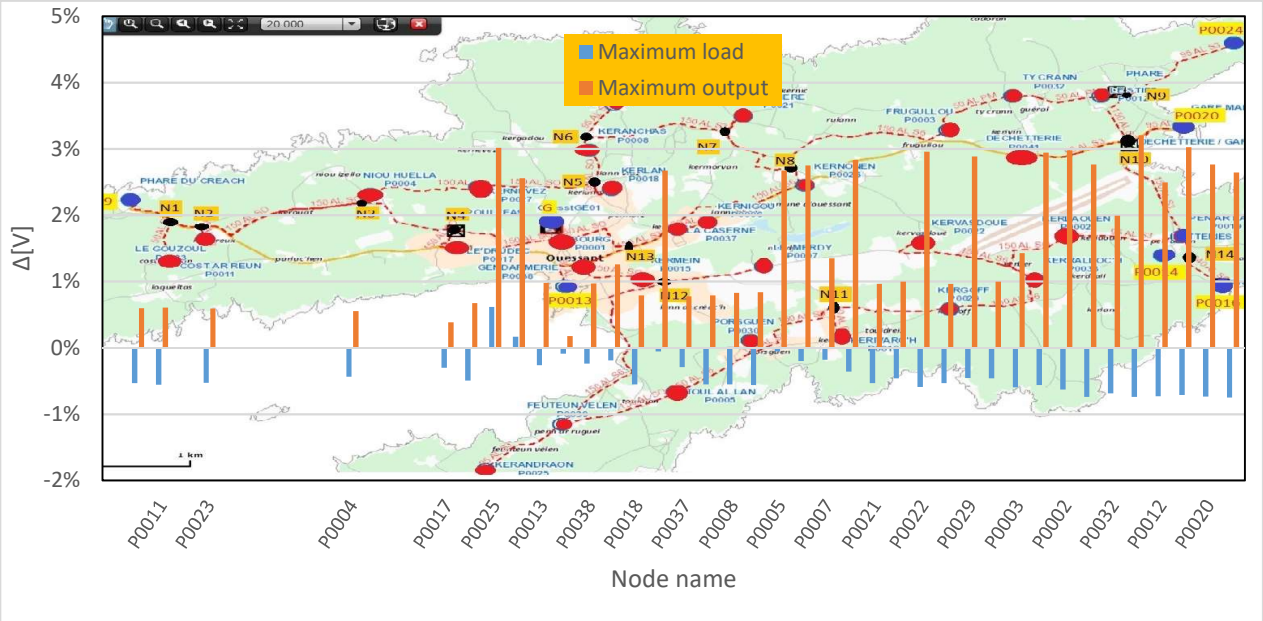

Figure 61: Voltage drop at each load node under high load demand and high generation power output (scenario 1)

Under the maximum load, the voltage drops are small in most of the load node (<0.8%). However, the voltage drops at load node P0025 and P0039 are positive which means the voltage at these nodes are higher than the network nominal voltage (5.5kV). This is due to these nodes are the nearest node to the wind turbine where the power is injected and the existence of the cable capacitors equivalent which boost the node voltage. Moreover, there is no controls modelled in the power flow. This phenomenon happens at the maximum power generation case where each node acts as a current source to inject power to the network. This is because the generated power from PV is higher than the demand load power at each node.

2.2.1.2 Scenario 2: Location WT_P0025

In this load case, the location of the wind turbine is located at node P0021. Figure 63 shows the location of the wind turbine and tidal energy. The cable capacity usage under two cases are shown in Figure 64.

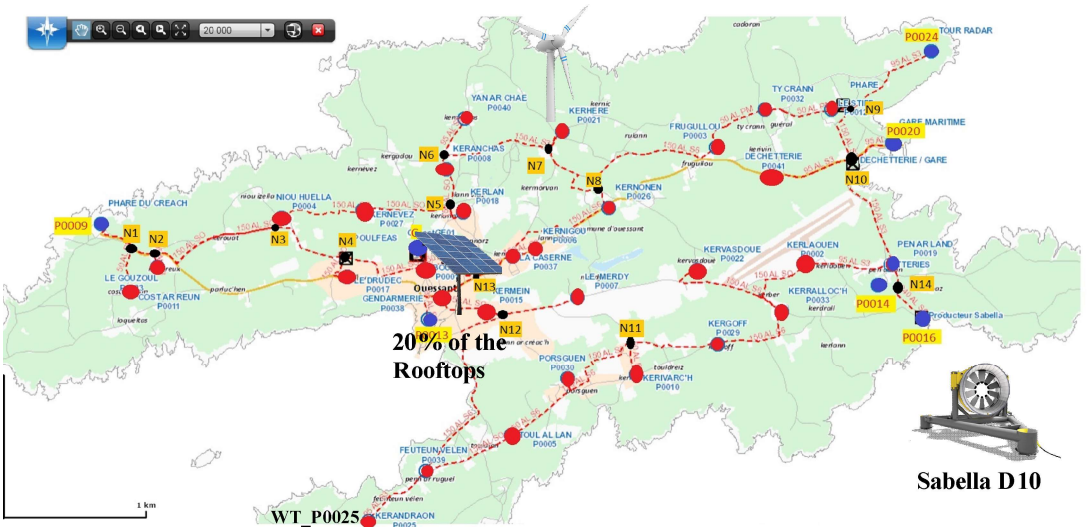

Figure 62: Scenario 2 for the location of the energy generation unit

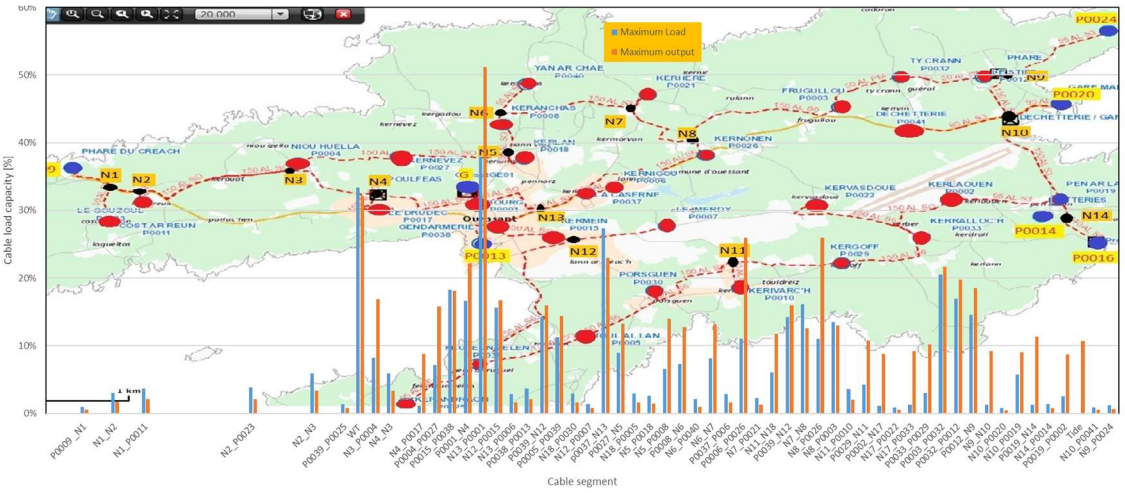

Figure 63: Cable used capacity under high load demand and high generation power output (scenario 2)

There is no much different between the two scenarios of the wind turbine location I term of the cable capacity usage. The wind turbine location at P0021 seems a little less in the cable capacity usage where the maximum is (52%).

Figure 65 shows the voltage drop at each load node. Under maximum load demand the voltages drops is little higher than the scenario 1. Here, the maximum voltage drops is more than 1% and all node. This voltage drops range is lower than the maximum voltage variation ranges according France grid regulations, 6%-8% (Republic 2003). Under the maximum generation, the voltage drops of the load node are positive as in scenario 1 and nearly the same as in scenario 1 but different variation across the load nodes.

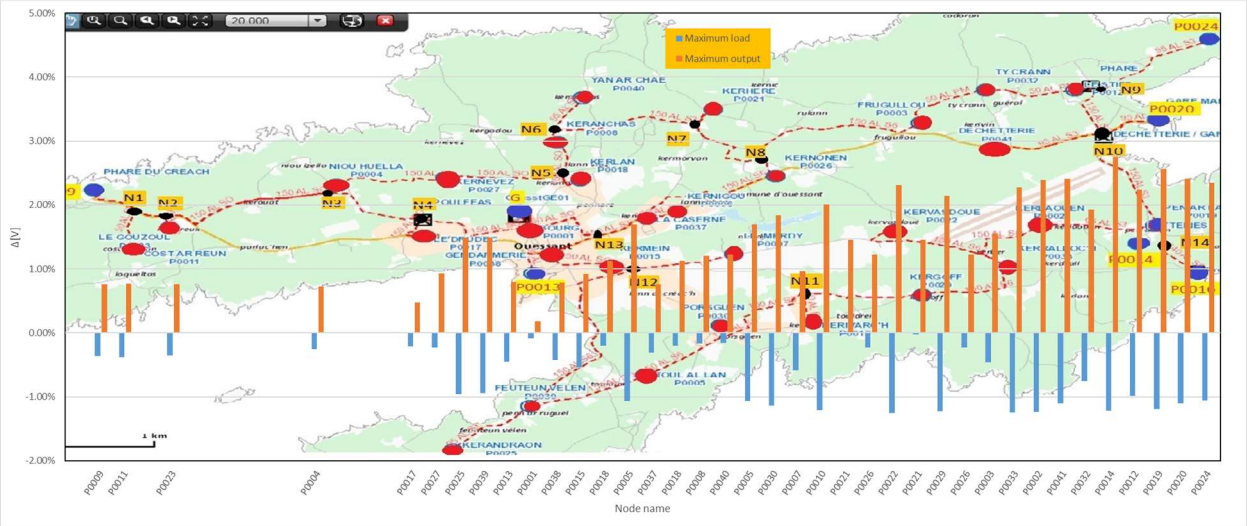

Figure 64: Voltage drop at each load node under high load demand and high generation power output (scenario 2)

2.2.2 Reliability Assessment of the Future Ushant Island Power Network

In this reliability study, there is no diesel generation units. For simplicity, the 20% of the PV rooftops is lumped to one PV system located at the city centre where the battery storage system is located. Two reliability studies are considered. The first one assuming all the reliability of the wind turbine, tidal energy and PV are the same of the diesel generator unit, which is mainly the AC generator. The second one is considering the reliability of the PV is the reliability of the power inverter. The reliability of wind turbine and tidal energy is an AC generator and power inverter as shown in Figure 66.

(a) (b)

Figure 65: Simplified model of PV (a) and wind turbine &tidal energy (b) for reliability study

According to the reliability data in Table 11, the reliability of the PV unit, wind turbine and tidal energy are shown in Table 15. For the fixed and equal reliability for all generator units, the failure rate for each load node are shown in Figure 67.

Table 15 reliability of the PV unit, wind turbine and tidal energy

	PV system	Wind turbine	Tidal energy
Reliability/year	0.9567	0.872	0.872

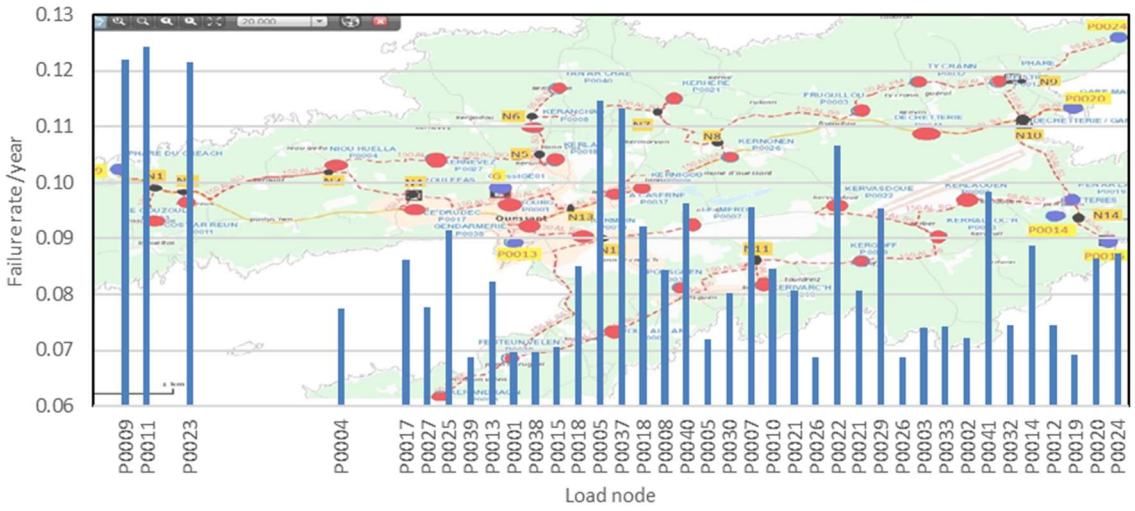

Figure 66: Failure rate for the load node under fixed and equal reliability for all generator units

It is worth to compare the failure rate of the Ushant grid under the diesel generators and the renewable energy sources. Figure 68 shows the failure rate of the load node under renewable energy sources compared with the diesel network operation. As it can be seen from Figure 68, the failure rates of the load nodes are decreased according to the close to the renewable energy sources.

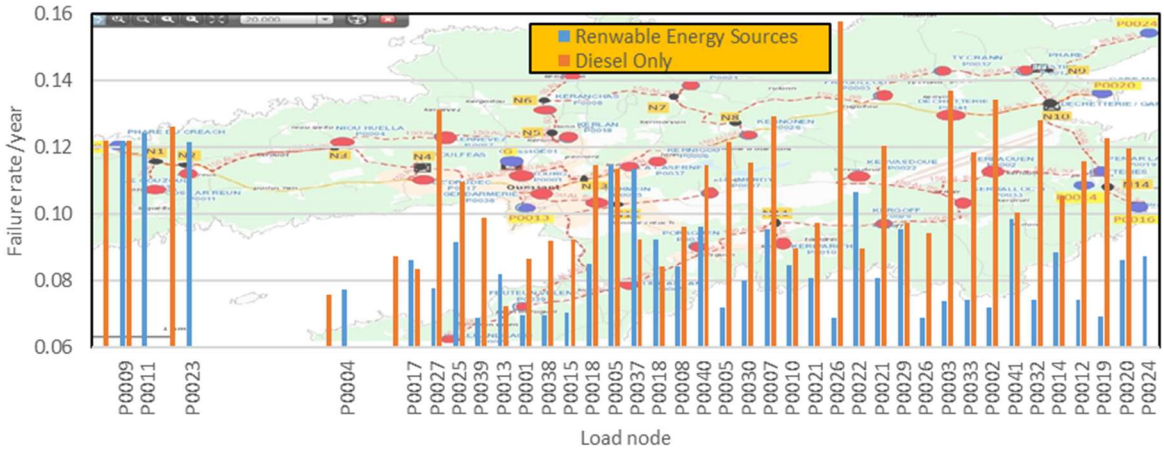

Figure 67: Failure rate for the load node under fixed and equal reliability for all generator units compared to the diesel generator units.

Under case two where the reliability of the PV is the reliability of the power inverter and the reliability of wind turbine and tidal energy is an AC generator and power inverter, the failure rate of the load node are shown in Figure 69.

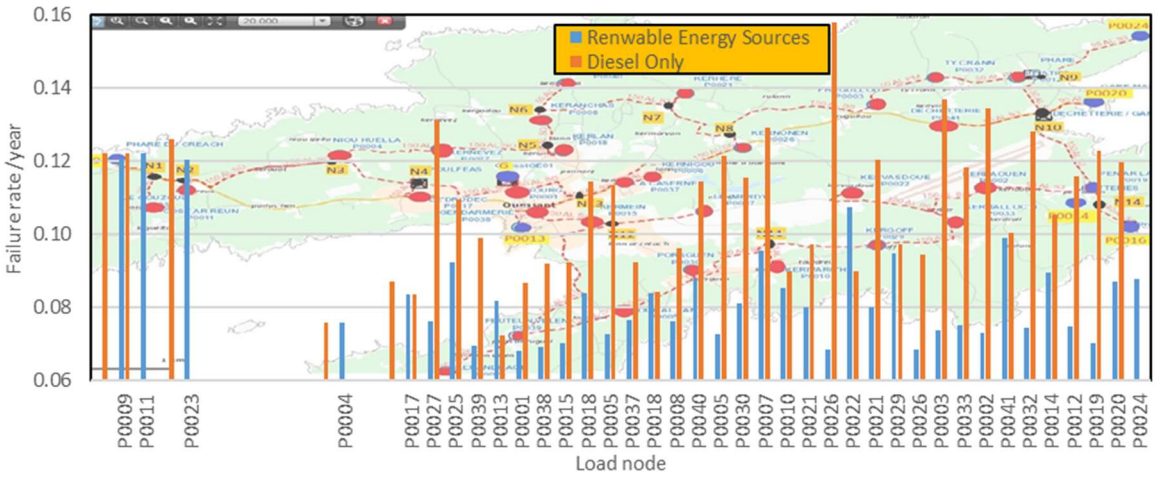

Figure 68: Failure rate for the load node under fixed reliability compared to the diesel generator units.

To show the effected of the replacing the diesel generator units with renewable energy sources, Figure 70 illustrates the comparison between the two cases in term of change the failure rate from the diesel generation operation.

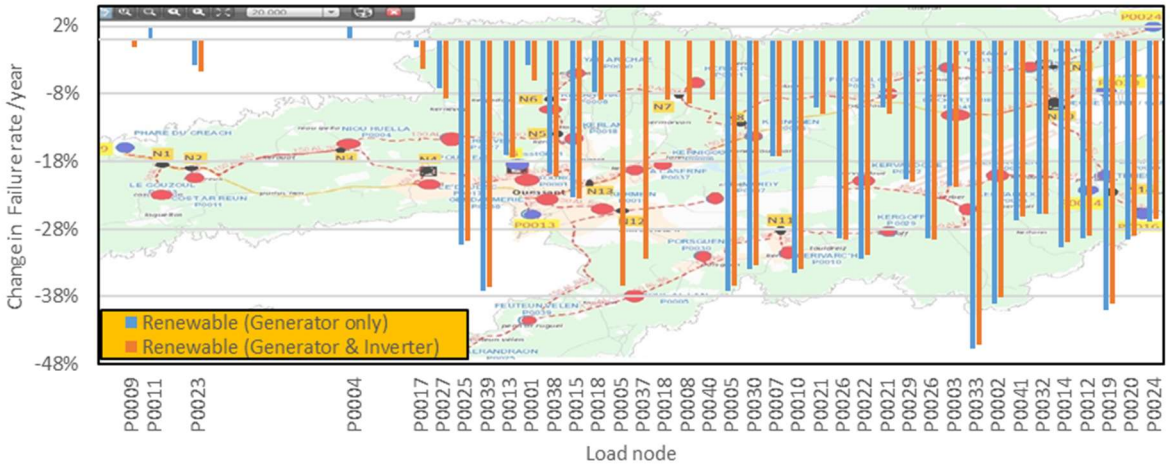

Figure 69: Change in the load node failure rate under fixed & equal reliability for all generator units and fixed reliability

The renewable energy sources reduce the failure rate of the load nodes (1% - 47%). In case 1, it seems that the failure rate of the load node at the city centre not change. This is due to they are near to the generator units. On the other hand, in case 2, the failure rate of the load node at city centre reduced significantly (up to 37%). This is because the PV that is mainly at the city centre have high reliability compared to the AC generator.

References

Busoniu, L., Babuska, B., Schutter, D., and Ernst, D., Reinforcement Learning and Dynamic Programming Using Function Approximator, Boca Raton, FL, USA: CRC Press, 2010.

Chen, S., Gooi, H. and Wang, M. (2012). Sizing of Energy Storage for Microgrids. IEEE Transactions on Smart Grid, 3(1), pp.142-151.

Danish Wind Industry Association. (2002). Roughness and Wind Shear. [online] Available at: http://drømstørre.dk/wp-content/wind/miller/windpower%20web/en/tour/wres/shear.htm [Accessed 17 Nov. 2017].

Davies, J. (2013). A Guide to Roof Construction. [online] Great Home. Available at: http://great-home.co.uk/a-guide-to-roof-construction/ [Accessed 18 Nov. 2017].

Du, P., and Lu, N., Appliance commitment for household load shedding, IEEE Transactions on Smart Grid, vol. 2, no. 2, Jun 2011.

EDF. (2016). Electricity – Tarif Bleu. [online] Available at: http://residential.edf.com/energy-at-home/offers/electricity/tarif-bleu-56121.html [Accessed 26 Nov. 2017].

Enercon (2015). Enercon product overview. E53. [online] Enercon. Available at: https://www.enercon.de/fileadmin/Redakteur/Medien-Portal/broschueren/pdf/en/ENERCON_Produkt_en_06_2015.pdf [Accessed 17 Nov. 2017].

EnergyPlus. (n.d.). Weather Data Sources - International Weather for Energy Calculations (IWEC). [online] Available at: https://energyplus.net/weather/sources#IWEC [Accessed 13 Nov. 2017].

EWT. (2016a). EWT DW52/54-250kW. [online] Available at: http://www.ewtdirectwind.com/wind-turbines/dw5254-250kw.html [Accessed 17 Nov. 2017].

EWT. (2016b). EWT DW52/54-500kW. [online] Available at: http://www.ewtdirectwind.com/wind-turbines/dw525461-500kw.html#c1517 [Accessed 17 Nov. 2017].

EWT. (2016c). EWT DW52/54/61-900kW. [online] Available at: h http://www.ewtdirectwind.com/wind-turbines/dw525461-900kw.html#c1514 [Accessed 17 Nov. 2017].

Fthenakis, V. (2012). Third generation photovoltaics. Rijeka, Croatia: InTech.

Gelažanskas, L., and Gamage, K. A. A., Forecasting Hot Water Consumption in Residential Houses, Energies 2015, 8, 12702–12717.

Google Earth Pro. (2017). Google, Version no.: 7.1.8.3036. [online] Available at: https://www.google.com/earth/download/gep/agree.html [Accessed 13 Nov. 2017].

Hardwick, J., Zheng, S., Smith, H. C.M., Fitch-Roy, O., Connor, P. M., Sundaram S., Iglesias G. and Williams, J., 2018. *ICE report T1.4: An overview of renewable energy supply potential*. ICE Project Report, Penryn, UK.

Homer Energy. (n.d.). Weibull k Value. [online] Available at: https://www.homerenergy.com/support/docs/3.10/weibull_k_value.html [Accessed 13 Nov. 2017].

IWEC Weather Files. (2012). ASHRAE. [online] Available at: https://www.ashrae.org/resources--publications/bookstore/international-weather-for-energy-calculations [Accessed 13 Nov. 2017].

Kalogirou, S. (2014). Solar energy engineering. 1st ed. Burlington, MA: Elsevier/Academic Press.

Marion, B., Riordan, C. and Rennè, D. (1992). Shining On. A Primer on Solar Radiation Data. [online] NREL. Available at: https://www.nrel.gov/docs/legosti/old/4856.pdf [Accessed 13 Nov. 2017].

Northern Power Systems (2015). NPS 100C-24. [online] Northern Power Systems. Available at: http://www.northernpower.com/wp-content/uploads/2014/09/20150212-brochure-NPS-100C-24-UK.pdf [Accessed 17 Nov. 2017].

Parajuli, A. (2016). A Statistical Analysis of Wind Speed and Power Density Based on Weibull and Rayleigh Models of Jumla, Nepal. Energy and Power Engineering, [online] 08(07), pp.271-282. Available at: https://www.researchgate.net/profile/Ayush_Parajuli/publication/306406852_A_Statistical_Analysis_of_Wind_Speed_and_Power_Density_Based_on_Weibull_and_Rayleigh_Models_of_Jumla_Nepal/links/57bd7b8308ae69182430214f/A-Statistical-Analysis-of-Wind-Speed-and-Power-Density-Based-on-Weibull-and-Rayleigh-Models-of-Jumla-Nepal.pdf [Accessed 17 Nov. 2017].

Ray, M., Rogers, A. and McGowan, J. (2006). Analysis of wind shear models and trends in different terrains. [online] Amherst, MA: University of Massachusetts, Department of Mechanical & Industrial Engineering. Available at: https://www.researchgate.net/profile/Jon_Mcgowan/publication/251965566_Analysis_of_wind_shear_models_and_trends_in_different_terrain/links/0c96052e8fb7b913fc000000/Analysis-of-wind-shear-models-and-trends-in-different-terrain.pdf [Accessed 17 Nov. 2017].

Ozdemir, S., Selamogullari, U. and Elma, O. (2014). Analyzing the effect of inverter efficiency improvement in wind turbine systems. 2014 International Conference on Renewable Energy Research and Application (ICRERA). [online] Available at: http://ieeexplore.ieee.org/document/7016449/ [Accessed 22 Nov. 2017].

RegenSW, (2016). Energy Storage - Towards a commercial model. Pathways to Parity - Market insight series. [online] Exeter: RegenSW.Available at: https://www.regensw.co.uk/Handlers/Download.ashx?IDMF=5e5a587b-0fc4-4467-a72a-6c253426df31[28 Nov. 2017].

Schiffer, J., Sauer, D., Bindner, H., Cronin, T., Lundsager, P. and Kaiser, R. (2007). Model prediction for ranking lead-acid batteries according to expected lifetime in renewable energy systems and autonomous power-supply systems. Journal of Power Sources, 168(1), pp.66-78.

System Advisor Model. (2010). NREL, Version no.: 2017.9.5. [online] Available at: https://sam.nrel.gov/download [Accessed 13 Nov. 2017].

Troen, I. and Petersen, E. (1989). European wind atlas. Roskilde, Denmark: Published for the Commission of the European Communities, Directorate-General for Science, Research, and Development, Brussels, Belgium by Risø National Laboratory.

Xiao, J., Bai, L., Li, F., Liang, H. and Wang, C. (2014). Sizing of Energy Storage and Diesel Generators in an Isolated Microgrid Using Discrete Fourier Transform (DFT). IEEE Transactions on Sustainable Energy, [online] 5(3), pp.907-916. Available at: http://ieeexplore.ieee.org/document/6787107/ [Accessed 26 Nov. 2017].

Zhang, M. (2015). Wind resource assessment and micro-siting. 1st ed. Singapore: Wiley.

"http://nepsi.com/."

. "http://plotdigitizer.sourceforge.net/."

A. E. Green, A. J. B. (1978). Reliability Technology Wiley-Blackwell.

AME (1992). "Reliability and availability of wave energy devices " Advanced Mechanics & Engineering.

Ammirato, V. J., J. Silecchia and W. Fairechio (2006). Predicting lead sheath cable failures. Conference Record of the 2006 IEEE International Symposium on Electrical Insulation.

Chengke Zhou, X. J., Zeyang Tang, Wei Jiang , Babakalli Alkali, Wenjun and a. J. Y. Zhou (2012). STATISTICAL APPROACHES FOR ANALYSIS OF FAILURE DATA IN POWER CABLES. CIGRE 2012. PARIS.

Gill, Y. (2011). "Development of an electrical cable replacement simulation model to aid with the management of aging underground electric cables." IEEE Electrical Insulation Magazine 27(1): 31-37.

Hassan M. Nemati, A. S. A., Sławomir Nowaczyk (2015). Reliability Evaluation of Underground Power Cables with Probabilistic Models. Int'l Conf0. Data Mining, DMIN'15 Las Vegas, Nevada, USA.

Jey K. JEYAPALAN, D. J. A. (2007). MAKING REMAINING LIFE PREDICTIONS FOR POWER CABLES USING RELIABILITY ANALYSES. International Conference on Power Insulated Cables, Jicable'07. Versailles , France.

Papathanassiou, S. A. and F. Santjer (2006). "Power-quality measurements in an autonomous island grid with high wind penetration." IEEE Transactions on Power Delivery 21(1): 218-224.

Republic, G. o. t. F. (2003). Décret n°2003-588 du 27 juin 2003 relatif aux prescriptions techniques générales de conception et de fonctionnement auxquelles doivent satisfaire les installations en vue de leur raccordement au réseau public de transport de l'électricité France: 11110-11115.

SINTEF (1984). Offshore Reliability Data Handbook.

YARD "Reliability of six wave power devices."